Mechanisms and interaction phenomena influencing releases in low- and medium-level waste disposal systems. Final report 1986-1990

Brodersen, Knud Erik; Nilsson, K.

Publication date:
1990

Document Version
Publisher's PDF, also known as Version of record

RISØ

Riso-M-2908

Mechanisms and Interaction Phenomena Influencing Releases in Low- and Medium-Level Waste Disposal Systems Final Report 1986-1990

Knud Brodersen
Karen Nilsson

Risø National Laboratory, DK-4000 Roskilde, Denmark
November 1990

Mechanisms and Interaction Phenomena Influencing Releases in Low- and Medium-Level Waste Disposal Systems Final Report 1986-1990

Risø-M-2908

Knud Brodersen
Karen Nilsson

Risø National Laboratory, DK-4000 Roskilde, Denmark
November 1990

Abstract. The report covers work done 1986-1990 at Risø National Laboratory as part of the third EC Research Programme on Radioactive Waste Management.

Waste product characterization:

- Leaching and volume stability of cemented ion-exchange resins. Wet/dry cycling was found to be an important degradation mechanism.
- Hygroscopic properties of cemented and bituminized radioactive waste. Water uptake from the air can be an important release mechanism when waste containing soluble salts are disposed of by shallow land burial.
- Water uptake and swelling of bituminized waste including studies on water migration in bitumen membranes and measurements of swelling pressures.
- Ageing of bituminized products was demonstrated to result in increasing stiffness of the materials.
- Nickel ferrocyanide in precipitation sludge was found to be unstable in contact with concrete.

Barrier material properties:

- The influence of the pore structure in concrete on the hydraulic or diffusive transport of water and ions through concrete barriers was investigated. The main parameter is the water/cement ratio. A theoretical interpretation is given.
- Healing of cracks in concrete barriers by precipitation of calcium carbonate was demonstrated experimentally and described by a simplified model.
- Transport of components between two thin plates of cement paste with different composition stored together in water was found to take place at a low rate.
- The structure of degraded cement paste was studied using SANS (small angle neutron scattering).

Interaction phenomena:

- Integral experiments with migration of radioisotopes from cemented waste through barriers made from kaolin, chalk or concrete were made under different external conditions. The results can be used for model validation and some preliminary work was done.

Final Report 1986-1990 for Contract No FI 1W-0089-DK-(B).

Work performed in the frame of
The Third EC Programme on Radioactive Waste Management,
Task 3, item 1 and 3: "Characterization of Low- and Medium-Level Waste Forms"
and "Barrier Materials".

ISBN 87-550-1694-4
ISSN 0418-6435

Grafisk service, Risø 1990

CONTENTS

ACKNOWLEDGEMENTS.

The authors wish to thank the following for contributions to the work reported here:

Arne Vinther, Gitte Larsen and Jesper Bohn Rasmussen from the staff of Risø Waste Management Section for analytical and general experimental work.

Lis Vinther from the Chemistry Section (supporting analyses) and Heinz Hansen and Alice Kjølhede (tritium analyses) from the Ecological Section of the Department for Environmental Research.

Kell Mortensen and Torsten Freltofte of the Department for Solid Physics for support during the SANS studies. A.J. Allen and D. Shofield, Harwell Laboratories for discussions in the initial phase of the SANS work.

Matching funds to the CEC contributions came from the Danish state appropriations to Risø National Laboratory.

1. INTRODUCTION AND SUMMARY

This final report covers work done in the 4-year period from July 1986 to June 1990 at Risø National Laboratory, Denmark under Contract FI 1W-0089-DK-(B) with the CEC. Conclusions and comprehensive summaries are given in the following for most of the investigations made in the period, but some further details are available in Progress Reports, etc. made during the period /1,2,3,4,5,6,7,8/.

The work has mainly been experimental and is concerned with long-term stability of waste forms and interaction phenomena between barrier materials and cemented or bituminized waste. It is of relevance for Task 3.1 and 3.3 of the EC research programme on radioactive waste management.

Where possible specifications based on the Task 3 reference materials (RMA's) were employed in preparation of simulated conditioned waste samples. However, the handbook /9/ was only available from late in the period and some of the materials studied are therefore prepared according to previous specifications /11/ or are of simplified composition.

All the experiments involving cement is based on Danish SRPC, i.e. a Sulphate Resistant Portland Cement with low alkali and alumina contents. Specifications are given in /1/. Danish Mexphalte 40/50 (Shell) were used in studies on pure bitumen, but considerable work has also been done on a sample of inactive Eurobitum prepared in an early cold run of the Eurochemic extruder. In addition some commercial available kaolin and bentonite were employed as barrier materials.

Work has been done within three main areas:

The first comprises general characterization of conditioned waste products and development of experimental methods for this purpose. Some degradation mechanisms not normally taken into account in waste characterization have been identified.
The following items should be mentioned:

- Leaching and volume stability of cemented ion-exchange resins.
  All the products swell in water. The tendency to swelling increases with increased Water/cement ratio and waste loading, but is decreased by silica-fume additive. Repeated drying/reweting resulted in complete failure of all samples based on pure Portland cement while the silica-fume containing samples were found to withstand at least 7 cycles. Dry/wet cycling is recommended as a screening test for volume stability of cemented waste.

- Hygroscopic properties of waste materials.
  Water absorption from high-humidity air may for hygroscopic waste materials lead to formation of free liquids inside waste packages. The mechanism has been studied for cemented and bituminized wastes containing larger amounts of soluble salts, but may also be relevant for similar polymer encapsulated waste. Water uptake from humid air could be of safety importance during long-term storage under unsuitable conditions, and in near-surface disposal where water as such may be absent, but where the humidity in air in pores or voids is likely to be high.

- Water uptake and swelling of bituminized materials.

  The large difference /10/ in swelling due to water uptake in real Eurobitum and products from early cold runs of the extruder is not well understood. Measurements of the swelling in water of the inactive product before and after γ-irradiation in combination with some (incomplete) experiments with water migration through bitumen membranes containing ß-emitters do not indicate that radiation is the important factor.

  Results from measurements of migration of tritiated water and Cs-ions through membranes of pure bitumen or bitumen containing salt crystals and/or sludge particles should be useable in modelling water uptake in bituminized materials. Variations in electrical conductivity over such membranes indicates, however, that the migration phenomena at least to some degree are stochastic: The soft bitumen films surrounding individual waste particles have at least some ability to self-healing of defects. The ability is probably more pronounced in soft bitumen, and this may possibly explain the above-mentioned difference in behavior since the real Eurobitum material is known to be considerably softer than the product from the early cold run.

  The development of swelling pressure in a confined sample of the inactive Eurobitum was followed through one year. The pressure leveled off at ~1.7 bar, but this may be due to system leakage. An alternative and much simplified system for measurement of swelling pressure due to water uptake in bituminized waste products has been developed and followed also for more than one year. So far a the pressure has reached ~4 bar for a 60 % $NaNO_3$/40 % bitumen sample confined by a concrete barrier. The pressure increases steadily without any tendency to levelling off. The method is found to be very promising. It is cheap and parallel systems can therefore be used to study parametric variations e.g. in waste loading, etc.

  Results from a study of ageing behaviour of some simulated bituminized products are also reported. A general increase in stiffness with time was found to be typical. Finally - as a supplement to the bitumen studies - some results from equilibrium extraction of Cs and Sr from nickel ferrocyanide and barium sulphate precipitation sluge indicate that high pH environments are unfavourable for the Cs-containing precipitate. An effect of micro-organisms on the extraction rates was not established.

The second main area comprises studies on barrier materials. It is pointed out that complete water impermeability cannot be expected for bitumen used as barrier material in relatively thin layers. However, the main emphasis has been on the study of concrete materials. The items investigated are:

- The influence of pore structure in concrete on transport properties.

  The dependence of the hydraulic conductivity and diffusive transport properties for water and Cs-ions in concrete on water/cement ratios and the use of silica fume as additive is demonstrated. A simple theoretical explanation for the differences in transport parameters measured in leaching and diffusion cell experiments is given. The measurements are relevant for water-saturated concrete.

The rate of water-vapour diffusion through various types of concrete has also been measured. This property is important when concrete is used as barrier in the unsaturated zone especially if disposal of hygroscopic waste is intended.

- Crack-healing in concrete.

  When a hydraulic gradient is present over a concrete barrier the flow of water will mainly be through any cracks or other interconnected voids present and not through the much finer poresystem in the material. Apperance and disapperance of such defects are therefore of considerable interest for safety assessments.

  Experimentally it has been demonstrated that a slow flow of bicarbonate-containing water (as typical for most groundwaters) is able to close at least minor cracks in concrete. However, the efficiency appears to be strongly dependent on crack dimensions, etc. A preliminary model of crack-healing by carbonate was developed.

  A study of equilibration between thin plates a calcium- and a silica-rich type of cement paste stored together in a small volume of water showed preferential migration of calcium from the more calcium-rich to the more silica-rich plates. The process is slow and does mainly influence the outer few tenth of millimeters of the plates, but under suitable circumstances such reactions may also contribute to crack-healing in concrete.

- Use of SANS for characterization of degrading cementitious materials.

  Small angle neutron scattering was found to give interesting supplementary information about the fine structures in cement paste. The SANS facility at the DR3 reactor at Risø was rebuild and much improved during the period.
  Some tentative results have been obtained concerning the effect of degradation in the form of corrosion and leaching on the microstructure of cement.

The third main area is possible interaction phenomena between waste and barrier (or different barrier materials). This reflects the title of the report and will partly be a component in some of the items mentioned above. However, some experiments of an integral type, i.e. comprising waste and barrier materials in the same set-up are included here:

- Integral experiments with diffusion in one-dimensional column systems.

  The diffusive release of Cs and Sr from cemented sodium nitrate waste through barriers made from kaolin, chalk or concrete was studied under various conditions. Results were obtained illustrating the influence of anoxic/oxic conditions (some indirect effect on Cs release), presence of corroding iron (slight), bicarbonate ions (strong decrease in Sr release), potassium leaching from the waste (competition with Cs retention in clay barrier), etc. The experimental method was found to be very versatile.

- Diffusion of tritiated water through bentonite influenced by contact with concrete.

  A preliminary set of experiments was made, but the results are too few to permit any conclusions.

2. WASTE MATERIAL CHARACTERIZATION

Low and medium-level conditioned waste materials can be of many types and within each type a wide range of compositions may occur in practice. In the following the study on cemented ion-exchange resin can be regarded as an example of the influence of compositional variations on material properties. As far as relevant degradation mechanisms are concerned the importance of storage conditions is underlined by the effects of wet/dry cycling. Another theme concerned with storage conditions are the possibilities for water uptake from humid air into hygroscopic waste materials. The phenomenon is demonstrated for cemented as well as bituminized waste in continuation of previous work /10,12/. Additional studies of water uptake and other properties of bituminized materials were made. As a sideline to this an investigation of degradation of precipitation sludges was also carried out.

2.1. Cemented ion-exchange resins (RMA3).

Large amounts of ion-exchange resins in bead form or as powdered material arise as waste at nuclear power stations. The material will normally be a mixture of e.g. 1:2 by volume (7/5 according to /9/) of strongly acid cation- and strongly basic anion-exchange resin, commercially available in many types, but always based on cross-linked polystyrene as the structural basis. The ion-exchange capacity may be covered by Li^+, Na^+, corrosion products, Cl^-, silicate, carbonate or borate ions including the fission- and activation products present in the reactor water. In most cases the capacity is only partly spent, so that some of the resins remain on H^+ and OH^- form, respectively. Activation products may also be present in form of crud particles retained in the resin bed by mechanical filtering effects. Futhermore, the waste material, especially the anion exchanger, is likely to be partly degraded due to radiation, thermal effects, etc. It follows that the IX waste can be a very variable material, with properties much dependent on its previous history.

2.1.1. Materials and compositions.

When the experimental study was initiated in 1986, no specification was available for reference waste form RMA3 (mixed ion-exchange resins on bead form solidified in cement /RMA/). In absence of such a specification a parametric study was conducted covering considerable variation in the IX-to-cement and water/cement ratios. The range of selected compositions was partly based on experimental work made in Sweden, Norway and Finland in the late seventies /13,14/.

8 different products were prepared from fresh an- and cation exchange resins (Amberlite IR 120 and IRN 78) on Cl^- and Na^+ form, respectively, mixed in the volume ratio 2:1. The "even-level", i.e. resin mixture just covered by water, contained ~0.344 g dry material/g. About 0.37 g water per g even-level mixture is supposed to be present as free interstitial water while 0.28 g/g is contained in the particles corresponding to a water content of ~45 %.

100 ml (~110 g even-level) mixed-bed resin on NaCl form contains about 67 meq Na^+ and 100 meq Cl^-. When mixed with the cement (Danish SRPC), considerable

regeneration of the resin takes place resulting in increased Cl^- and Na^+ concentrations in the pore water. The total contents in the products investigated here were from 16 to 21 mg Cl/cm³ and 8 to 10 mg Na/cm³.

The interstitial water in the even-level mixture, any extra water which was added, and some of the water in the resin beads may be consumed in the cement-hydration reactions. However, it is reasonable to assume that the fast initial setting of the cement paste takes place while the beads are still completely swelled. This defines a relatively large hollow into which each resin bead is nested. The distance between adjacent beads will depend on the waste loading and has for the products studied here typical values beween 0.3 and 0.4 times the diameter of the completely swelled particles (mean diameter ~0.6 mm). The volume fraction filled with cement paste varies between 0.69 and 0.72 and the product density between 1.70 and 1.86 g/cm³ /1/.

Recipies for the 8 investigated products are given in Table 1. Fig. 1 shows the cement-to-IX ratios plotted against the w/c ratios.

Later, when water is removed from the beads by the hydration reactions or by simple drying of the sample, the resin beads contract to about half the volume of the completely swelled particles. This, in itself, should be of no concequence for the product stability. In principle, the hollow surrounding each particle should also be sufficiently large to permit reswelling to the original bead size if a dry product later gets into contact with water, but in practice this appears not to be the case for some products, as shown in the following.

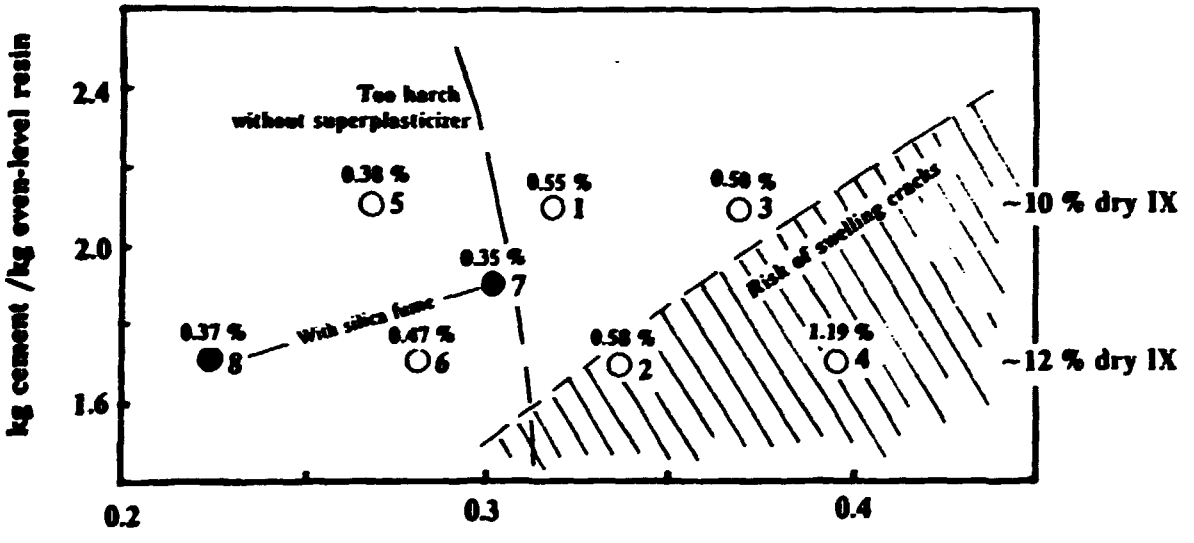

Fig. 1. Relationships between w/c ratios and the amounts of cement and additional water added to 1000 g even-level mixed IX resin. Limitation for suitable mix-proportions are according to Swedish work. The circles indicates sample compositions used in the present study. Vol% swelling after 246 days in water is given at each point.

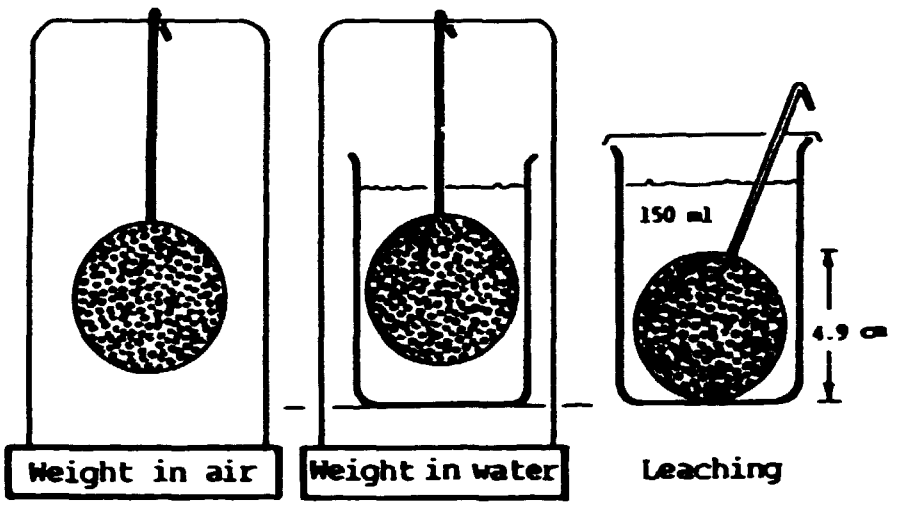

Fig. 2. Weighing in air and in water and leaching of spherical samples of cemented ion-exchange resins.

2.1.2. Experimental method and results.

Samples of the 8 different products were cast in spherical form (d=4.9 cm) using silicone-rubber moulds. The samples were hardened 28 days in a high-humidity environment but without contact with liquid water. They were then weighed in air and again after immersion in 150 ml 'pure' water of the same temperature (20°C) as the sample, see Fig. 2. After increasing periods of storage in the water (in contact with laboratory air) the weighings were repeated and the water replaced. The solutions were acidified and analysed for Na^+, Ca^{++} and Cl^-. Leach rates for the macro-components were calculated from the analyses and were also used to estimate the total amount of leached material. The change of weight in air plus the amount of leached material is a measure for the water uptake in the sample. The change in weight immersed in water is, according to the Archimedes' principle, a measure of the volume change.

Figure 3 shows as an example the leach curves for the four main components for sample No. 1. Na^+ is leached rapidly in a short initial period followed by a period where the amount of released material increases nearly but not quite liniarily with $\sqrt{t}$. The initial behaviour is similar for Cl^-, but after about 10 days the leach rate drops to very low values corresponding to Cl^- concentrations of only about $2 \cdot 10^{-5}$ mol/l in the leach water. Solubility limitations for a Cl-containing mineral in the concrete is the most probable explanation. The Ca^{++} release is influenced and decreased by CO_2 interference which will also influence the OH^- release, here somewhat arbitrarily calculated from the electro-neutrality principle.

The leach curves for Na^+ cannot be fitted with the simple analytical expression for diffusion-controlled leaching from a spherical sample /15/. However, it has been found that excellent fits of the experimental results can be obtained if the total leached amount is regarded as the sum of material leached one-dimensionally from a rapidly depleted

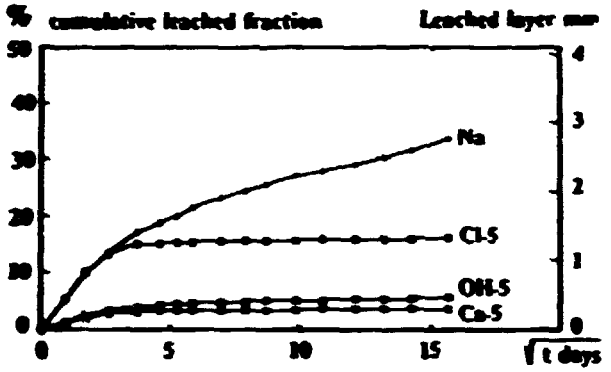

Fig. 3.
Leaching of major components from sample No. 1.

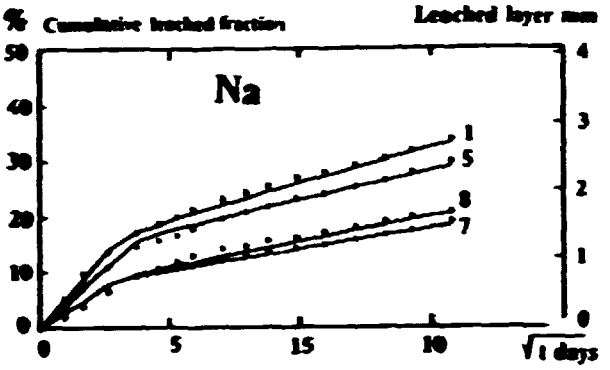

Fig. 4.
Leach curves for Na^+ for 4 of the samples compared with model calculations based on diffusive leaching from a surface layer plus leaching from an inner sphere.

0.5 to 2 mm thick surface layer and material leached at a somewhat lower rate from a sphere reduced correspondingly in diameter. This is demonstrated for the Na^+ results in Figs. 4. The two diffusion coefficients and the layer thicknesses are given in Table 1. That a good fit can be obtained by a model with three independent parameters is not surprising, but it appears reasonable to treat the surface layer - which may be structurally different and in much better contact with the water - differently from the more protected material in the middle of the sample. The thickness of the layer is seen to increase with decreasing quality of the product. The diffusion coefficients obtained for the spherical part of the samples are supposed to be representative for the properties of the bulk material. Whether this is the case, and the surface-layer model as such is reasonable, can be investigated by scaling experiments.

Figures 5a-h show the results of the weight-increase measurements for samples No. 1, 5, 7 and 8, the first two without and the last two with silica-fume additive.

After a short period of rapid water uptake the process continues at a much slower rate. The water uptake was for all 8 samples accompanied by some swelling. The maximum values after 24% days in water are given in Table 1 and are also indicated on Fig. 1 The volume stability is seen to decrease with increasing water/cement ratio and increasing IX content. Sample 4 (~1.2 vol % swelling) was in an area where swelling cracks according to /13/ could be expected. The swelling as such is small compared with the micro-heterogenity of the materials.

After the first long period of immersion the samples were dried in the laboratory air (~50 % RH, 20°C) for about 22 days and then reimmersed in water. This treatment led to complete disintegration of 4 of the samples. No. 1 was also very fragile with pronounced deep-going cracks. It broke on the second reweting. The results of the weighings for this sample are shown in Figs. 5ab. It is seen that the drying is accompanied by contraction which rapidly is converted to increased swelling when the sample is reimmersed in water.

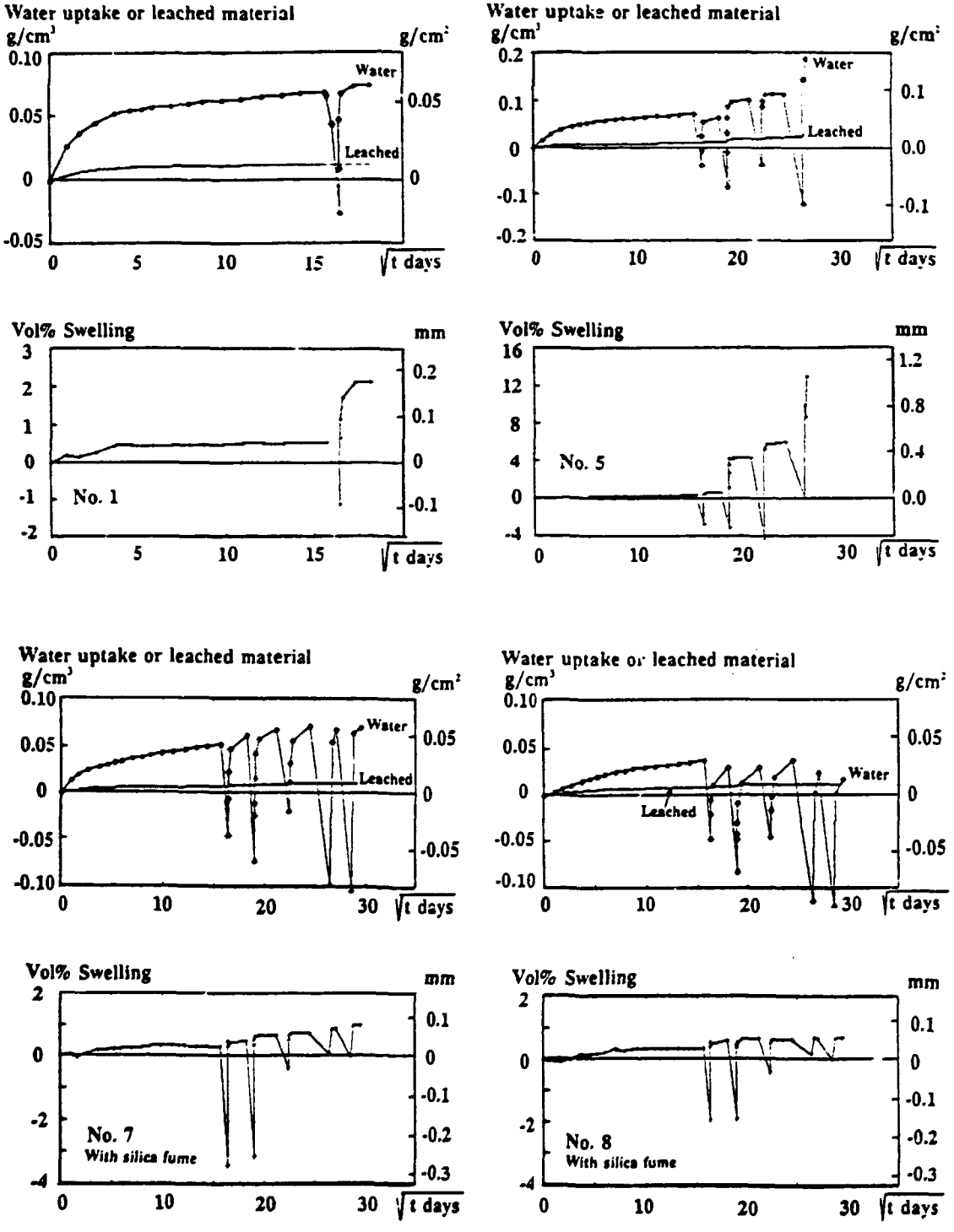

Fig. 5a-h Water uptake, leached material and swelling of samples of cemented ion exchange resin exposed to dry/wet cycling.(The amounts of leached materials were not determined systematically and may be higer than indicated. The water uptake is therefore somewhat underestimated.)
Sample No. 1: 10.1% IX in pure SRPC paste with w/c=0.32 at 45% water in the resin beads
Sample No. 5: 10.4% IX in pure SRPC paste with w/c=0.27 - " -
Sample No. 7: 10.4% dry IX, 10 g silica fume/100 g SRPC, w/c=0.30 - " -
Sample No. 8: 11.8% dry IX, 10 g silica fume/100 g SRPC, w/c=0.22 - " -

Only the samples with very low w/c ratio (No. 5) and/or with silica-fume additive (Nos. 7 and 8) appear to withstand such a dry/wet cycling. However, it is seen (Fig 5d) that the swelling of sample No. 5 is increasing drastically during the second, third and fourth rewetting. After the fourth rewetting this sample desintegrated completely.

The samples with silica fume are more resistant. For sample No. 8 the swelling after 5 cycles has only reached about 0.8 vol%. Swelling is also moderate: about 1.0 vol% for sample No. 7 with higher w/c ratio. The beneficial influence of silica fume on volume stability of cemented ion-exchange resin is clearly demonstrated by this experiment. However, it should be noticed that the contraction during the drying periods has diminished considerably during the later cycles, maybe indicating defects formed inside the samples.

Table 1. Mixing proportions and results from investigation of 8 samples of cemented mixed-bed ion-exchange resin.

Sample No:	1	2	3	4	5	6	7	8
Even-level mixed bed g	100	100	100	100	100	100	100	100
Extra water g	30	20	40	30	20	10	20	0
Cement (SRPC) g	210	170	210	170	210	170	190	170
Superplasticizer g					0.25	0.4	1.0	3.3
Silica fume g							19	17
Consistency		soft	soft	soft		harsh		
w/c ratio at 45% water in the resin beads	0.32	0.34	0.37	0.39	0.27	0.28	0.30	0.22
Dry ion exchange resin%	10.1	11.9	9.8	11.5	10.4	12.3	10.4	11.8
Density g/cm³	1.81	1.73	1.75	1.70	1.85	1.80	1.81	1.86
Effective diffusion coefficients for Na-leaching, unit: 10^{-9} cm²/sec								
Sphere:	1.55	2.1	2.4	3.9	0.95	1.34	0.44	0.62
Surface layer:	7.7	10.8	14.2	23	2.4	7.1	2.4	2.0
Layer thickness: mm	1.0	1.2	1.5	2.0	1.0	1.0	0.5	0.5
After 246 days in water:								
Water uptake mg/cm²	72	75	74	75	72	72	51	36
Swelling vol %	0.55	0.60	0.50	1.2	0.39	0.48	0.37	0.37
After the first air drying and re-immersion in water:								
Sample condition	cracked	disinte-grate	disinte-grate	disinte-grate		disinte-grate		

2.1.3. Conclusions.

Cemented IX resins with 10 to 12 weight % dry mixed-bed resin and covering a wide range of w/c ratios have been investigated with the following results:

- Na^+ is leached readily. The rate is increasing with increasing w/c ratio and IX loading and is decreased by the use of silica-fume additive. The behaviour can be modelled by a diffusion mechanism if a lower quality surface layer is assumed.
- Cl^- is only leached to a minor degree, maybe due to formation of a chloride-containing mineral in the cement paste.
- Water uptake proceeds rapidly in an initial period followed by a prolonged period with slow uptake. The rate is decreased by silica-fume additive.
- All products swell in water, but to a different degree. The swelling is increasing with increasing w/c ratio and IX loading and is decreased by silica-fume additive.
- When exposed to repeated drying and rewetting the samples made with pure SRPC failed completely. The use of silica-fume considerably improves the volume stability under dry/wet cycling at least when the w/c ratio is reasonably low.

In summary: The use of pure cement of the Portland type as solidifying matrix material for ion-exchange resins cannot be recommended. However, acceptable products may still be obtained adding sand and gravel as specified for RMA3 /9/, silica fume as demonstrated in the present investigation, or by use of e.g. blast furnace slag cement as recommended in UK. Low w/c ratios (using superplasticizers to ensure sufficient workability), decreased waste loading or thermal pretreatment of the resins to reduce the swelling tendencies, are other possibilities for improvement of the product stability.

The experimental methods employed were demonstrated to be well suited for the study of cemented waste products. Wet/dry cycling may - like the freeze/thaw method - be used as a screening test to study volume stability. The effects of dry/wet cycling may also have direct safety implications for waste materials stored for long periods above ground.

2.2. Hygroscopic waste materials.

Samples of cemented, bituminized or polymer-encapsulated waste may change in weight due to water uptake or water loss when exposed to high- or low-humidity air, respectively. The process continues until a certain equilibrium water-vapour pressure is attained. This equilibrium vapour pressure is a function of the porewater composition and is strongly influenced by the contents of easily dissolvable salts such as $NaNO_3$, Na_2SO_4 or NaOH in the products.

The phenomenon has been studied for various cemented and bituminized waste materials (see also Section 2.3.1).

2.2.1. Hygroscopic properties of cemented sodium nitrate (RMA8).

Spherical samples (d=4.8 cm) cast from the simulated RMA8 product described in Section 4.1. (~9.4% $NaNO_3$, w/c=0.4, ^{134}Cs activity) and small broken pieces (~5 mm) of the same material were kept at 20°C in 98, 80 and 50 % relative humidity environments for about 10 months, see Fig. 6a. The spheres as well as the beakers with the spheres, and the beakers with the broken pieces were weighed at increasing intervals. The results are shown in Fig. 6b.

After about 14 days droplets of solution began to appear on the surface of the sphere stored at 98 % RH. It dripped into the beaker and was collected there. On the sample surface it is probably present as a nearly concentrated sodium nitrate solution, but in the beaker it will be further diluted by absorption of additional water from the air. At the end of the experiment 15.5 g water had been collected containing 2.9 g dry material, mainly $NaNO_3$. It means that about 27 % of the sodium nitrate originally present in the sphere was leached by the procedure. About 21 % of the ^{134}Cs present in the sample was also leached. Since the weight of the sphere is nearly constant (slightly declining at the end) the leached $NaNO_3$ must be replaced by a corresponding amount of water retained in the pores of the sample. In the beaker with the small broken pieces water was accumulating in contact with the sample resulting in leaching of 56 % of the sodium nitrate and 50 % of the ^{134}Cs.

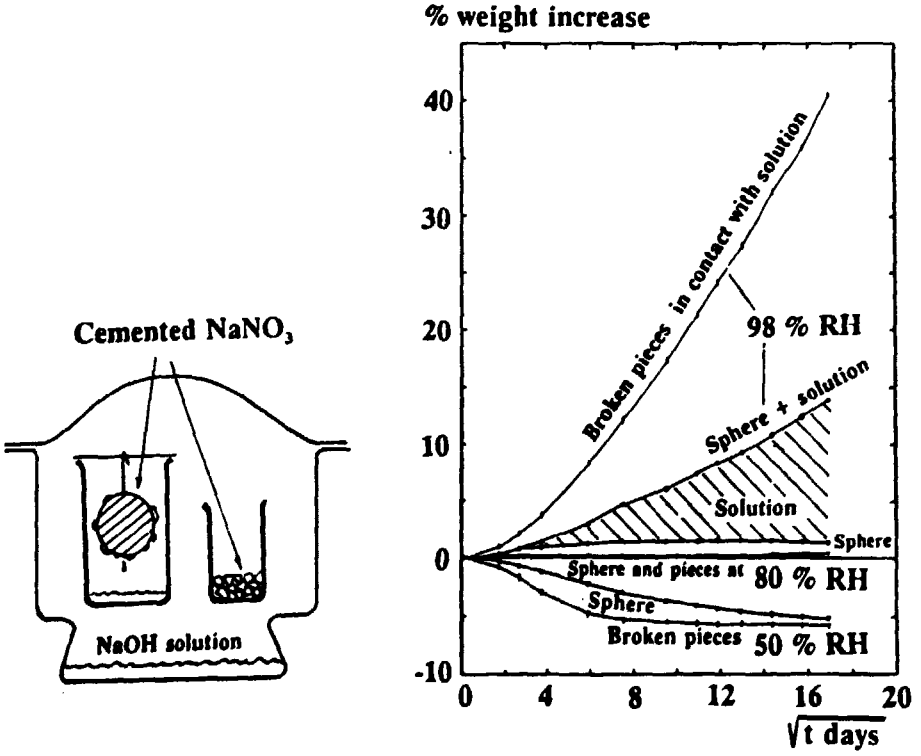

Fig. 6a,b. Experimental set-up and water uptake and accumulation measurements for samples of simulated RMA8 (cemented sodium nitrate) stored in 98 %, 80 % and 50 % relative humidity environments.

At 80 % RH only very slight weight increases (<0.5 %) and no free liquid were observed for both systems. This indicates that 80 % relative humidity corresponds quite well to the equilibrium water vapour pressure for the material.

At 50 % RH a weight loss corresponding to about 6 % can be extrapolated for both systems although the spherical sample is not yet quite in equilibrium. This corresponds to ~21 % of the original water content or a reduction in w/c ratio from 0.4 to 0.32.

The weight increases for the spherical samples of RMA8 have been compared with the results for similar samples cast from SRPC paste with w/c = 0.4 but without addition of $NaNO_3$ or activity. At all three RH levels the tendency to water absorption or retention was considerably less than for the simulated RMA8 material. The limit for actual water uptake, as indicated by positive weight increase, is probably considerably above 90 % RH for the pure paste while it for RMA8 is slightly below 80 % RH.

2.2.2. Comparative study of water uptake and volume stability of cemented waste forms during leaching or exposure to high-humidity air. (RMA1,3,8 and 10)

As a follow-up on the studies of leaching, water uptake and volume stability of cemented ion-exchange resins reported in Section 2.1, and to the above-mentioned experiment with water uptake from high-humidity air in samples of cemented sodium nitrate, a comparative experiment was set up to study leaching, water uptake and volume stability of samples of various types of cemented waste exposed to water or high-humidity air.

Five types of materials were prepared:

1) 100 g even-level ion-exchange mixture + 40 g water + 210 g SRPC.
This corresponds to sample No. IX-3 in Table 1 and the composition:
16.5 g dry IX + 13.3 g water in the IX + 36.6 g water + 100 g SRPC.

2) 10.4 g Na_2SO_4 + 37 g water + 100 g SRPC.
This corresponds to a previously investigated material /8/, but at that time based on an Italian OPC.

3) 13.2 g $NaNO_3$ + 37 g water + 100 g SRPC.
This is an inactive version of the material used for the experiments in Section 2.2.1.

4) 13 g (mainly) wood ash + 37 g water + 100 g SRPC.
The ash contains: 0.67% Na, 2.97% K, 1.02% Ca, 2.11% SO_4^- and 2.1% CO_3^-

5) Pure cement paste: 37 g water + 100 g SRPC.

The first four simulate, or are of a type reasonably similar to RMA3, RMA1, RMA8 and RMA10, respectively, while the pure cement paste is included as reference.

Three spherical samples (series A B and C with d≃4.8 cm, surface area ~72 cm^2) and a cylindrical sample in the bottom of a beaker (series D with d≃6.5 cm, exposed upper surface ~33.2 cm^2) were cast from each type of material. After hardening one of each set of samples was exposed to water in an ordinary leaching experiment (series A) while the other two spherical samples and the sample in the beaker were exposed to CO_2-free, high-humidity air (RH~95 %) using systems similar to those shown in Fig. 6a.

The weight changes of the samples and the accumulation of solution dripping from some of the spherical samples or collecting on top of the samples in beakers have been followed for 435 days. The matrix of experiments are shown in Fig. 7.

The samples in series **B** and **C** are treated in the same way, except that solution accumulating on and eventually dripping into the beaker under samples of type **B** are permitted to remain there, while samples of type **C** are exposed to a short immersion in water in connection with each weighing of the systems. From the weight changes when immersed in water the swelling can be calculated for samples of type **A** and **C**. The sample is then wiped carefully to remove adhering water and weighed again in air. The leached amounts of Na are also measured for the samples of type **A** and **C** (supplemented with Ca analyses for type **A**). From this the total amount of leached dry material is estimated and the uptake of water into the samples can be obtained as difference.

The results are given in more detail in /5/. Table 2 contains a summary of the end-values obtained after 435 days.

For the normally leached samples of type **A** it is seen that a considerable fraction (60-90 %) of the sodium in all cases has been leached, and that there is not much difference between the water uptake into the various products: 0.07 - 0.1 g/cm² surface area. In the case of the sodium sulphate or nitrate-containing samples a nearly corresponding amount calculated as dry material has been leached out. For the other three products the amounts of leached solids are considerably less than the water uptake.

Table 2. Leached fraction of sodium, swelling, water uptake and total leached material for five different types of cemented waste after 435 days of normal leaching (**A**) or exposure to high-humidity air (**B C** and **D**).

Type			IX	Na_2SO_4	$NaNO_3$	Ash	Cem
A	Leached Na	%	81.5	70.6	58.6	81.3	87.1
C	Leached Na	%	2.0	33.7**	32.0	3.9	5.7
D	Leached Na	%	-	~24	~14	-	-
A	Swelling	vol%	0.12	0.41	0.43	0.28	0.16
C	Swelling	vol%	~0.005	0.92*	0.62	~0.03	~0.07
A	Water uptake in sample	g/cm²	0.068	0.098	0.085	0.065	0.086
	Leached material	-	0.024	0.090	0.084	0.005	0.015
B	In sample: water uptake-leached	g/cm²	0.009	0.049	0.033	0.031	0.012
	In sample + drip.solution	-	0.010	0.242	0.277	0.033	0.013
C	Water uptake in sample	g/cm²	0.0065	0.054*	0.080	0.036	0.017
	Leached material	-	0.0005	0.015*	0.052	0.0003	0.0003
	In sample: water uptake-leached	-	0.008	0.049*	0.031	0.039	0.017
	In sample + drip.solution	-	0.010	0.073*	0.279	0.040	0.019
D	In sample + accum.solution	-	0.065	0.544	0.703	0.091	0.054

* At 119 days when sample broke.
** Some broken pieces in direct contact with solution in beaker.

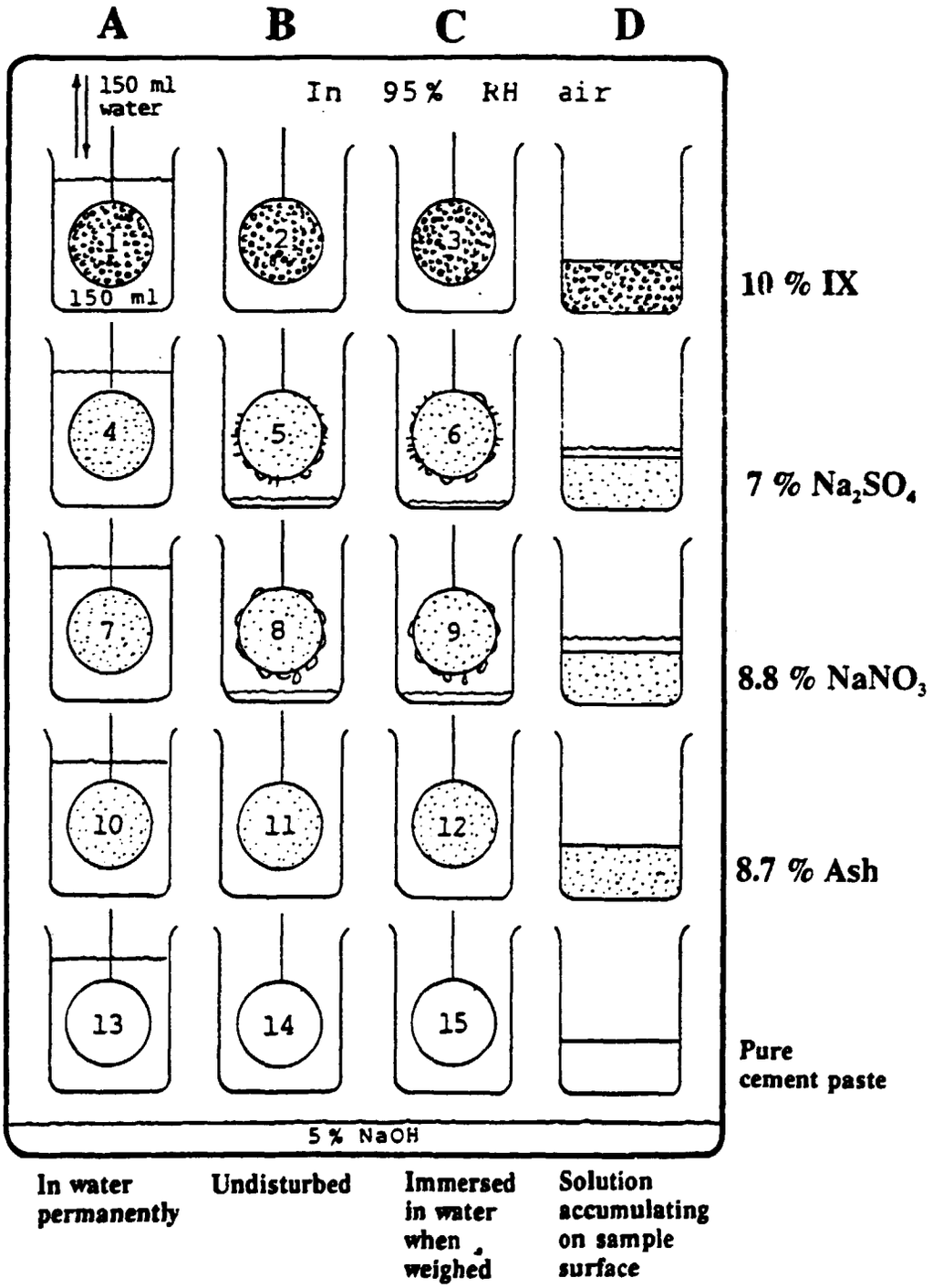

Fig. 7. Experiment comparing the effects of normal leaching conditions with water uptake from high-humidity air for four different types of cemented waste and pure cement paste.

Comparing with the similar set of values for the systems of type C it is seen that the water uptake in the samples kept in high-humidity air is somewhat less, but still considerable, especially for the sulphate and nitrate-containing samples. The amount of "leached" Na - i.e. sodium which has been removed from the sample mainly by solution dripping down from the spheres - is reduced to about 30 %. For the IX, Ash and Cem samples, where free liquid has not been observed on the surface, the water uptake is considerably less than for the corresponding A-samples. The slight amount of leached Na is in this case due to wash-out from the surface during the short immersions.

The simple weight-gain measurements for wiped samples of type C and B should correspond to the difference between water uptake into and total leached solid material from the sample. With reasonably accuracy this is demonstrated in the type C experiments where independent values for leached materials could be estimated from the chemical analyses. It is also seen that the weight-gain measurements for the C and B samples are fairly similar indicating that the short immersion periods for the C-samples do not influence the general behaviour of the system very much. The use of this method for swelling measurements is therefore permissible.

The sodium sulphate-containing sample of type C was partly broken after about ~120 days. Some big pieces laying at the bottom of the beaker in contact with the solution gave rise to a steep increase in solution accumulation. Also the corresponding type B sample developed deep cracks and broke completely after about one year.

All the samples treated according to procedure C, B and D and containing larger amounts of soluble salts, i.e. $NaNO_3$ or Na_2SO_4, are accumulating free solution on the top (D) or dripping down from the samples (B and C). The amounts are not negligible since they would correspond to accumulation of a 1-cm water layer on top of the two D samples in about 2 to 3 years.

In the case of the spheres the rate of accumulation is only about half of this value probably because the strong solution collecting on the surface of these samples has possibility to run off and is not kept nearly concentrated by leaching in direct contact with the product. (This is probably also why the solution contact with the broken pieces from the sulphate-containing C sample results in an increased rate of weight gain for this system).

The water uptake for the IX, Ash and Cem samples of type D are somewhat greater than for the corresponding spherical samples. Free liquid has not been seen on any of these samples so the "leaching" explanation is not immediately relevant. However, the exposed surface area of the sample in the beaker may possibly be somewhat greater than the assumed 33 cm^2 since no special precaution has been taken against gabs between the sample and the beaker wall.

The end-values for the swelling of samples in series A and C are also given in Table 2.

For the type A samples under permanent immersion the sulphate product contracted a little during the first ~50 days of the leaching period while all the other products swelled 0.1 to 0.2 vol%. Later the sulphate and nitrate products swelled slowly corresponding to a total volume increase of about 0.40 vol% while the other products and the cement paste samples remained nearly volume-stable.

For the type C samples stored in high-humidity air the swelling of the sulphate product was especially large: 0.9 vol% at 119 days when the sample disintegrated partially. One cannot say whether the disintegration is due to the swelling, or the large measured swelling is due to cracks formed by a minor degree of volume change in the product. However, exposure to high-humidity air appears to be worse for this product than simple leaching in water.

The swelling of the nitrate-containing sample was similar to the one under ordinary leaching. For the other three types of samples the swelling measurements were somewhat variable and the swelling rather low, near the sensitivity of the method.

2.2.3. Summary and general comments

The employed experimental methods were found to give interesting information about the behaviour of cemented waste in contact with water or humid air, but the phenomena are not restricted to cemented waste: Most of the comments given below will also be relevant for bituminized waste (see section 2.3.1) and maybe also for certain types of polymer-encapsulated wastes.

It has been demonstrated that activity can be released from hygroscopic waste products without direct water contact by formation of a liquid phase from condensed water vapour. This may occur during storage under unsuitable circumstances or disposal in moist, but unsaturated, geological formations.

- Releases by 'leaching' in such high-humidity air environments were found to be only slightly less than by total immersion.
- The accumulation of water is accelerated when the solution stays in contact with the waste sample so that a high concentration of easily dissolved salt is maintained by leaching from the material. The rate will also be dependent on the possibilities for vapour transport through pore structures, etc.
- The tendency to water accumulation is a function of the relative humidity in the environment and of the contents of easily dissolved salts in the waste. Below ~80% RH the water uptake will probably be insignificant in most materials.
- A difference in material stability during high-humidity exposure compared with leaching i liquid water is indicated for sulphate-containing cemented waste and may be important for the degradation of such materials under certain circumstances.

At a given humidity the amount of solution generated by the content of easily dissolved salts in a waste unit is defined by the condition about water-vapour equilibrium between solution and the environment. Whether this will result in releases from the unit or the near-field materials will depend on the amount of solution relative to the retaining capacity of the pore structure of the materials.

The phenomenon may be important for storage of waste units under unsuitable conditions or for disposal in the unsaturated zone where it - in combination with percolating rain water may constitute an important release mechanism.

2.3. Water uptake in bituminized materials.

An experimental study of inactive RMA 9.2 (Eurobitum) has been conducted in continuation of previous general work /10,12/ on water uptake and transport in bitumen and bituminized waste. Some further studies of the mechanism of water and ionic transport through bitumen membranes were also made.

The inactive Eurobitum material was received from Mol in April 1987. The product is from an early, cold run of the Eurochemic extruder. The composition is assumed to correspond to the specifications for RMA 9.2, i.e. the $NaNO_3$ content is ~25 % /9/. The same material was included in characterization work performed at Mol /7,10,16/.

2.3.1. Hygroscopic properties of Eurobitum.

Samples of the inactive Eurobitum material were cast as 0.6 cm tick layers in glass Petri dishes and stored at 20°C in 98, 75 and 50 % relative humidity environments. The weight of the samples were followed through ~220 days. In some cases solution collecting at the surface of the samples was removed in connection with the weighings. The results are shown in Figs. 8a,b.

Weight increases of dishes originally containing crystals of pure sodium nitrate were also included in the experiment. At 75 % RH the weight increase levelled-off at 117 %, corresponding to a 46 % $NaNO_3$ solution. At 98 % RH the weight was still slightly increasing at 760 % weight gain, corresponding to a ~12 % $NaNO_3$ solution.

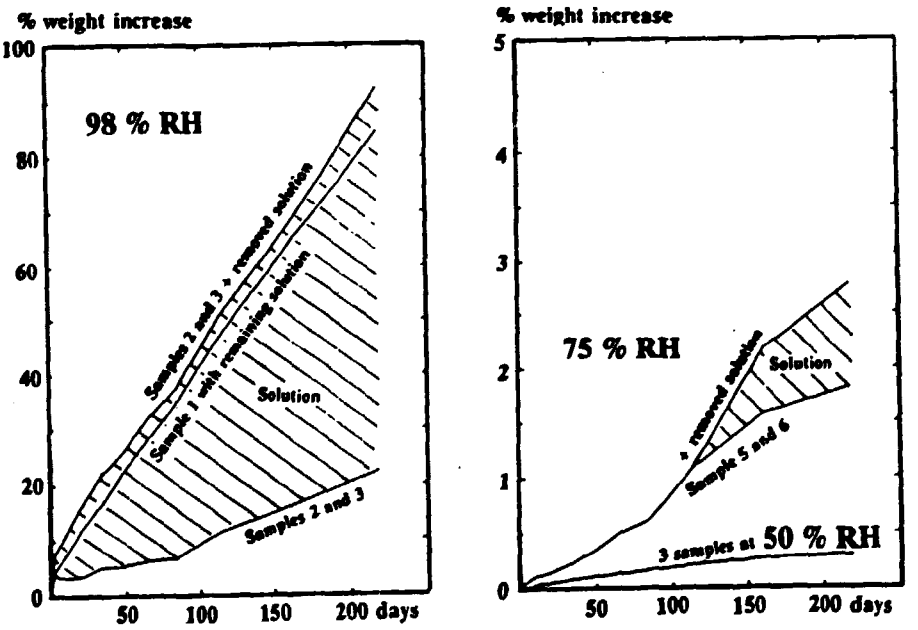

Figs. 8a,b. Water uptake and accumulation measurements for samples of inactive Eurobitum stored in 98, 75 and 50 % relative humidity air.

Since the bituminized product contains ~25 % $NaNO_3$ it can be assumed that the weight increase of these samples would reach about 180 % in 98 % RH and 30 % in 75 % RH air. The measured end-values after 220 days were ~90 % and ~3 % respectively, see Fig. 8, but obviously the samples were still taking up water when the experiment was closed.

At 50 % RH no weight increase was found for the sodium nitrate crystals but the bituminized product increased slightly (~0.3 %) in weight. This is supposed to be due to water uptake in the bitumen matrix which typically contains ~0.5 % water when saturated.

2.3.2. Unrestricted swelling of Eurobitum in water.

Samples of inactive Eurobitum were cast in stainless steel rings (h=2.0 cm, d=4.2 cm, giving a surface-to-volume ratio: $S/V = 1\ cm^{-1}$). The samples were stored in beakers in 200 ml pure water which was replaced at increasing time intervals. The solutions were analysed for Na and the swelling was calculated from weighing of the samples in air and suspended in the pure water. The results of the measurements are shown in Fig. 9a. The reproducibility for two identical samples was excellent.

Swelling is clearly demonstrated for these unconfined samples, but is not nearly as pronounced as for the active samples investigated at Mol (7,10,16). The swelling shown in Fig. 9a can be described approximately by:

$$\Delta x = 0.0038 \cdot \sqrt{t} - 0.007 \text{ cm} \qquad (t \text{ in days})$$

and the volumetric swelling by:

$$\Delta V = 100 \cdot (S/V) \cdot \Delta x \quad \text{vol \%}$$

The expressions are probably valid while the sample can be regarded as 'infinitly thick' as far as leaching of $NaNO_3$ is concerned.

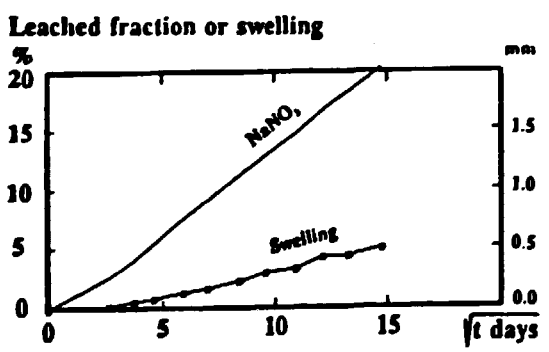

Fig. 9a.
Na-leaching and volume increase due to water uptake for sample of inactive Eurobitum.

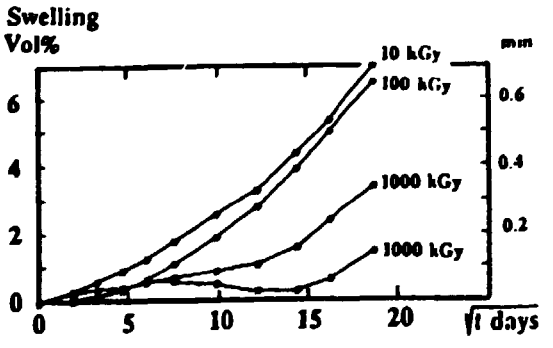

Fig.9b
Volume increase for 4 samples of γ-irradiated inactive Eurobitum immersed in water.

The equivalent leached thickness for Na is given by:

$$L = 0.0142 \cdot \sqrt{t} - 0.008 \quad \text{cm} \qquad (t \text{ in days})$$

corresponding to an effective diffusion coefficient $D_e = 1.8 \cdot 10^{-9}$ cm²/sec.

In principle, the formulas should also be applicable on bigger samples. The swelling of of the contents in a 200 l drum (d=58 cm) exposed to water from the top only should then be about 1 vol % i 100 years. However, it appears from the above-mentioned experiments in Mol that the sample of inactive Eurobitum cannot be regarded as representative for the real active material.

2.3.3. Effects of radiation on rate of water uptake.

Increased rate of water transport due to radiation damage in bitumen might be the reason for the observed high swelling of active Eurobitum in water. It was therefore thought worthwhile to investigate whether external γ-radiation was sufficient to induce a tendency to increased swelling in the inactive material.

Four samples similar to the inactive ones described in Section 2.3.1. were irradiated at 37°C in a ^{60}Co source facility to 10, 100 or 1000 kGy (two samples), respectively. The samples were stored in water at 20°C, and the swelling was measured at intervals by weighings in air and immersed in water. Sodium leaching was also followed. The results are shown in Figs. 9b.

The two samples which have recieved the lowest doses behaved practically like the unirradiated material. However, the increasing slope of the later part of the curves is of interest. The results for the two samples exposed to 1000 kGy indicate that the water uptake in this case result in none or low swelling, or rather in a long delay before swelling is initiated. This is thought to be due to a counteracting contraction process caused by outdiffusion of gases produced by the irradiation. The γ-doses had no significant effect on sodium leaching.

The general conclusion drawn from this experiment is that external γ-radiation before exposure to water does not produce a significantly increased tendency to water uptake. However, external radiation during the water exposure and/or radiation by internal sources, especially alpha-emitters, may still play a role in swelling due to water uptake in bituminized material: The rate of water-vapour transport through the thin films of bitumen surrounding the individual salt crystals may well increase due to defects caused by the radiation, but the defects may only be temporary and disappear again due to repair mechanisms in the soft bitumen. In that case the effect can only be demonstrated if continuous external or internal irradiation is employed.

This was investigated using the membrane technique described in the following. 0, 1 or 5 MBq ^{45}Ca ß-activity was incorporated as $CaCO_3$ in 2 mm thick membranes of Mexphalte 40/50. The transport behaviour of tritiated water in the membranes was not established with certainty, but the results indicate that the effect of continuous ß-radiation is insignificant. Further studies using α-activity should be made, but so far it must be concluded that radiation is of minor importance for the rate of water uptake.

2.3.4. Diffusion of water and ions through bitumen membranes.

Previous work /10/ on diffusion of tritiated water and ions through membranes of bitumen or bituminized waste materials have been continued.

2.3.4.1. Pure Mexphalte 40/50

Simple diffusion cells - as shown schematically in Fig. 10 - were used to study simultaneous migration of tritiated water (TOH) and $^{134}Cs^{+}$ and $^{60}Co^{++}$ or ($^{60}Co(CN)_6^{4-}$) through ~0.5 to ~1.3 mm thick bitumen membranes cast against siliconized paper and reinforced by nylon net. One side of the cell was permanently filled with a strong solution containing the diffusing species while the weak solution on the other side was replaced and analysed by γ-spectroscopy and (after destillation) by liquid scintillation counting. The influence of membrane thickness and macro-chemistry of the solutions was studied using 8 systems kept at 20°C.

An example of the break-through curves is also shown in Fig. 10. The results are presented as the cumulative normalized amount of strong solution which should have passed the membrane to give the amounts of activity found in the weak solution.

Table 3 contains the specification for the various systems together with values for the transport coefficients estimated from the shape and slope of the break-through curves. (Definitions: the effective diffusion coefficient $D_e = \lambda \cdot x^2/6$ where λ is the timelag and x the thickness of the membrane. The diffusive permeability coefficient $P = \alpha \cdot c \cdot x/\Delta c$ where α is the slope of the break-through curve, c is the concentration in the strong solution and $\Delta c/x$ the concentration gradient over the membrane, see also Section 3.1).

Typical time-lags of the order of 6 days were used to estimate the D_e values for TOH given in the table. The break-through curves for TOH tend to have two slopes: an initial one corresponding to the time-lag and assumed to be associated with transport of water as vapour through the membrane, and a later one (partly) due to transport through water-filled micro-defects in the membranes and accompanied by migration of ions.

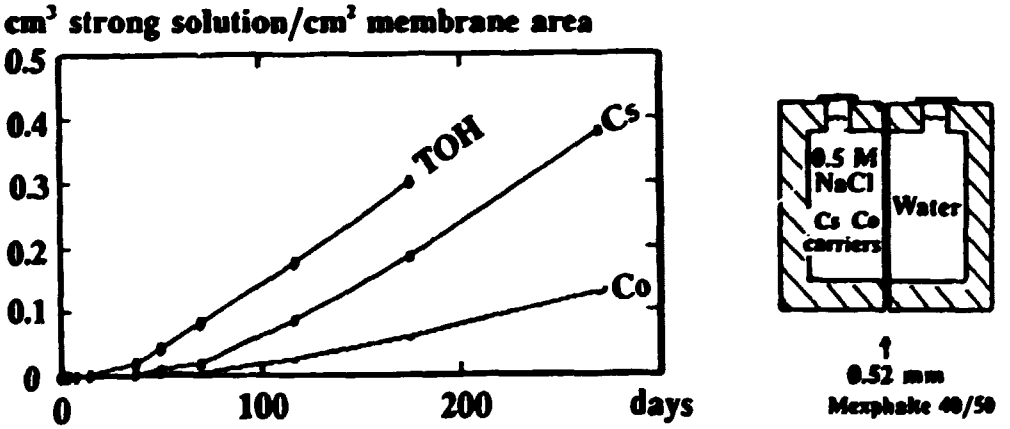

Fig. 10. Diffusion cell and break-through curves for tritiated water (TOH), $^{134}Cs^{+}$ and $^{60}Co^{2+}$ ions at room temperature for a 0.5 mm thick membrane of pure Mexphalte 40/50 with water on one side and 0.5 M NaCl and 0.001 M Cs^{+} and Co^{2+} carriers on the other.

This is especially the case for the systems with thinner membranes (0.5-1 mm, Nos 15-18) where the long-term diffusive permeability is nearly the same for TOH and Cs^+ indicating that the transport is mainly through the liquid phase. The large concentration gradients of macro-ions (NaCl) over membrane Nos. 16 and 18 is apparently not resulting in different behaviour from membrane Nos. 15 and 17 with water or thin carrier solution on both sides.

For the 1.3 mm membranes, where in addition the macro-chemistry is the same on both sides (Nos. 11-14), the diffusive permeability for Cs^+ remains much lower than for TOH during the whole experiment. The tendency to generation of defects has therefore been less for these systems.

The P values for Co^{2+} are in all cases somewhat lower than for Cs^+, probably due to some retention capability for Co^{2+} on the asphaltenes in the bitumen (also demonstrated in equilibration experiments /7/).

Table 3. Diffusion and permeability coefficients for TOH, Cs^+ and Co^{2+} or $Co(CN)_6^{4-}$ obtained for membranes of pure Mexphalte 40/50 at room temperature.

Unit for D_e and P: 10^{-12} cm^2/sec

Membrane No:		11	12	13	14
Thickness:	mm	~1.3	~1.3	~1.3	~1.3
Solution on	strong side:	1 M Na_2SO_4 + carrier		0.01 M H_2SO_4 + carrier	
	Weak side:	1 M Na_2SO_4		0.01 M H_2SO_4	
D_e	TOH	5600	6700	7100	8000
P	TOH short term	29	33	80	30
	TOH intermediate	36	36	102	35
	Cs^+ long term	0.19	0.013	0.007	0.004
	Co^{2+}		0.003		0.002
	$Co(CN)_6^{4-}$	0.034		0.008	
Membrane No:		15	16	17	18
Thickness:	mm	~0.5	~0.5	~1.0	~1.0
Solution on	strong side:	Carrier	0.5 M NaCl	Carrier	0.5 M NaCl
	Weak side:	Water	Water	Water	Water
D_e	TOH	*	6100	25000	34000
P	TOH short term	(460)	51	34	36
	TOH long term	940	1300	370	480
	Cs^+ long term	970	1080	200	180
	Co^{2+}	290	350	52	37

2.3.4.2. Thick membranes.

Four modified diffusion cells were used to determine transport of tritiated water through 0.6 cm or 1.0 cm thick layers of pure Mexphalte 40/50 simultaneously with measurement of electrical conductivity over the layers. Two of the systems were filled with 0.1 M NaCl solution and the other two with 0.1 M NaOH. Tritiated water was present on one side of the membrane.

The electrical resistance was followed over a period of nearly one year. In most cases no conductivity could be measured, indicating that no solution-filled defects had developed in the thick membranes. After about 10 months the 1 cm membrane in NaOH solution gave indications of slight but very variable conductance.

Water samples from the weak side of the cells were analysed for tritium. The break-through curves are shown in Fig. 11 and values for the transport parameters are given in Table 4. It is seen that the D_e values obtained from the time-lags (110-140 days) are of the same order as for the thinner membranes in Table 3. Also the P values are approximatly the same as for the 1.3 mm membranes without defects. However, the transport in the strongly alkaline systems appears to be somewhat slower than in the neutral or acid systems. The reason for this is not obvious.

Table 4. Diffusion and permeability coefficients for tritiated water obtained for thick membranes of pure Mexphalte 40/50 at 20°C.

Membrane No:		T1	T2	T3	T4
Thickness:	mm	~6.3	~6.3	~10	~10
Solution on	strong side:	0.1 M NaCl		0.1 M NaOH	
	Weak side:	0.1 M NaCl		0.1 M NaOH	
D_e TOH		6600	15000	6300	14000
P TOH long term		87	138	20	7

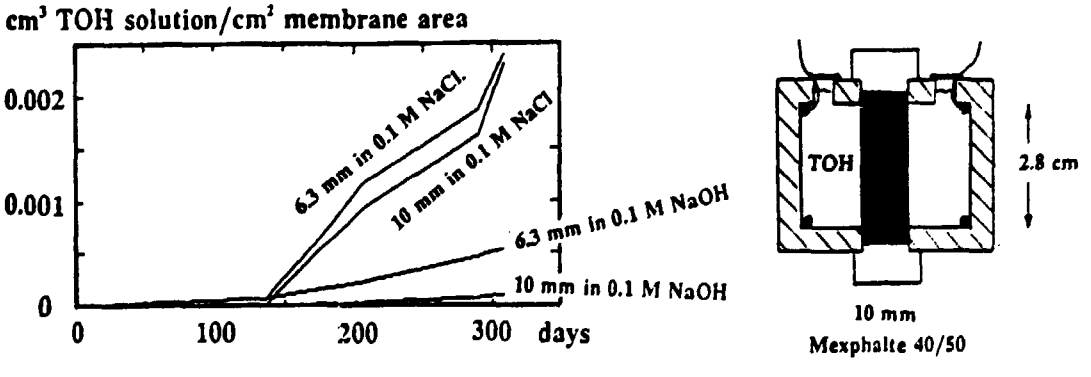

Fig. 11. Break-through curves for tritiated water for 4 thick membranes of pure Mexphalte 40/50.

2.3.4.3. Eurobitum.

In bituminized waste containing soluble salts the thickness of the bitumen films separating the individual crystals is much less than ~0.3 mm, the minimum thickness possible to handle in the diffusion-cell experiments described above. If in addition the product contains precipitation sludge particles the properties of the bitumen membranes surrounding the salt crystals may be modified by inclusion of the much smaller sludge particles. The influence of embedded particles may be studied using membranes containing salt crystals and/or sludge particles.

A set of three about 2 mm thick membranes were employed. Two were cast from the inactive Eurobitum material mentioned above and one from the same material, but after extraction of the $NaNO_3$ content by hot water.

The three membranes were mounted in diffusion cells as shown in Fig. 12b and a solution containing tritiated water and $^{134}Cs^+$ in 0.001 M Cs carrier was placed in the left side of the cells. The diffused material was sampled from the right side at increasing time intervals. One of the untreated Eurobitum membranes was stored with saturated $NaNO_3$ on both sides. The other membranes had pure water (except for the Cs-carrier) on both sides. The results are shown in Figs. 12a,b.

It is seen that the TOH-penetration rate is considerably higher for the $NaNO_3$-containing membrane stored in water compared with the one in concentrated sodium nitrate solution. This must be due to defects produced by leaching of the salt crystals. However, these defects are not so large that they have much influence on the Cs-transport and a considerable part of the water transport may still be in form of vapour.

For the membrane cast from pre-leached Eurobitum the TOH- and Cs-penetration rates are very low for the first 100 days where they suddenly increases to a much higher and nearly identical rate for the two species (the appearent difference is due to a scale factor 10 between figure a and b.) This similarity must be interpreted as due to the generation of very fine channel(s) permitting transport in solution through the membrane.

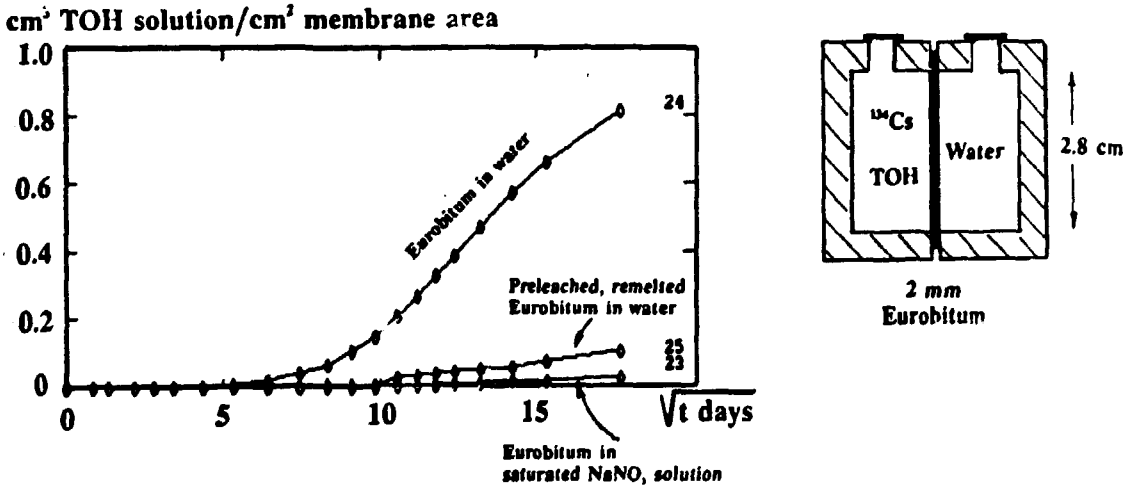

Fig. 12a,b. Diffusion cell and break-through curves for tritiated water and $^{134}Cs^+$ ions for 3 membranes of inactive Eurobitum.

No. 24: Water or weak Cs^+ solution.

No. 25: Preleached Eurobitum, water or weak Cs^+ solution.

No. 23: Saturated $NaNO_3$ solution on both sides.

Table 4. Diffusive permeability coefficients for tritiated water through various membranes of bituminized materials at 20°C.

Membrane No:	23	24	25
Material	Eurobitum	Eurobitum	Leached Eurobitum
Thickness: mm	~2	~2	~2
Solution on strong side	Ca. 10 M $NaNO_3$	0.001 M Cs^+	0.001 M Cs^+
Solution on weak side	Ca. 10 M $NaNO_3$	Water	Water
Permeability coefficients TOH	280	8800	870
Unit: 10^{-12} cm^2/sec Cs^+	0.3	600	760

The diffusive permeabilities for TOH as calculated from the slope of the curves are given in Table 4. Tentative values for Cs are also given.

Values between 40 and 100 • 10^{-12} cm^2/sec were found for the diffusive permeability of TOH in pure Mexphalte 40/50 or R 90/40 at room temperature, see Section 2.3.3.1. and /10/. By comparison it follows from the experiment described here that the presence of dissolving salt crystals and to some degree also undissolved crystals and sludge particles will result in an increased rate of transport of water through the bituminized material.

2.3.4.4. Electrical measurements on bitumen membranes.

While the transport of water in bitumen membranes at least partially is thought to take place in the vapour phase, the transport of ions in solution requires the presence of an interconnected network of solution-filled channels through the membrane. Measurement of the electrical conductivity over the membrane should give a good indication of the presence or development of such channels.

The experimental cells are similar to the ones used for diffusion experiments except that they are fitted with platinum wire electrodes along the circumference of the bottom of the cell chambers. Before the experiment the conductivity S_o is determined for the system filled with solution but without the membrane. After mounting the membrane both cell chambers are filled with the same solution. The conductivity over the membrane is then followed for a period of some months. The instrument employed is a Radiometer CDM 83 conductivity meter using 0.07-50 kHz alternating current.

The two initial experiments will be described:

A: An ~1.2 mm thick membrane of pure Mexphalte 40/50 mounted in a cell with 0.1 M NaCl on both side. The conductivity was followed for 75 days.

B: An ~1.25 mm thick membrane of Mexphalte 40/50 containing 10 weight% very fine-grained $NaNO_3$ mounted in a cell with 0.5 M $NaNO_3$ solution on both sides. The conductivity was followed for 160 days. The sodium nitrate solution is strong

enough to ensure that conductivity changes due to leaching of $NaNO_3$ from the membrane are not important, but it is far from saturated so leaching should not be suppressed significantly.

The results are shown in logarithmic form in Figs 13ab. The right-hand scales indicates the approximate fraction F of the membrane area which must be occupied by solution-filled channels (with turtuosity 1, i.e. going right through the membrane, and with the same solution concentration as in the cell chambers) to explain the measured conductivity S:

$$F = \frac{S \cdot x}{S_o \cdot L}$$

where x is the membrane thickness and L the distance between the electrodes.

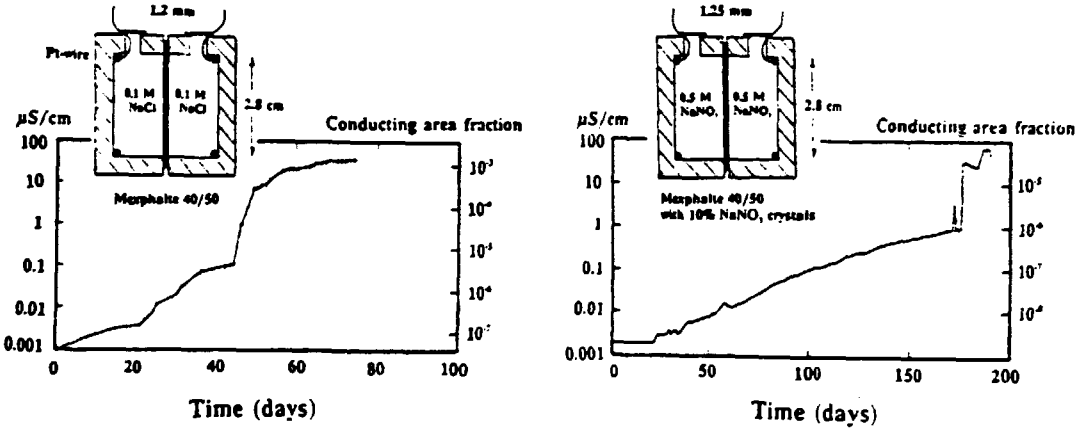

Fig. 13a,b. Electrical conductivities of two bitumen membranes.
a) Pure Mexphalte 40/50 in 0.1 M NaCl.
b) Mexphalte 40/50 + 10 % $NaNO_3$ crystals in 0.5 M $NaNO_3$ solution.

The membrane of pure Mexphalte 40/50 appears to generate defects in a stepwise manner with especially large ones occuring between 40 and 50 days. When stopped, about 0.1% of the membrane area must be regarded as perforated.

The membrane with 10 % $NaNO_3$ crystals showed for an unexpectedly long time a continuous but low increase in conductivity. At about 180 days a peak in conductivity was observed followed by a recovery period of some days and then some more permanent but still variable larger increases in the conductivity. Less than 0.01% of the membrane area was perforated when the experiment was terminated.

This behaviour is interpreted as an effect of repair mechanisms in the soft bitumen films surrounding the dissolving salt crystals. In addition to a fine network of small solution-filled defects, relatively coarse interconnecting pores may also be formed, but with at least some tendency to reclosure. Such a stochastic mecanism must be dependent on the flow properties of the bitumen and may therefore explain differences in swelling behaviour of waste products based on soft and hard bitumens. It may also contribute to the explanation of the high degree of swelling of real active Eurobitum compared with the simulate, since the real product is known to be considerably softer.

The electrical measurements were found to be a valuable supplement to ordinary diffusion-cell experiments. The possibility of combining the two types of measurements in the same cell should be persued and was tried in case of the thick (0.5-1 cm) membranes of pure Mexphalte 40/50 mentioned in Section 2.3.3.2. However, in this case only a very slight indication of conducting channels was obtained during the 11 months experiment, no doubt due to the larger thickness of the membranes.

2.3.5. Swelling pressure due to water uptake in bituminized materials.

Swelling pressure may develop in waste units containing bituminized materials with a content of soluble salt, if water can penetrate into the units while swelling is restricted by the containers.

2.3.5.1. Inactive Eurobitum.

The pressure development in a sample of inactive Eurobitum has been followed using equipment previously employed to investigate swelling pressure in bituminized ion-exchange resins /1,10/. The apparatus is shown as an insert in Fig. 14. The sample is cast on mercury which transmits the swelling pressure to the measurement system. The upper surface of the sample is covered by a dialysis membrane supported by filter paper and a porous disk of stainless steel. This permits water access (and some leaching of sodium nitrate by diffusion) but prevents swelling of the sample. The system was followed for about one year. The pressure development is shown in Fig. 14. Apparently the pressure is levelling of at about 1.7 bar, but this could be an artefact of a slight mercury leakage detected in the system.

The leached $NaNO_3$ sampled from the top reservoir corresponds to an equivalent leached thickness of ~1.2 mm. The corresponding leached thickness for a freely exposed sample would have been about twice as much.

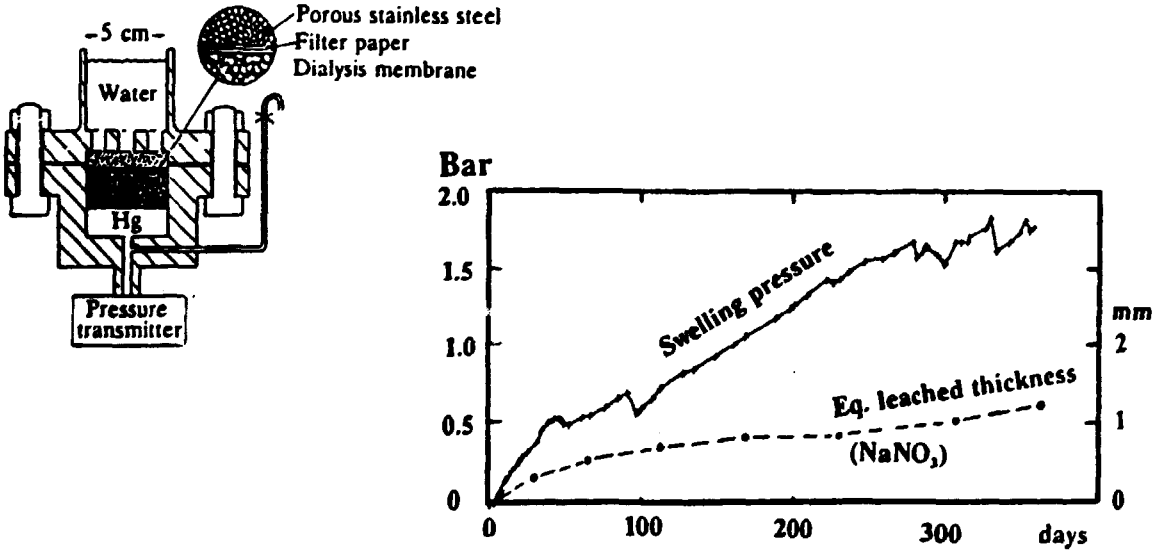

Fig. 14. Long-term pressure development due to water uptake in a confined sample of inactive Eurobitum.

2.3.5.2. Simplified system for measurement of swelling pressure.

A simple system for the measurement of swelling pressure due to water uptake in bituminized materials containing soluble salts has been developed and tested through a period of 14 months.

A spherical glass-flask is used as container, see Fig. 15a. The sample of bituminized waste product was cast on top of a small amount of mercury around a piece of capillary glass tubing. After complete cooling a layer of concrete was cast on top of the bituminized product and allowed to harden for some days. The system was then placed in a thermostated bath at 22±0.1°C and some water was added on top of the concrete.

The water is able to diffuse through the concrete and will then be taken up in the bituminized product. Since volume expansion upward is prevented by the concrete the swelling will squeeze some mercury up through the central capillary tube. The height of the mercury is a direct measure for the pressure increase in the system. The rate of water uptake is obtained from the volume of displaced mercury after correction for material leached from the bituminized material.

The system is much simpler and cheaper than the one described in Section 2.3.4.1. Previous problems with leakage of mercury is avoided since the bituminized product itself is used as a most efficient sealant. In addition there is no doubt about calibration of the pressure measurement. The use of concrete as water-permeable barrier is also more representative for a real situation in a waste container.

The system will for practical reasons be limited to the measurement of maximum about 4 bars overpressure. Much higher pressures can be generated by osmotic forces, but they are not likely to occur in practice in burial systems since a few bars overpressure often will be sufficient to break surrounding concrete barriers.

To obtain a rapid signal the system was tested using somewhat atypical materials: 60 % fine grained-$NaNO_3$ crystals + 40 % Mexphalte 40/50 as the waste product and a concrete with water/cement ratio 0.7 as barrier. The pressure development versus time is shown in Fig. 15c.

After an initial delay period of about 10-20 days the pressure increased steadily. Up to ~100 days the rate was about 0.6 cm Hg/day increasing to 1.35 cm Hg/day between 130 and 190 days. The pressure did reach a value slightly above 2 bars when a mercury leakage developed at a plastic tubing connecting the short piece of capillary tube cast into the system with the ~2 m tube on top of it. Another type of connection was made and has efficiently prevented renewed leakage. The pressure increased again at a slightly higher rate: 1.7 cm Hg/day declining to 0.95 cm Hg/day in the period between 265 and 413 days.

There may be various explanations for the variations in the rate of water uptake at the beginning of the experiment. Some contraction of the bituminized product due to out-diffusion of gases may well take place during the initial few months of the experiment. This phenomenon was noticed in previous experiments with bituminized waste /18/ and will partly compensate for a simultaneous swelling. The internal diameters of the sections of cappilary tubes was measured after the experiment and did vary considerably.

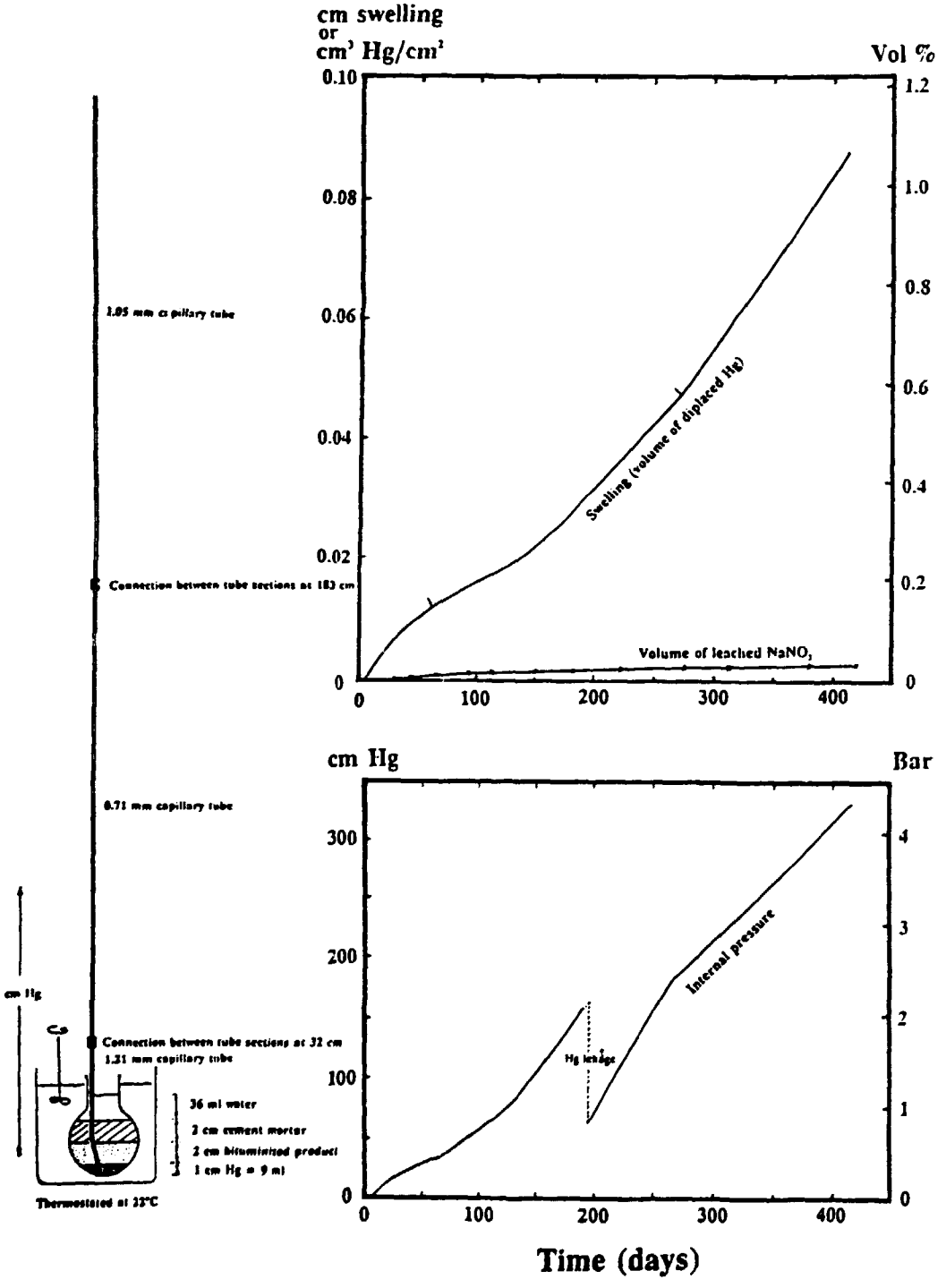

Fig. 15a,b,c. Simple system to follow over-pressures generated by water uptake in bituminized materials containing soluble salt. The measured overpressure as function of time is given for a sample of 60% $NaNO_3$ crystals in 40 % Mexphalte 40/50 when confined under a layer of porous cement mortar (w/c=0.7) covered by water. The swelling and the volume of $NaNO_3$ crystals leached from the bituminized material normalized against the area (29.2 cm^2) of contact between sample and concrete barrier are also shown.

The volume of displaced mercury given in Fig. 15b is calculated on this basis. The change in swelling rate around 130 days is probably due to some change in mechanism for the water uptake. The increase in slope of the nearly straight-line curve above 266 days (and 183 cm Hg) may be explained as an effect of the lower rate of pressure increase in the upper tube with larger cross-section. The swelling at the end of the 413 days experiment was ~0.9 mm or ~1.1 vol% based on the about 50 ml bituminized product. In previous experiments /18/ with unconfined samples of the 60% $NaNO_3$ - 40% Mexphalte 40/50 product the swelling was quite moderate: ~0.1 mm in 150 days, so the tendency is worse for the confined sample in the present experiment.

Clogging by bitumen squeezed into the pores of the concrete by the pressure would lead to decreasing swelling rate and does apparently not take place. When taken apart after the experiment the 2-3 mm layer of bitumen product nearest the concrete surface was found to be structurally weak and contain many ~0.1 mm droplets in a spongy mass of bitumen. The layer could be scraped away leaving a light yellow but otherwise clean surface on the moist concrete.

The leaching of $NaNO_3$ from the bituminized material was followed by Na-analyses of the water on top of the concrete barrier. The volume of $NaNO_3$ crystals corresponding to the sodium leached from the bituminized material was calculated from the water analyses after correction for a small amount of Na leached from the concrete layer. In total after 413 days the volume is about 0.013 ml i.e. about 2 % of the 2.54 ml Hg displaced from the system. Leaching of the nitrates is therefore rather insignificant under these circumstances. The equivalent thickness of the leached layer is only ~0.003 cm after the 413 days. This is less, but not too different, from the unconfined sample mentioned above where the value reached ~0.01 cm in 150 days.

That the water uptake and the swelling are much greater than the amount of leached sodium nitrate is in accordance with the general tendency to generation of osmotic forces within confined samples of bituminized materials containing soluble salts when exposed to water. The material investigated here has an atypically high content of soluble salt (60 % $NaNO_3$), but this is thought mainly to influence the rate of water uptake, not the pressure levels as such.

The experimental system is simple and cheap and should therefore be well suited for systematic studies of the influence of various parameters on the generation of swelling pressure in confined bituminized materials.

2.4. Viscosity change in ageing bituminized materials.

Ageing of bitumen and bituminized waste may result in changes in material properties even if radiation is excluded as a contributing factor. Changes in rheological properties are probably the most sensitive indication for aging reactions. One possible mechanism could be increased ordering of the large hydrocarbon molecules present in the maltene phase of the bitumen resulting in increased stiffness of the material. Slow oxidation or other chemical interactions may also take place.

In connection with a Nordic study /20/ a series of samples consisting of pure Mexphalte 40/50, Mexphalte + ion-exchange resins or Mexphalte + sodium nitrate crystals (75-150 μm) were cast as 0.5 cm thick layers between circular brass plates. Samples cast from bitumen filtered through a steel net from these products after typically 1.5 hours contact time at 200°C were also prepared. The flow properties of the samples have been measured using a simple plate viscometer at ~1 day, 1 month, 3 months and 3.5 years after the casting. In the periods between measurements the samples were stored at 20 ± 1 °C with the plates locked in a fixed position. For further details, see /1/.

The materials show considerable visco-elastic behaviour and are certainly not ideal Newtonian liquids. However, for sufficient loads reproducible 'viscosities' could be obtained from curves over the displacement versus time. The values are shown plotted against the square root of storage time in Figs. 16a,b. $\sqrt{t}$ is used as a convenient way to compress the time scale, but it does also result in nearly linear curves, maybe reflecting that the mechanisms resulting in increased stiffness are diffusion related.

For pure Mexphalte and all the products containing solid simulated waste materials the viscosities are increasing with time. A factor 4 in 3.5 years appears to be typical. The effect is pronounced also for the 40% $NaNO_3$/60% Mexphalte 40/50 product kept at 200°C for 5 hours. However, it is the only material where the sample cast from bitumen

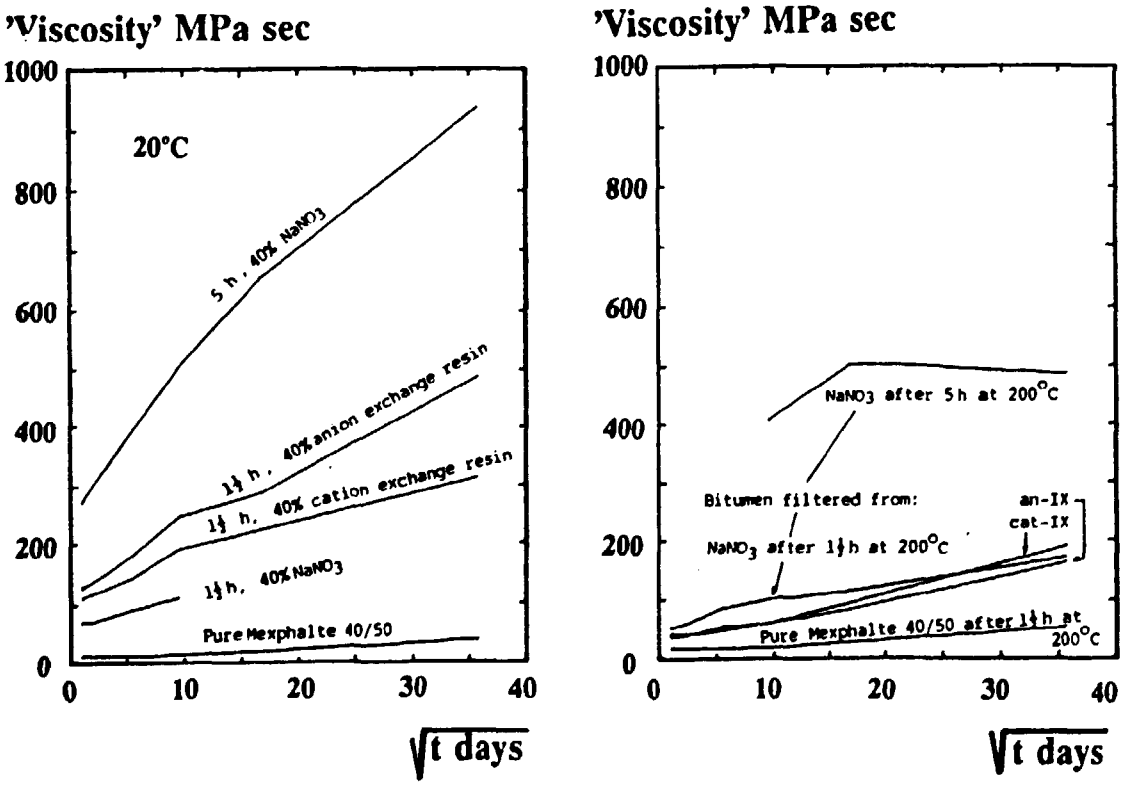

Fig. 16a,b. Change in viscosity of Mexphalte 40/50 and some simulated bituminized waste materials during long-term storage at 20°C. Figure b shows the viscosity development of bitumen which has been in contact with the waste, but where the waste particles as such were removed by filtering through a steel net before the samples were cast.

and filtered rapidly from the molten product did not show the typical increase in viscosity at the last measurement. Otherwise it is a general trend that bitumen filtered from the products have a higher viscosity than pure Mexphalte which has not been in contact with the foreign materials.

As a supplement the plate viscometer was also employed to measure the 'viscosity' of freshly recast but 'old' inactive Eurobitum, the material employed in the swelling and diffusion studies described above. The value was found to be about 7400 MPa·sec, i.e. 1 to 3 orders of magnitude higher than the values in Fig 16a. The high vicosity may partly be due to the use of bitumen with low penetration in the Eurobitum process and to the contents of sludge and sodium nitrate particles, but the repeated remeltings which has been necessary to obtain the sample and to cast the disk used for the measurements may also have increased the viscosity due to oxidation etc. This illustrates one of the difficulties in preparing representative samples.

2.5. Equilibrium extraction of precipitation sludges by cement and/or bitumen-conditioned water.

The leaching of Cs, Sr and other radionuclides from bituminized waste is greatly reduced if the isotopes are fixed within the bitumen matrix in form of particles of a solid, difficult soluble compound. This is done for example with reprocessing sludge by co-precipitating Cs with nickel ferrocyanide and Sr with $BaSO_4$ before the bituminization. The precipitation sludges may also contain CoS and titanium hydroxides /9/.

The long-term safety value of this chemical treatment must, however, to some degree depend on the stability of the precipitated compounds within the bitumen matrix before and after water - and maybe dissolved components from the outside - have penetrated into the bituminized material.

In continuation of previous experiments /2/ the extraction of ^{134}Cs, ^{85}Sr and ^{60}Co from unprotected precipitation sludge particles has been studied. This is a more sensitive method to obtain trends in behaviour than ordinary leaching experiments with monolithic blocks of bituminized sludge, but the results are of course not directly applicable on the conditioned material.

Four portions of sludge, each containing 0.33 g $Ni_2Fe(CN)_6$ + 0.233 g $BaSO_4$ + 0.092 g CoS, were prepared by precipitation from one litre solutions. The decontamination factors were about 400 for ^{134}Cs and 10 for ^{85}Sr and ^{60}Co. The sludges were transferred to polyethylene centrifuge-bottels resulting in the following experimental systems:

No. 15: 0.55 g sludge
No. 16: 0.55 g sludge + 10 g Mexphalte 40/50 as a ca. 1 mm thick coating on the inside of the bottle.
No. 18: 0.55 g sludge + 10 g hardened granulated cement paste (SRPC).
No. 19: 0.55 g sludge + 10 g Mexphalte coating + 10 g granulated cement paste.

In addition two control systems without sludge were also included in the experiment:

No. 17: 10 g Mexphalte coating or
No. 20: 10 g Mexphalte coating + 10 g granulated cement paste

All the systems contained 150 ml of a nutrient solution (0.01 M K_2SO_4 + 0.05 M $NaNO_3$ + 0.002 M Na_2HPO_4) and were inocculated with a mixed population of bitumen-degrading soil micro-organisms. After one week equilibration at room temperature (while the solids were kept in suspension by slow rotation of the bottles) the systems were centrifuged and 100 ml solution was sampled and replaced by fresh nutrient solution. The samples were analysed for ^{134}Cs, ^{85}Sr, ^{60}Co, pH, and COD (chemical oxygen demand). The activity analyses were made before and after filtering through 0.22 μm Millipore filters.

The results for Cs and Sr extraction are presented in Figs. 17a and c in form of cumulative leached fractions based on the analyses of unfiltered as well as filtered (designated f) solutions. The results are plotted against the cumulative amounts of extraction water per g $Ni_2Fe(CN)_6$ and $BaSO_4$, respectively.

Figs. 17b and d show the corresponding concentrations relative to the concentration remaining in solution after the original precipitation, and as Mol/L (right-hand scale) based on the carrier contents. The concentrations are plotted against the cumulative extraction time.

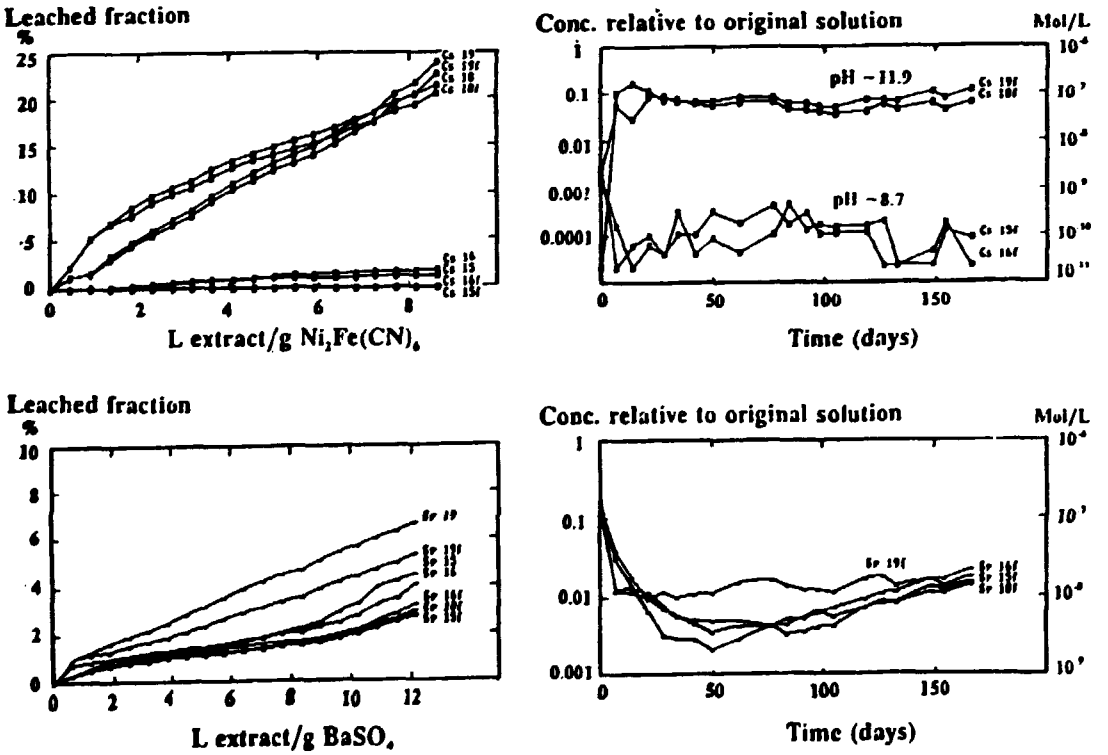

Fig. 17a,b,c,d. Leached fractions of ^{134}Cs and ^{85}Sr from $Ni_2Fe(CN)_6$ and $BaSO_4$ in precipitation sludge in water (15), in contact with bitumen (16), in contact with concrete (18), and in contact with bitumen + concrete (19).
The suffix f to a system number indicates that the samples were filtered before analysis.

The solution pH in the systems with concrete (Nos. 18,19,20) decreased from ~12.3 to ~11.8 during the experiment, while the systems with sludge (15) or sludge + bitumen (16) had pH between 8.7 and 9. The system with bitumen alone (17) had pH ~7 and the nutrient solution used for the extraction pH 8.35.

The COD determinations were somewhat variable, but the tendency is a decrease from inital high values in the systems with sludge to values around 10-20 mg O/L in the high pH systems, and 2-10 mg O/L in the systems with sludge or sludge+bitumen. In the system with only bitumen the COD increases from 6 to 10-20 mgO/L indicating growth of micro-organisms.

It is probable that the inocculation with bitumen-degrading micro-organisms did not succeed for most of the systems maybe due to high pH or other toxic effects. Test cultivation on agar after the 12th sampling indicated some, but not very vigorous growth in systems Nos. 18, 19 and 20.

Effects of micro-organisms in connection with the extraction and/or degradation of the sludge particles cannot be said to be clearly demonstrated in this experiment, but some interesting conclusions may still be drawn:

- Cs is leached much more rapidly from nickel ferrocyanide in a high pH environment than in more neutral solutions. The Cs is probably in true solution at the high pH since in this case it is not much influenced by filtration. Comparison of the slope of the curves for system Nos. 18 and 19 indicates that there may be a synergistic effect of the simultaneous presence of bitumen and concrete.

- Sr is leached in more or less the same manner in three of the systems, but the fourth (No. 19) shows also for this component a tendency to increased release in the case of simultaneous presence of bitumen and concrete.

- Results for Co are not presented since they are rather uncertain due to low countings. However, it can be seen that Co is leached at a very low rate in all systems, although the high pH systems show an initial large release of about 5% of the activity. During the experiment the black colour of the cobalt sulphide disappeared relatively early. This must be due to oxidation but it has not led to any significant release of the cobalt. In the high pH systems Co may be fixed on the cement paste, but another mechanism - which may function i all four systems - is substitution for Ni in the nickel ferrocyanide.

The general conclusion is that it is of considerable interest to study the leaching behaviour of bituminized products based on precipitation sludges not only in ordinary water, but - if the intention is to place the material in disposal facilities with concrete constructions or together with cemented waste - also in high pH water. Synergistic effects of concrete, bitumen and/or micro-organisms may or may not be important in this connection. In monolithic samples of bituminized sludge the effects will be slower in development than in these experiments with unprotected sludge, but the tendencies should probably be the same.

3. BARRIER MATERIALS

Materials used when making waste containers, as back-fill or for construction of engineered barriers in disposal facilities may partly be the same as those used in waste conditioning. The material properties relevant for a matrix material and for a barrier material may be quite the same, but the major difference is probably that only thin films of matrix material are surrounding individual waste particles in a conditioned waste product while much thicker layers are used in barrier construction. Diffusion and other types of transport mechanisms are relevant in both cases, and although different aspects of the processes may be important it follows that the experimental methods used to characterize matrix and barrier materials can be partly the same.

Concrete used in barriers is the main topic treated in the following. However, some aspects e.g. connected with the pore structure are obviously also relevant for cement paste used as conditioning material.

Bitumen has also been proposed as barrier material to prevent water contact. As described in Section 2.3.3.2. it has been shown that migration of water vapour through even relatively thick bitumen layers (~1 cm) is possible. Slight and variable electrical conductance through solution-filled defects was also detected at the end of this 11-months experiment. This agrees with earlier experience at Risø with a full-scale underground demonstration facility /21/ where the electrical resistance over bitumen layers of similar thicknesses between individual (empty) waste units was lost during 2-3 years of burial in contact with groundwater.

3.1. Pore structure in five types of concrete.

The pore structure in hardened concrete or cement paste is primarily a function of the water/cement ratio. Water not used in the cement hydration (w/c > ~0.2) remains in the product as free pore water forming an increasingly coarse and interconnecting network with increasing w/c ratio. Values about 0.4 is common in ordinary construction concrete, but easily castable mixtures can also be obtained with lower w/c ratios by use of small amount of organic superplasticizers. Products much stronger and with much finer pore structure can be made by the combined use of silica fume and superplasticizers. The work described in the following is a continuation of previous studies /21/.

3.1.1. Leaching compared with diffusion through slabs.

A set of experiments has been conducted where one-dimensional leaching of ^{134}Cs and tritiated water from thick samples cast from 5 different types of concrete were compared with diffusion of the same species through ~1 cm thick disks of the same materials. Some experiments with uptake of activity from water into thick samples of the inactive materials were also made.

The objective was to study the transport behaviour of species assumed to have weak or no chemical interaction with the concrete so that the transport mainly is determined by the pore structure. The leaching experiments have no direct relevance for cement-conditioned waste since major waste components (salts, sluges, etc) were absent.

3.1.1.1. Experimental procedure and results.

The composition of the 5 materials are specified in the upper part of Table 6. The experimental set-up is shown in Fig. 18.

The leaching and uptake systems were sampled every week, while increasing time intervals were used in the case of the diffusion cells. The water samples were analysed for ^{137}Cs by γ-spectrometry, for TOH by liquid scincillation counting (after purification by destillation), and in the case of the leaching experiments also for Ca, Na and K by flame photometry or AAS. The leaching experiments were conducted using deionized as well as synthetic cement-equilibrated water as replacement after sampling. No significant differences in TOH and Cs leaching could be seen due to this difference in leach medium.

At the end of the experiment the concentration profiles in the concrete samples were obtained using a HCl etching technique where the thickness of the etched layer is estimated from Ca analyses of the etch-solution.

A complete set of the experimental results are given in /1/. Only a few typical examples are described here:

Figure 19 shows the leach curves for the sample of material a - the one with the highest w/c ratio - when leached at 20°C in deionized water without CO_2 access. The relative positions of the curves are typical, with the Na^+-leach curve as the upper one followed by the K^+, the Cs^+ and finally the Ca^{2+} curve. With the relatively large water-exchange rate employed in these experiments also the Ca-leaching appears to be diffusion- and not solubility-controlled.

The TOH-leaching is decreasing less rapidly with increasing fineness of the pore structure than the leaching of K^+ and Cs^+. This can be seen by the values given in Table 6 for the effective diffusion coefficient D_e calculated from the slope of the leach curves according to:

$$L = 2\cdot\sqrt{(D_e\cdot t/\pi)} + b \qquad \text{cm}$$

Etching of the samples at the end of the experiment gave Cs-concentration profiles decreasing more or less liniarily from low values at the surface to the original concentration in the material in the deeper layers. The profiles correspond reasonably well to the amounts of leached Cs. Only sample e - containing silica fume - is an exception, here a slight enrichment of Cs in the layers slightly below the surface could be seen. Meaningful profiles for TOH could not be obtained, probably because some tritium is retained as -OT groups in the silicic acid remaining after the etching.

Fig. 20 shows the rate of uptake of TOH from a solution containing tritiated water into thick inactive samples of the 5 concrete materials. The values are obtained as differences between large numbers, which explain the somewhat erratic behaviour. The relative positions of the TOH-uptake curves reflect the increasing fineness of the pore structure when going from material a to e. Effective diffusion coefficients 'D_e', related to, but not identical with the D_e values obtained from the leaching experiments, can be calculated from a formula similar to the one shown above. Values for 'D_e' are given in Table 6.

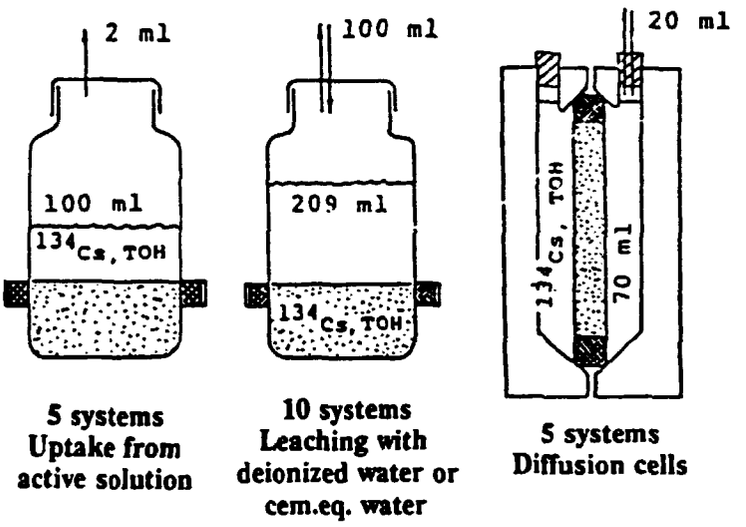

Fig. 18. Systems used in comparative experiments with the five types of cement mortar.

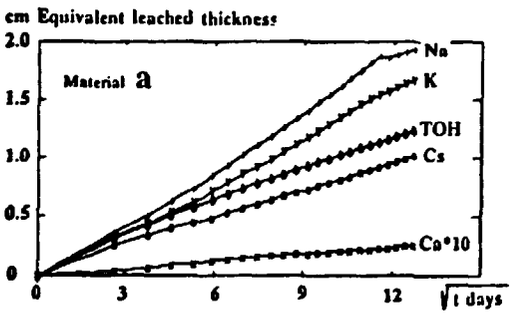

Fig. 19.
Leaching of ^{134}Cs, TOH, Ca, Na, and K from cement mortar. Product a.

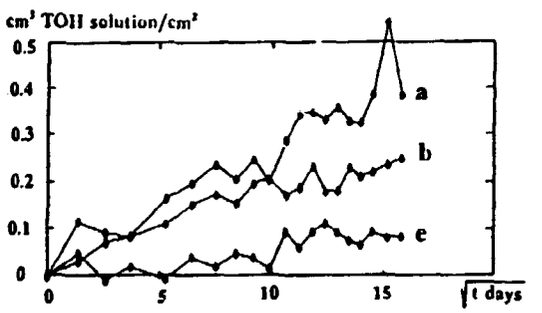

Fig. 20.
Uptake of TOH in three types of cement mortar Products a, b and e.

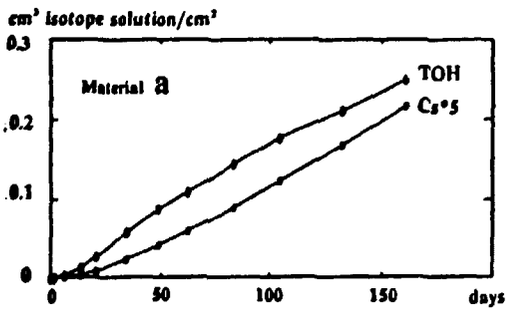

Fig. 21.
Diffusion of ^{134}Cs and TOH through slab of cement mortar. Product a.

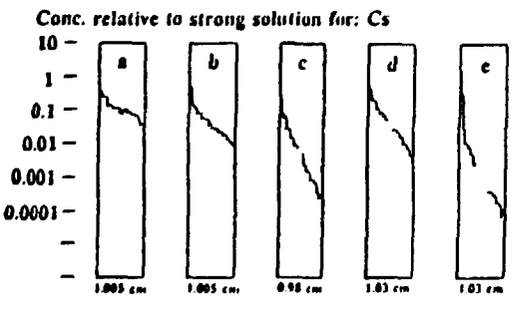

Fig. 22.
^{134}Cs profiles obtained by etching of the five slabs after the experiment.

The corresponding ^{134}Cs-curves are more difficult to interprete. However, it appears that some chemical absorption of Cs takes place in material e. The result is Cs-enrichment in the surface layer of the sample as confirmed by the HCl etching. The Cs-profiles in the other samples had the expected shape. Meaningful TOH-profiles could not be obtained.

Figure 21 shows a comparison between TOH and $^{134}Cs^+$ diffusion through an about 1 cm thick slab of material **a**. The tendency that TOH is diffusing about a factor 10 faster than Cs^+ through concrete is confirmed also for the other 4 materials. The Cs-transport through the other slabs is, however, much more irregular than the TOH transport. Unexpected increases or decreases appears to be possible, see the complete set of curves given in /2,8/. The phenomenon may be associated with changes in a few micro-defects in especially the more dense concrete samples. Sample **a** is - due to the higher w/c ratio - more porous in general and therefore less influenced by such defects.

The effective diffusion coefficient for transport through an ideal membrane of thickness x cm can be obtained from:

$$D_e = x^2/(6 \cdot \lambda) \qquad cm^2/sec$$

Determination of the time-lag λ requires that the break-through curve over a reasonable period can be approximated by a straight line. For porous materials, like the concrete samples here, the initial break-through may be determined by transport of a small amount of dissolved material at a high rate trough a few micro-defects. This tends to give high D_e values, independent of the material and approaching the diffusion coefficient in water. Later a more massive break-through may occur due to transport through the finer pore system characteristic for the material. Occasionally it is possible to calculate a second D_e value valid for longer time, but in most cases only the flux through the slab can be obtained from the measurements.

The flux can be represented by the diffusive permeability P as determined from:

$$P = \alpha \cdot c \cdot x/\Delta c \qquad cm^2/sec$$

where α cm/sec is the slope of the break-through curve, c is the concentration in the strong solution and $\Delta c/x$ the concentration gradient over the slab.

Nummerical values of D_e and P for the 5 materials, as obtained from the inital and from the later part of the break-through curves are also given in Table 6.

Etch profiles for ^{134}Cs obtained by HCl etching simultaneously from both sides of the slab are shown for all 5 samples in Fig. 22. Note that the Cs-concentration in the concrete is given in logarithmic scale relative to the concentration of Cs remaining in the strong solution at the end of the experiment. The concentration through the slabs is therefore decreasing faster than linearily with distance and the profiles can therefore not be explained only by Fick-law diffusion in a homogeneous material (or diffusion combined with simple equilibrium ion-exchange retardation).

Table 6. Composition of the five types of concrete together with effective diffusion coefficients and permeabilities obtained from the leaching, uptake and diffusion-cell experiments. The ratios S and R are defined in Section 3.1.1.2.

The unit for D_e and P is 10^{-12} cm^2/sec

Material		a	b	c	d	e
Cement SRPC	g	100	100	100	100	100
Sand 0.3-1 mm	g	200	140	140	100	100
Silica fume	g				20	20
Superplasticizer	g				1.7	1.7
Water	g	45	38	28	28	28
Density	g/cm^3	2.33	2.32	2.31	2.47	2.45
w/c ratio		0.45	0.38	0.28	0.28	0.28
Cs-leaching						
De_{leach}		51000	20000	3000	3100	90
Cs-dif.cell						
$De_{short\ time}$		132000	-	220000	-	250000
$De_{long\ time}$		76000	-	136000	-	-
$P_{short\ time}$		2800	910	20	2.3	12
$P_{long\ time}$		3700	730	24	50	0.3
$S = P_{long}/De_{long}$	%	4.9	-	0.018	-	-
$R = De_{slab}/De_{leach}$		1.5	-	45	-	-
TOH-leaching						
De_{leach}		74000	38000	8700	8400	2400
TOH-dif.cell						
$De_{short\ time}$		240000	300000	112000	114000	260000
$De_{long\ time}$		-	500000	49000	85000	94000
$P_{short\ time}$		26000	8800	1800	4200	60
$P_{long\ time}$		18000	8500	4400	5300	160
$S = P_{long}/De_{long}$	%	-	1.7	0.9	0.6	0.17
$R = De_{slab}/De_{leach}$		3.2	13.2	5.6	10.1	39
TOH-uptake						
'De'		5600	1100	1600	490	720
Na-leaching						
De_{leach}		260000	122000	15000	75000	15000
K-leaching						
De_{leach}		190000	91000	10000	20000	1700
Ca-leaching						
De_{leach}		3	23	4	11	2

- the shape of the curve prevents estimation of the parameter value.

Before initiating the diffusion experiments the hydraulic conductivity of the materials were determined by appiying a pressure difference (~69 mmHg) over the slabs when mounted in the cell and measuring the water flow as function of time. This was done partly to eliminate any slabs with major defects. The obtained hydraulic conductivities are shown in Fig. 23. The $2 \cdot 10^{-9}$ cm/sec found for material **a** and **b** is reasonably constant and typical for normal construction concrete (sample **b** may have had a slight defect). The behaviour of materials **c**, **d** and **e** with low w/c ratio is different since they gave low conductivities rapidly declining with time. A possible explanation could be that the flow in such materials is preferably through relatively few micro-defects which, however, have a tendency to closure when water is forced through the sample.

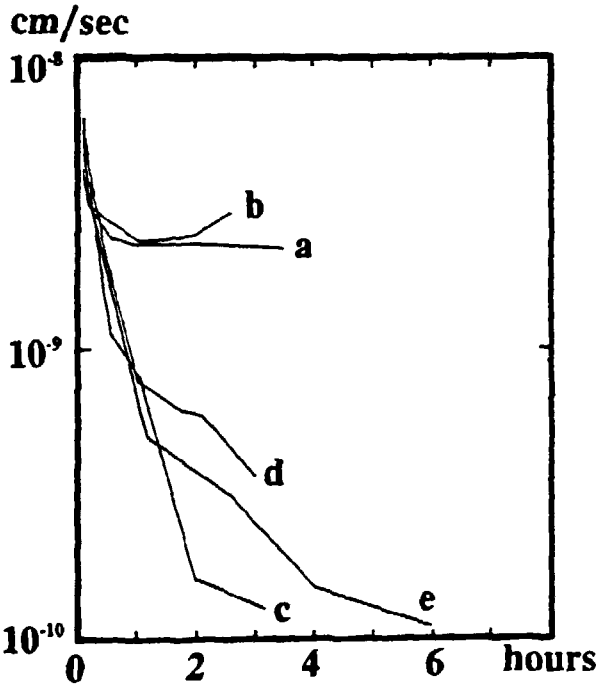

Fig. 23. Hydraulic conductivities for slabs of the five different types of cement mortar.

3.1.1.2. Theoretical interpretation.

The results may be seen on the background of a relatively simple model of the pore structure in porous materials such as concrete. The theory was developed in connection with previous work for the CEC, see appendix 1 in /21/.

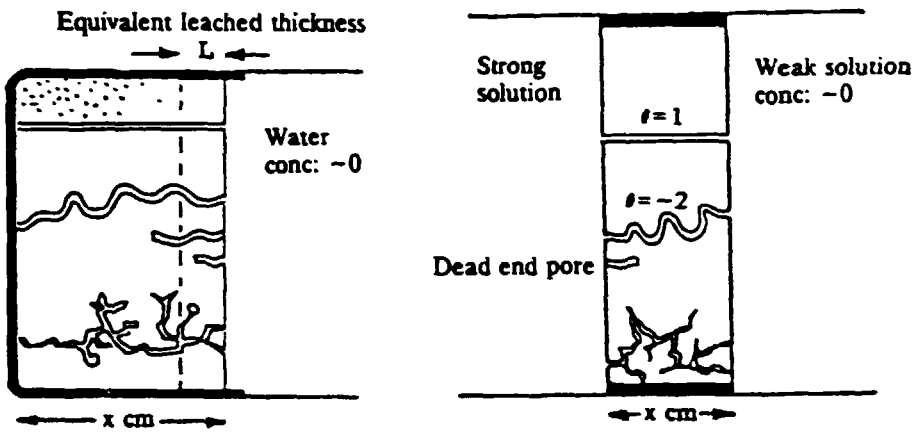

One-dimensional leaching **Diffusion through slab**

Fig. 24. Idealized presentation of a slab in a diffusion-cell experiment and a sample leached in one-dimensional geometry.
Channels with different tortuosities and penetration depths are indicated together with more 'realistic' systems of interconnected pores.

Refering to Fig. 24 it is assumed that the pore structure in a x cm thick sample can be approximated by a system of independent channels extending right through the slab and consisting of n groups of channels of equal length x_n and total cross section a_n. Within each group, the total cross section can be divided into i_n channels with uniform length but different cross section a_{ni}, which however, are assumed to be uniform along each channel, i.e.

$$a_n = \sum_i a_{ni}$$

The transport through the slab is then supposed to take place by diffusion through this water-filled channel system. The transmitting fraction of the total sample area A is:

$$S = \frac{\Sigma a_n}{A}$$

For such a system the relationship between the diffusive permeability P and the effective diffusion coefficent D_e is:

$$P = S \cdot D_e$$

The flux through the slab is given by:

$$F = \alpha \cdot c = P \cdot \frac{\Delta c}{x}$$

The transport through the total area of the slab is $A \cdot F$, but this is also given as the sum of transport through all the individual channels, i.e:

$$A \cdot F = \sum_n a_n \cdot F_n = \sum_n (\sum_i a_{ni} \cdot D \cdot k_i \cdot \frac{\Delta c}{x_n})$$

where D is the diffusion coefficient for the investigated species in water and k_i is a factor taking chemical retardation and pore size related retention for the i^{th} channel of the n^{th} group into account.

Introducing the definition for tortuosity:

$$\theta_n = \frac{x_n}{x}$$

and disregarding the possible dependence of retardation on variation in pore sizes the following simple relationships are obtained by combination of the formulas above:

$$P = D \cdot k \cdot \Sigma \frac{a_n}{A \cdot \theta_n}$$

$$D_{e\,(slab)} = D \cdot k \cdot \frac{\Sigma(a_n/\theta_n)}{\Sigma a_n}$$

or if all channels had the same tortuosity:

$$D_{e\,(slab)} = \frac{D \cdot k}{\theta}$$

Since typical values for D is $\sim 10^{-5}$ cm^2/sec the tortuosity θ must be in the order of 100 if the experimental D_e values in Table 6 shall be explained by tortuosity alone.

In the case of diffusion-controlled leaching from an 'infinitely' thick sample of a porous material the equivalent leached thickness L at time t is given by:

$$L = 2\sqrt{(D_{e\,(leach)} \cdot t/\pi)}$$

and the total amount of leached material is:

$$Q = A \cdot L \cdot c^*$$

where c^* is the bulk concentration of the leached species in the sample material.

For a channel-like structure, similar to the one described for the slab, the porosity is given by:

$$\epsilon = \frac{\Sigma(\theta_n \cdot a_n)}{A}$$

and for a non-adsorbed species the concentration in the pore water is:

$$c = \frac{c^*}{\epsilon}$$

It follows that

$$Q = c \cdot 2\sqrt{(D_{e\,(leach)} \cdot t/\pi)} \cdot \Sigma(\theta_n \cdot a_n)$$

The total amount of leached material is also given by the sum of material diffused out of the individual channels:

$$Q = \Sigma q_n = 2\Sigma(a_n \cdot c \cdot \sqrt{(D \cdot k \cdot t/\pi)})$$

Therefore by combination:

$$D_{e\,(leach)} = D \cdot k \cdot (\frac{\Sigma a_n}{\Sigma(\theta_n \cdot a_n)})^2 = D \cdot k \cdot (\frac{S}{\epsilon})^2$$

For the more general case with chemical ion-exchange retardation the relationship is:

$$D_{e\,(leach)} = D \cdot k' \cdot (\frac{S}{\epsilon + (1-\epsilon) \cdot \rho \cdot K_D})^2$$

where k' retains the pore size-related part of the retardation while chemical retardation is described by the usual distribution coefficient K_D. ρ is the density of the minerals.

Combining with the corresponding formula for diffusion through a slab one obtains a measure for the ratio:

$$R = \frac{D_{e\,(slab)}}{D_{e\,(leach)}} = \frac{\Sigma(a_n/\theta_n) \cdot (\Sigma(\theta_n \cdot a_n))^2}{(\Sigma a_n)^3} = (\frac{\epsilon}{S})^2 \cdot \Sigma \frac{a_n}{\theta_n \cdot \Sigma a_n}$$

or $R = \theta$ when the tortuosity is the same for all the pores.

It is therefore not surprising that D_e values obtained from diffusion experiments tend to be higher than values from leaching experiments. This is especially the case for materials with finely divided pore structures and therefore a high degree of tortuosity, e.g. the silica fume-containing material e, where the experimentally determined R value for TOH was found to be 39, see Table 6. High R values were also found for Cs in material e and in previous experiments /21/ with type e materials.

Values of $S = \Sigma a_n/A$ calculated for the slabs where both P and D_e values were available are also given in Table 6. They vary in a reasonably consistent way from ~5 % to ~0.2 % going from sample a to e. This reflects that an increasingly smaller fraction of the cross-sectional area is available for transport when the w/c ratio is decreased and/or silica fume is added. The total water-filled porosity will be decreasing somewhat with decreasing w/c ratio, but the major changes in the S values are probably due to increased numbers of dead-end pores in low w/c and/or silica fume-containing concrete.

The concept of dead-end pores can also explain the deviation from straight-line concentration profiles in the slabs, see Fig. 22. The concentrations in the pores connected to the surface in contact with the strong solution will of course be increased to high values if they do not permit further transport into the interior of the sample. For further discussion see /21/.

The general conclusion is that tortuosity, the presence of dead-end pores and chemical retardation and/or retardation due to geometrical restrictions in very narrow pores in combination are able to explain most of the phenomena observed in these comparative experiments. However, it would be of interest to evaluate whether S and θ and therefore also P are functions of the sample thickness x. This is especially the case since the diffusive permeability P is the parameter of primary importance in connection with calculation of transport through concrete barriers.

3.1.2. Diffusion of water vapour through concrete barriers.

The rate of transport of water vapour through porous concrete is of importance for the hygroscopic water uptake in waste materials stored in concrete containers or in other ways sealed in or contained by barriers made from concrete.

A comparative study of the above mentioned 5 types of concrete has been made. The compositions are given in Table 7 together with results from the water-vapour permeability measurements.

Samples of 1, 2.2 and 5 cm thicknesses were employed. They were precast and hardened for one month in a high-humidity atmosphere before they were mounted as lids in cylindrical polyethylene containers. A beaker with concentrated sulphuric acid ensured a low relative humidity inside the systems. They were stored at 20°C in a 95% relative humidity atmosphere and the weight increases were followed for a period of 3-5 months.

The weight of the systems was found to increase nearly linearily with time. The weight inrease is a measure for the amount of water transported through the slab - except for possible changes in the weight of the slab itself - and values for the water-vapour-permeability coefficient P_v can therefore be derived from the slope of the curve α g/cm²/day using the formula:

$$P_v = \alpha \cdot \frac{x}{p_1 - p_2} = \frac{\alpha \cdot x}{24 \cdot 3600 \cdot (\Delta RH/100) \cdot 0.0123 \cdot 0.0012}$$

where x is the thickness of the slab, p_1 and p_2 are the partial vapour pressures on the two sides of the slab and ΔRH % the corresponding difference in relative humidity. 100% RH is equal to 1.25 vol% H_2O in the air at 20°C and the density of (dry) air at 20°C and 760 mmHg is 0.0012 g/cm³.

The P_v values for all three slab thicknesses are given in Table 7. No systematic dependence on the thickness can be seen and the mean values can therefore be regarded as characteristic for the pore structure in the products.

Table 7. Composition of five types of concrete used in the comparative experiment with diffusion of water vapour through samples of 3 different thicknesses and values for the water vapour permeability coefficients.

Material type			a	b	c	d	e
Cement: SRPC		g	100	100	100	100	100
Sand: 0.3-1 mm		g	200	140	-	140	140
Silica fume		g	-	-	-	-	20
Superplasticizer		g	-	-	-	1.7	1.7
Water		g	45	38	28	28	28
Slab thickness:							
1 cm	Permeability		0.0037	0.0029	0.0020	0.0022	0.0004
2.2 cm	coefficients:		0.0048	0.0033	0.0014	0.0022	0.0004
5 cm	P_v	cm^2/sec	0.0033	0.0022	0.0015	0.0022	0.0008
	Mean values:		0.0039	0.0028	0.0016	0.0022	0.0005

The water-vapour permeability follows the expected trend with water/cement ratio, i.e. highest for **a** followed by **b** and then **c** which is similar to **d** while **e** has a much lower permeability due to the silica-fume additive.

A previous experiment /3/ using a 2 cm thick slab of concrete with composition 425 g sand + 100 g SRPC + 70 g water has given a P_v value of 0.0074 cm^2/sec, well in line with the results in the table as illustrated by Fig. 25. Results from this earlier experiment

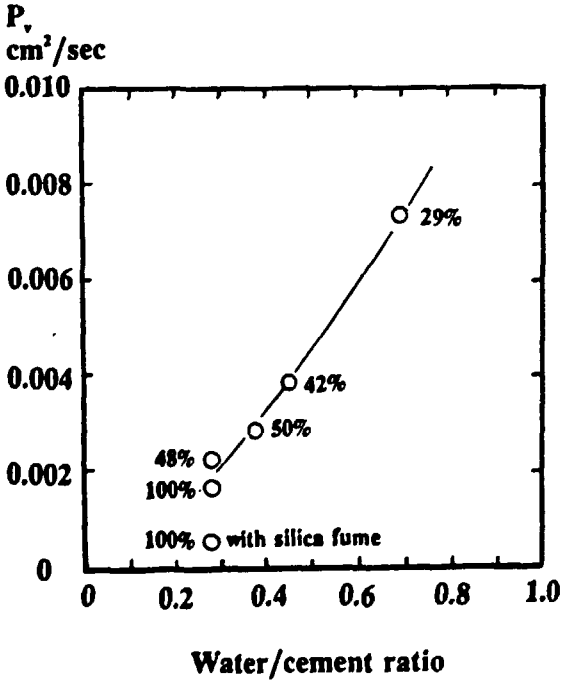

Fig. 25. Permeabilities for water vapour as function of water/cement ratio in the cement mortar. The percentages indicate the weight contents of cement gel, the rest is sand particles.

are shown in Fig. 26ab where transport of water vapour through the porous concrete barrier was demonstrated to result in solution accumulation on top of an hygroscopic waste type, system H2.

None of the concrete types investigated are impermeable to water vapour. Concrete may therefore only retard, but cannot prevent water uptake in hygroscopic materials contained inside barriers made from concrete.

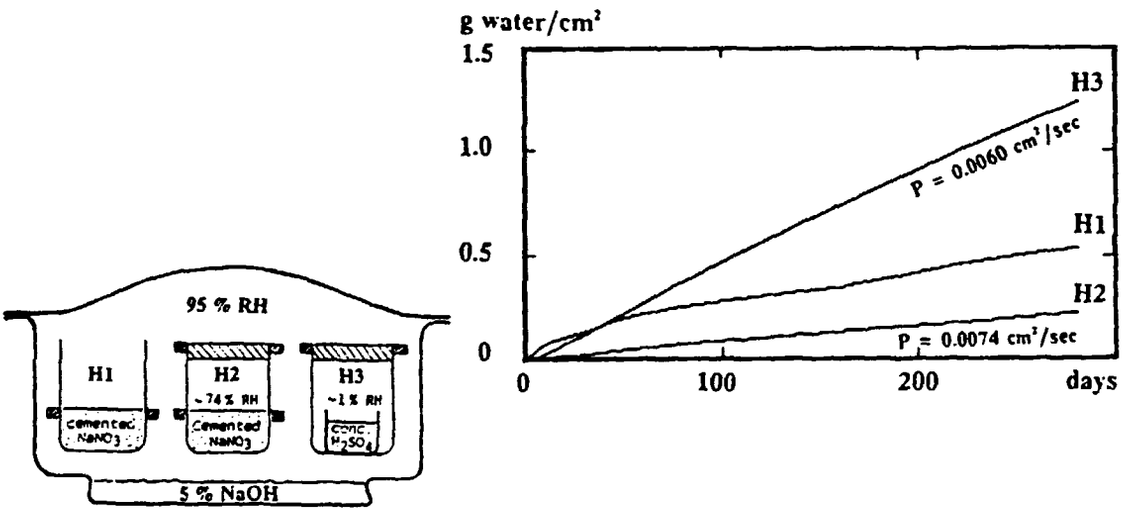

Fig. 26a,b. Experimental system and accumulative water uptake in three systems with hygroscopic materials where two (H2 and H3) are closed with a disk of low-quality cement mortar (w/c=0.7).

The concrete itself will contain different amounts of water depending on the humidity in the environment and the type of concrete. Water uptake in ~98 % RH air and water loss in ~50 % RH were studied using cylindrical samples (h=8.5 cm, d= 4.5 cm) of the 5 types of concrete. Weight changes were followed through ~460 days starting from 2 days after casting. Equilibration is slow and the sample weights were still changing slightly at the end of the experiment.

Expressed as % of the cement content the four samples without silica fume gained about 3 % in weight at 98 % RH and lost from 8 to 15 % at 50 % RH. The weight loss is strongly dependent on the content of free pore-water as given by the water/cement ratio. The silica fume-containing sample e gave a water loss of only about 5 %. This is probably because the equilibrium water-vapour pressure is reduced in material with small diameter pores. This effect was also demonstrated in an equilibration experiment using granulated paste with different silica-fume contents /1/.

3.2. Crack-healing in concrete.

The rate of diffusive transport of dissolved materials through concrete is - as discussed in the previous section - much dependent on the pore structure.

Water flow caused by hydraulic gradients over concrete barriers will, however, mainly take place through coarse channels such as cracks or macro-pores. Such defects may be present from the beginning due to manufacturing problems, or they may arise - especially in form of cracks - due to mechanical failure of the barrier.
Under certain circumstances the defects could be enlarged by dissolution processes caused by the water flow. This is especially the case if the incoming water is relatively pure or chemicaly aggressive in some way. However, in the case of underground constructions the water will typically be conditioned by contact with surrounding minerals or possibly by contact with other parts of the concrete construction. This should normally make the water less aggressive and may result in a tendency to deposition of solid material due to reactions between dissolved components and calcium hydroxide or other materials from the concrete.

The possibility of autogenous crack-healing in concrete constructions is of considerable interest for the safety evaluation of waste disposal. A literature review is available /22/.

3.2.1. Preliminary experiments.

Some preliminary experiments were run to develop methodology and get a feeling for the phenomena.

In one case a slow flow (~8 ml/h, gravity driven through a narrow tube) of deionized water was equilibrated through a column with granulated silica fume-containing concrete before it passed through a cylindrical (d=4.4, h=4.4 cm) sample of ordinary concrete with an artifically induced crack. The hydraulic head requiered to maintain the flow through the system was followed over a period of 150 days.

The hydraulic conductivity decreased steadily from $2 \cdot 10^{-1}$ cm/sec to $2 \cdot 10^{-3}$ cm/sec, but this was found to be due to closing of the pores in the column with granulated concrete. The conductivity of the crack as such was nearly unchanged. However, taking the column out of the flow system and exposing the cracked sample directly to a flow of deionized, but CO_2-containing water led to a rapid decrease in conductivity to values about 10^{-5} cm/sec. This must be due to precipitation of calcium carbonate which probably also was responsible for the previous clogging of the column.

In a new set of experiments a peristaltic pump with high quality tubes was used as the feeding system. The principle is simple as shown in Fig. 27a. Four systems could be tested simultaneously. Three samples of ordinary concrete and one of low w/c ratio silica fume-containing concrete were employed. The samples were more than 3 years old before they were cracked and mounted in the rubber-tube holders used as the outer container. The two parts of the samples were fitted together and pressed closely against each other by an external rubber + steel tightening ring. The cracks were therefore very narrow.

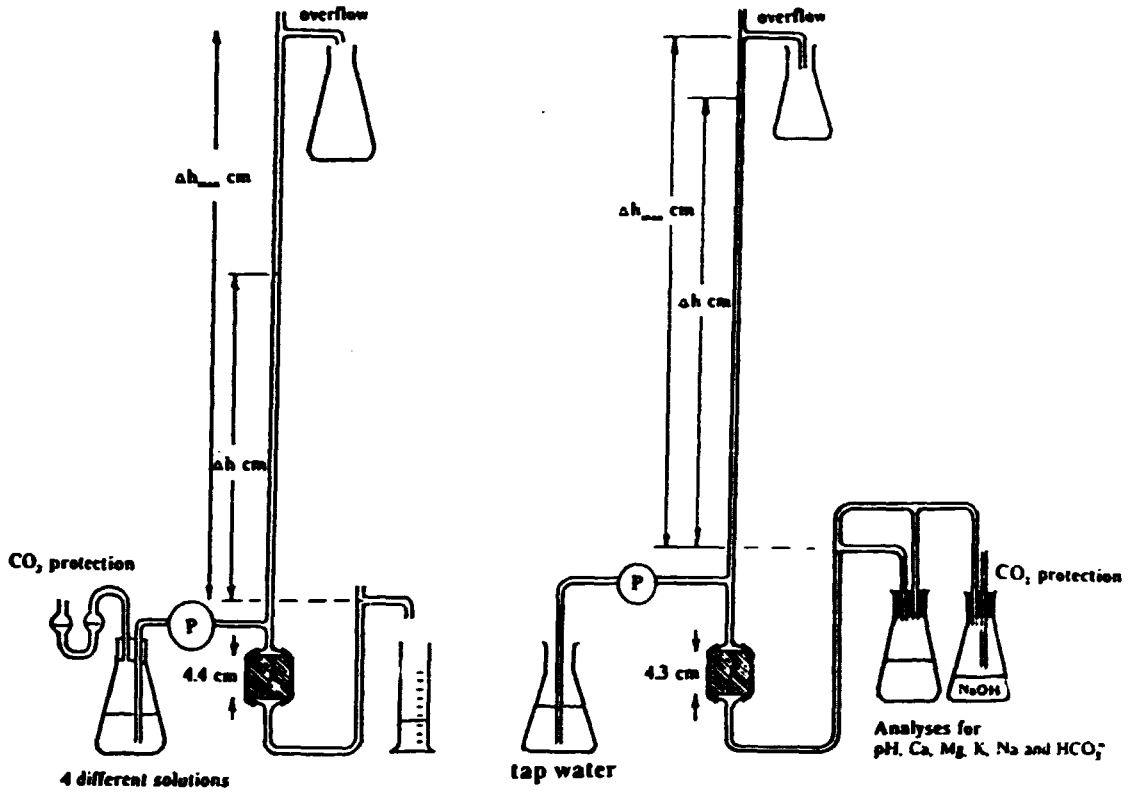

Fig. 27a,b. Experimental set-up used in the crack-fill experiment with four different solutions (a) and in the experiment with tap water and detailed analyses of the out-flowing water (b).

The samples of ordinary concrete were exposed to either ordinary tap water (containing $Ca(HCO_3)_2$), water equilibrated for 2 weeks with 1 g/L of granulated hardened cement + 20 % silica fume, and water equilibrated with lumps of silica gel. The silica fume-containing sample was exposed to a synthetic solution corresponding to equilibration of 10 g ordinary concrete with one litre water: (1.77 g $Ca(OH)_2$ + 0.044 g NaOH + 0.006 g $Na_2SiO_3 9H_2O$ per litre). The three last solutions were prepared from CO_2-free water and kept protected from CO_2. The solution equilibrated with silica-fume containing cement paste gave problems with precipitation of silicic acid clogging the tubes in undesirable places, but otherwise the experiment run quite smoothly for 34 days with initial water flows about 4.5 ml/h.

The crack in all four samples closed more or less rapidly. The hydraulic heads increased to 1.5 m H_2O pressure (maximum in this set-up) whereafter the water flow decreased steadily in most cases to zero. The sample of ordinary concrete exposed to tap water was taken apart and remounted once. The closing of the crack occured even faster the second time. Visual inspection showed that the precipitated minerals (here $CaCO_3$) mainly were concentrated in a narrow band closing the upper few mm of the crack. The sample was remounted a second time where the crack were kept at some tenth of a mm width by inserting small strips of plastic foil. This appeared to prevent a renewed closing.

Interpretation of the results for the other samples are more difficult. Some analyses for dissolved silica, before and after the water has passed through the crack, were made and

indicate precipitation or reaction of silica. When the samples were taken apart the precipitate in the cracks looked like silica gel. Crack closure by silica or silcates is of considerable interest, but the mechanism requirs considerable further investigation, which was not attempted here.

3.2.2. Experiments with crack-closure by calcium carbonate.

The experimental system was then used in a study of crack-healing by calcium carbonate precipitation from tap water. A flow rate of ~5 ml/h was maintained for about 4½ months through artificially induced cracks in cylindrical concrete samples (4.3 cm high, dimeter 4.4 cm). The composition of the concrete (100 SRPC + 140 sand + 38 water) corresponds to material b in Table 6 in Section 3.1.

The initial width of the two cracks: 0.15 mm for sample A and 0.23 mm for sample B, were estimated from the time and the pressure drop required for the flow of a small water volume through the cracked samples.

The pH of the tap water entering the crack was ~7.6 and the contents of Ca, Mg and HCO_3 were 2.6, 0.65 and 4.1 mMol/L, respectively.

The water leaving the crack was collected without contact with atmospheric CO_2 and analysed for pH, HCO_3^- (titration) and Ca^{2+}, Mg^{2+}, Na^+ and K^+ (AAS). Some results for sample A (with the 0.15 mm crack) are given in Figs. 28b and c. The two parallel lines shown for each component corresponds to ± the standard deviation around the mean value of the analyses for the tap water. The results for sample B were rather similar, see /5/. After a short initial period it is seen that the Na and K concentrations are nearly the same as in the incoming water although some slight leaching can still be noticed especially for potassium.

On contact with the alkalis leached from the wall of the crack, some of the Ca^{2+}, Mg^{2+} and carbonate ions in the tap water react and precipitate as $CaCO_3$ and $Mg(OH)_2$. In the early part of the experiment Ca, Mg and carbonate concentrations are therefore strongly decreased, but later they return to values near the mean values for the tap water. The Mg concentration may even rise slightly above this value indicating that previously precipitated $Mg(OH)_2$ is redissolved.

After a short initial period with rapid leaching of the surface layers in the crack, the release of hydroxide from the concrete is decreasing. The pH measurements - shown as OH^- concentration in Fig. 28c - indicate that some dissolution of alkaline materials are still going on. This is also reflected in a slight continuing decrease in the Ca-concentration in the out-flowing water.

Based on this and other mass-balance considerations the amount of deposited $CaCO_3$ given as % crackfill have been calculated, see Fig. 28d. In principle the crack should be closed when % crackfill = 100, but some of the calcium carbonate has no doubt been deposited in the pores in the concrete or on top of the sample, see below. In the case of the somewhat wider crack in sample B the degree of crackfill reached only 95 %.

As indicated by the curves for the flow rate and the hydraulic head (delta-h) over the crack, Fig. 28a, complete closure were not attained. However, partial closure of the thinner crack in sample A gave rise to a temporary decrease in water flow from 5 to ~2

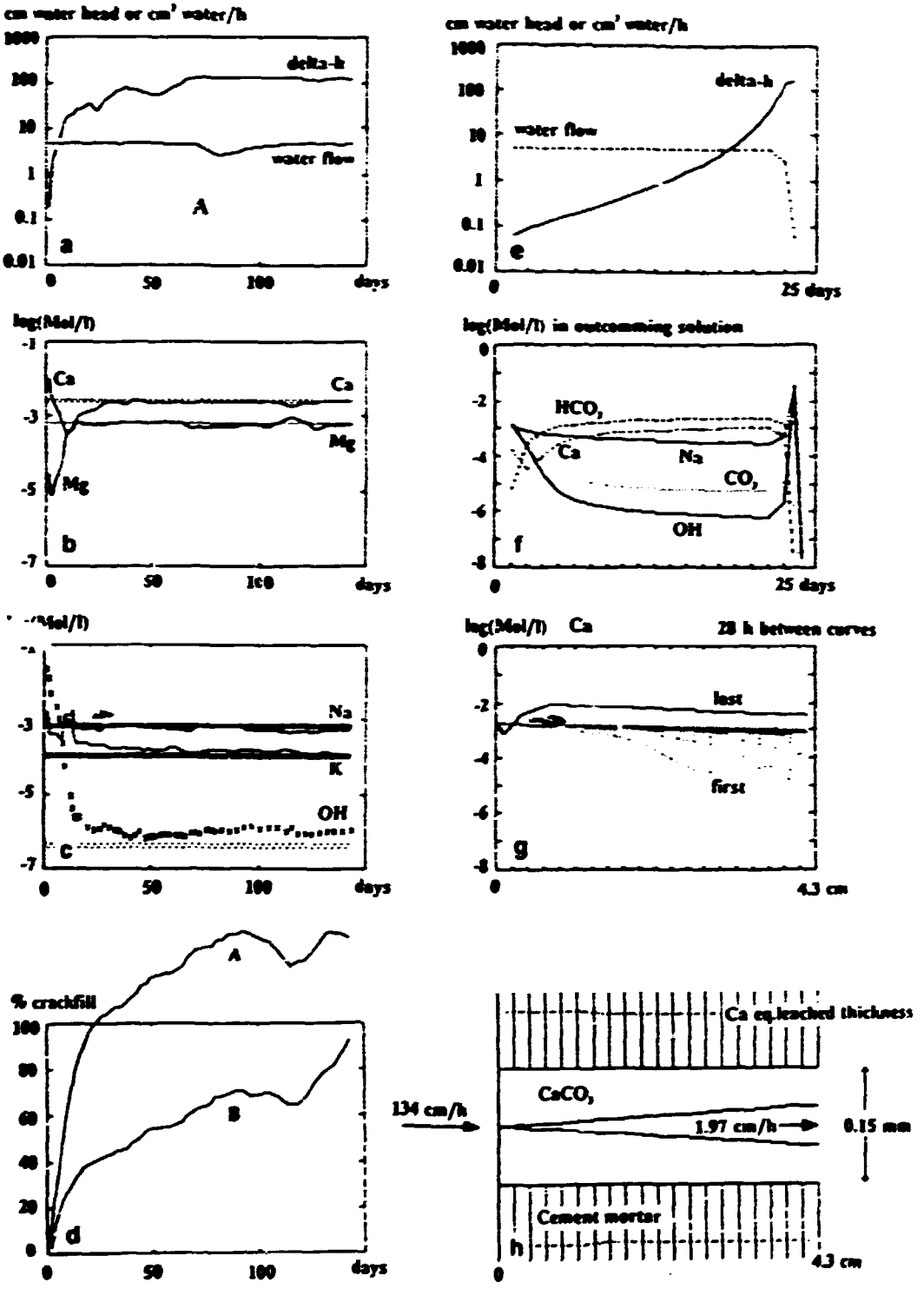

Fig. 28a-h. Experimental results with crack-healing due to calcium-carbonate precipitation in an originally ~0.15 mm wide crack in concrete. Results from model calculations on a similar system are shown in the right-hand figures.

ml/h. With sample B the hydraulic head did not reach the maximum value of ~145 cm H_2O possible in the experimental set-up (see Fig. 28b) and the water flow remained at 5 ml/h.

The observed temporary variations in hydraulic head and/or flow rate indicate that the structure of the deposits in the crack is unstable either physically or chemically. One possibility is that local redissolution take place due to temperature variations (the systems were simply kept at room temperature which did vary considerably), but a short period with changed chemical composition of the tap-water is thought to be a more probable explanation.

At the end of the experiment the two samples were taken apart and inspected visually. The entire inner surface appeared to be covered by a thin carbonate layer slightly thicker at the entrance side. The precipitates were somewhat less clearly delineated than in the preliminary experiments mentioned, above where the crack was thinner and where the water flow relatively rapidly ceased completely. Some carbonate had also precipitated on the ends of the cylindrical samples.

The preliminary conclusion of this experiment is that crack-filling by calcium-carbonate precipitates is strongly dependent on the width of the crack and may be incomplete for even quite narrow cracks.

3.2.3. Modelling.

A simple model simulating $CaCO_3$ precipitation in a crack in concrete exposed to tap water was developed and is described in more detail in /3/.

The crack is modelled as a flat narrow channel and the surrounding concrete as a number of independent columns, perpendicular to the channel. Each column is supposed to release an amount of $Ca(OH)_2$ and NaOH corresponding to diffusive leaching from the exposed column cross-section into the water flowing through the crack. Values for the Ca and Na+K concentrations and the effective diffusion coefficients determining leaching from the columns are taken from Table 6 in Section 3.1.

The precipitation reaction is assumed to occur instantly when the amount of out-diffusing hydroxides in a time-step dt is mixed with the volume of 0.002 M calcium bicarbonate solution (representing tap water) passing by in the same time step. The amount of precipitated material is calculated from mass-balances, from the solubility products for $CaCO_3$ and $Ca(OH)_2$ and from the pH dependence of the CO_3^{2-} and HCO_3^- concentrations. Mg^{2+}-ions and $Mg(OH)_2$ precipitation is not taken into account, KOH is included in the amount af leached NaOH, and chemical activities are disregarded.

The hydraulic head is calculated from the expression for pressure drop involved in laminar flow between two parallel plates. It is proportional to the water viscosity and therefore temperature dependent. 20°C is assumed.

An example calculation is given in /3/. The four diagrams to the right in Fig. 28 show results from modelling of the experiment with sample A described above. Qualitatively there is seen to be reasonable agreement with the experimental results presented to the left in the figure.

The hydraulic head increases steadily until the maximum and then there is a rather rapid decrease in flow rate. This occurs much later in the real experiment and the following rate of decrease in flow is much less and not permanent, see Fig 28a. The reason for this is not known, but new channels must have been opened within the deposited material. Such phenomena cannot be described by the model.

The shape of the curves for the calculated OH^-, $HCO3^-$, Ca^{++} and Na^+ concentrations in Fig. 28f is also in general agreement with the measured concentrations shown in Figs. 28b and c for the solution leaving the sample, although the effects of the calculated large decrease in flow rate was not attained in the experiment.

With Ca as an example Fig. 28g shows how the solution concentration is calculated to change during the passage through the crack at various times during the experiment. A passage takes at the beginning about 200 seconds, but the contact time will be considerably shorter when the crack is partially filled with deposits. The model is based on equilibria and may therefore give too high deposition if the contact time in reality is too short for equilibration.

The calculated profile of the deposits inside the crack when it is nearly closed is shown in Fig. 28h. A degree of crack-filling of about 80 % of the total volume is indicated, i.e. considerably less than found in the experiment, see Fig 28d. It should, however, be mentioned that an amount of Ca corresponding to about the width of the crack at the same time has been leached from the walls. (The equivalent leached thickness is indicated by the dot-and-dash lines in the figure.) Since Ca constitutes about 15 % of the concrete this may have resulted in some widening of the original crack boundaries, explaining part of the 140 % crackfill calculated from mass-balances.

The model can - like other models - be used in parameter studies. An example is shown in Fig. 29, which for various crack-widths show the time it takes before the hydraulic head must rise to 150 cm to maintain a water flow of 5 ml/h. Sample dimensions, concrete properties and the water composition are the same as in the calculations above.

It is seen that the time required for closing of the crack is increasing rapidly with crack-width. However, it follows from the mathematics of the model - as it presently stands - that a crack of any width will close if sufficient time is available.

In reality this cannot be the case, but theoretical considerations indicates that the ratio between length and width of the crack is important and that longer cracks may close more easily. Also a decreased flow rate will probably result in a slower, but more efficient closure of the cracks: even though the incoming amount of bicarbonate will be less the ability to maintain high pH inside the crack will be improved resulting in a more efficient precipitation.

In a real system some additional resistance to the diffusive release of OH^- from the concrete by the precipitate of $CaCO_3$ forming on the surface inside the crack can be expected, but a mechanism of more importance is probably that part of the carbonate precipitation may take place inside the pore structure of the concrete and not in the crack itself. The following qualitative explanation may be given:

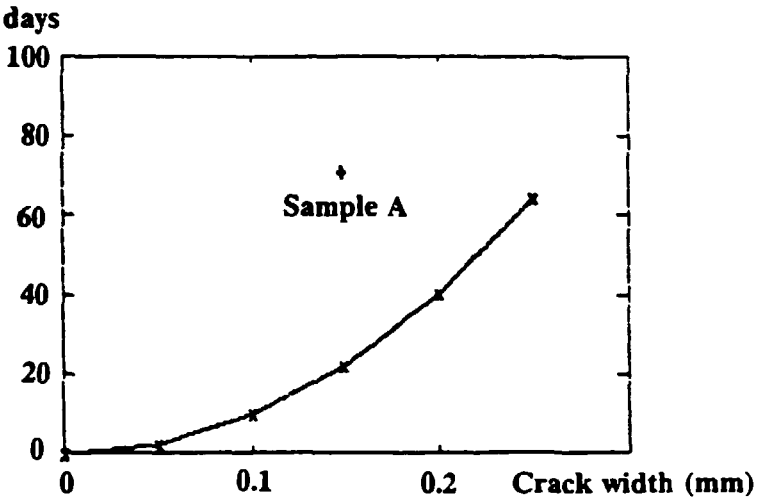

Fig. 29. Calculated time as function of crack-width before a crack in concrete is nearly closed by calcium-carbonate precipitate produced by reaction between alkaline materials from the concrete and a slow flow of a calcium-bicarbonate solution simulating ground water.

The mobility of the OH^- ion in the pore water is relatively high, but - disregarding the small amount moving as dissolved NaOH or KOH - the OH^- ions are only able to leave the pore structure when accompanied by Ca^{2+} to balance the charge. However, after the initial ~15 days-period with low pH values in the water in the crack, the concentration gradient for Ca^{2+} is not favorable for outward diffusion. At the later stages a more probable candidate for charge balancing is therefore the indiffusion of HCO_3^- which then at the higher pH value inside the pore system reacts with OH^- and Ca^{2+} forming precipitates of calcium carbonate.

Quantitatively this should result in only half the amount of OH^- reaching the water in the crack, but the mechanism is more complex since the concentration profiles will be influenced by the precipitation reaction.

Some indications for possible improvements and extensions of the model and for further experimental work follow of the discussion above. It may be possible to model part of these phenomena using the DIFMIG program described in Section 4.1.

3.2.4. Equilibrium studies using thin plates.

An experimental method for study of material transport between concretes with different compositions or concrete and environmental materials has been investigated. The intention was to investigate whether contact through a common water phase between a sample of normal Portland cement phase containing free calcium hydroxide and a more silica-rich cement product might lead to precipitation on the later. The study can be regarded as a supplement to the preliminary experiments with crack-filling due to silicates, see Section 3.2.1.

Thin plates with dimensions ~4 • 1.5 cm and thickness 2, 1, 0.5 and 0.3 mm were cast from SRPC paste with and without (30 %) silica-fume additive as described in /1,20/. Half of the plates were made using neutron-activated cement powder containing ^{45}Ca as

Table 8. Normalized values (% of total amounts in system) for transfer of Ca and ^{45}Ca and total solids between 1 mm thick plates kept at 20° and 40°C.

Equilibration time: days		14				28			56			112			316		
		SRPC	water + cont.	SRPC + SF	SRPC	water + cont.	SRPC + SF	SRPC	water + cont.	SRPC + SF	SRPC	water + cont.	SRPC + SF	SRPC	water + cont.	SRPC + SF
1 mm plates		•	II.2b		•	III.1a		•	III.1b		•	III.1c		•	III.1d	
20°	^{45}Ca	-1.9	1.4	0.5	-2.6	1.5	1.1	-3.4	0.1	3.3	-2.8	1.5	1.3	-2.8	1.3	1.4
	Ca	-2.0	1.7	0.3	-1.1	1.4	-0.2	-4.4	0.7	3.7	-5.2	0.3	4.9	0.6	1.6	-2.2
	weight	-1.1	1.1	0.0	-0.5	0.9	0.4	-0.3	0.5	-0.1	-0.3	0.4	-0.0	-0.7	0.8	0.1
			II.6b	•		III.3a	•		II.3b	•		III.3c	•		III.3d	
	^{45}Ca	0.0	0.4	-0.4	0.4	0.4	-0.8	0.9	0.0	-0.9	0.4	0.4	-0.8	0.7	0.8	-1.5
	Ca	?	1.5	?	-2.2	1.2	1.0	-1.8	0.7	1.0	-5.0	0.2	4.8	-6.1	4.9	1.2
	weight	-1.1	1.0	0.1	-0.8	0.9	-0.1	-0.7	0.6	0.1	-0.6	0.2	0.4	-0.8	0.7	0.1
1 mm plates					•	III.2a		•	III.2c		•	III.2c		•	III.2d	
40°C	^{45}Ca				-2.6	1.5	1.1	-4.5	0.3	4.3	-3.9	1.4	2.5	-3.9	1.2	2.6
	Ca				-6.1	1.2	4.9	-1.0	0.6	0.4	-5.7	0.3	5.3	-0.3	1.0	-0.8?
	weight				-0.5	0.7	-0.2	-0.6	0.3	0.3	-0.2	0.4	-0.2	-0.8	0.7	0. 1
1 mm plates					III.4a	•		III.4b	•		III.4c	•		III.4d	•	
40°C	^{45}Ca				0.9	0.3	-1.1	1.5	0.5	-2.0	1.1	0.3	-1.4	1.6	0.5	-2.1
	Ca				-2.0	1.4	0.6	0.5	0.8	-1.3	-3.5	0.3	3.3	-1.7	1.0	0.7
	weight				-1.2	1.1	0.1	-0.4	0.4	-0.0	-0.5	0.3	0.3	-1.0	0.6	0.4

• indicates that the ^{45}Ca activity originally was present in this plate.

the predominant radio-active isotope. After ~28 days hardening, the plates were placed two and two together in about 10 ml water in closed polyethylene containers as shown in Fig. 30a. Inactive samples of paste with or without silica fume are combined with the opposite type cast from activated cement. The systems were stored CO_2-protected at 20° or 40°C

After equilibration for 7, 14, 28, 56, 112 or 316 days the samples were removed, and their weight changes determined after drying. The total Ca contents were measured by chemical analyses (AAS) and the ^{45}Ca contents by ß-counting. The calcium and the activity contents in the water and in precipitates, which may have accumulated on the container walls, were also determined. From this information it should be possible to calculate the transport of calcium and total solid materials which has taken place in the equilibration period. Values normalized to give constant activity and Ca contents in the closed systems are shown for the 1 mm thick plates in Table 8. The complete set of results are available in /5/.

In general the dry weight of the silica fume-containing plate tends to be constant while the Ca content is somewhat increased. Conversely the ordinary SRPC plates show weight-losses of the same order as the amount of material found in solution (or precipitated on the container wall, in most cases a minor part) together with some Ca

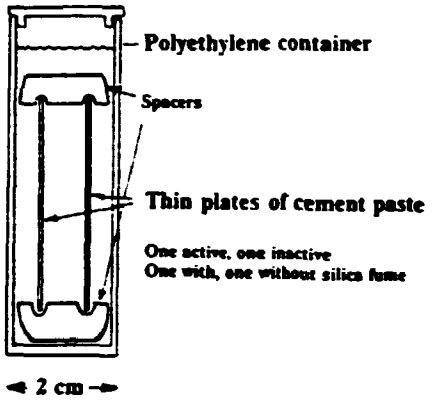

Fig. 30a.
The experimental system with the two thin plates.

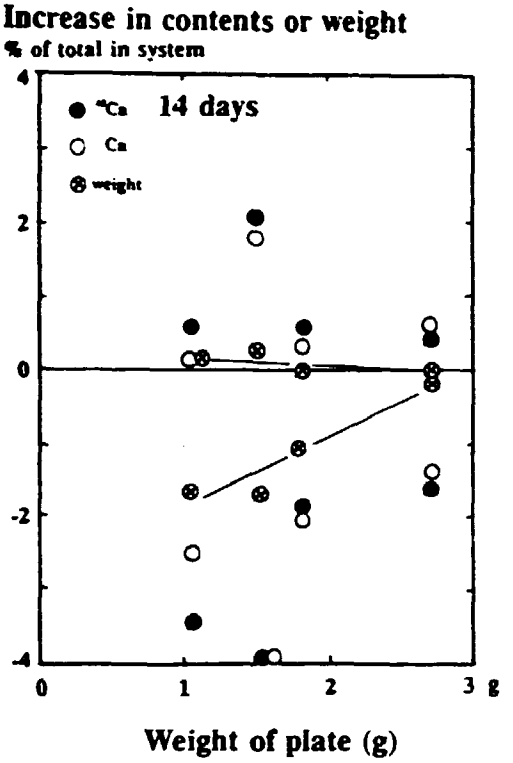

Fig. 30b.
The relative transport of ^{45}Ca, Ca and "total solids" from plates kept at 20°C for 14 days as function of the total weight of the two plates in the systems. The activity was in the pure SRPC plate.

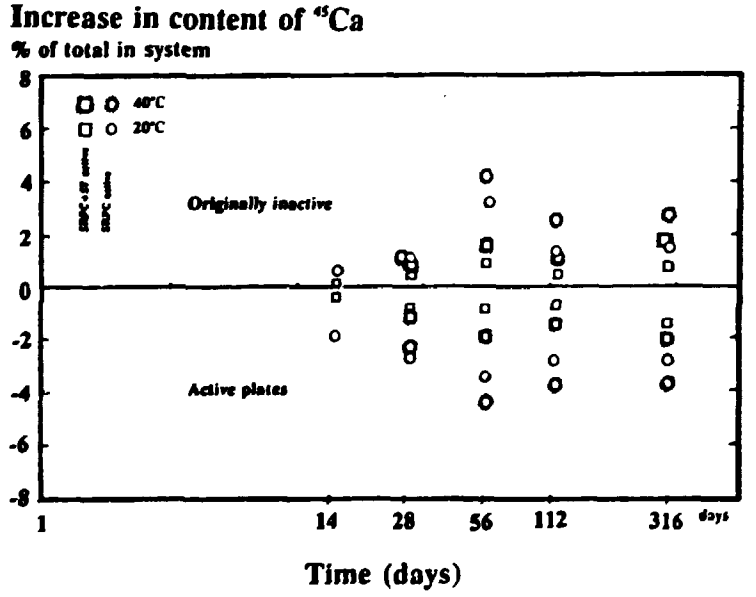

Fig. 31. Relative amounts of ^{45}Ca transported from the active plate (points below the 0% axis) to the inactive plate (points above the axis) as function of time at two temperatures and for different thicknesses of the plates.

losses. When the pure SRPC plate is the active one more of the ^{45}Ca activity is transferred to solution and to the inactive plate than when the activity originally were in the silica fume-containing plate, although some activity also was lost from these plates. Unfortunately the calcium analyses were too uncertain to obtain a detailed interpretation of the Ca transport.

The fractional transfer of Ca and ^{45}Ca to the other plate or the solution tends to decrease with sample weigth or thickness as illustrated by Fig. 30b. The variation with time and temperature in the degree of transport of ^{45}Ca from the active to the inactive plate is shown in Fig. 31. The time dependence is not very great or systematic, but at tendency to increased transfer with time and temperature can be seen.

The idea with the experiment was to demonstrate that transport and redeposition of calcium (and other species) will take place in systems where cement paste of different composition are in contact through a common solution. Such phenomena may be of importance e.g. for crack-healing in concrete when CO_2 is not present. There is no doubt that some transport will take place, but the degree of reaction as well as the rate appear to be low. The analytical possibilities available were not quite sufficient to obtain the needed small differences in Ca contents, but in principle the experimental method is thought to be sound.

The analytical uncertainties make the results somewhat difficult to interprete, but at least some indications for the Ca migration can be derived:

- The transfer of ^{45}Ca from the active to the inactive plates increases slowly with time.
- The transfer of ^{45}Ca is more rapid at higher temperature.
- The fraction which has moved from one plate to the other is in general less than 2 to 4 %. Calcium in the interior of the samples is probably only participating to a minor degree in the exchange.
- When the activity is present in the silica fume-containing plates the percentage of activity released and especially the amount taken up in the inactive plate is less than when the activity follows the 'natural' flow of Ca from an active plate of pure SRPC to an inactive and more silica-rich plate containing silica fume.
- A tendency to slight weight increases of the thinner silica fume-containing samples indicate build-up of material on these silica-rich samples.
- The releases from the pure SRPC plates increases systematically with decreasing weight, but the reason is simply that a larger fraction of the lighter plates must go into solution to reach concentrations in quasi-equilibrium with the hydrated calcium-silicate phase in the plates.
- The plate without silica fume is in most cases found to be the major contributer to the calcium content in the solution.
- No significant difference is seen when using nearly saturated $NaNO_3$ solution instead of water as equilibration medium.

The general conclusion is that some transport of Ca from ordinary Portland cement paste to a more silica-rich paste will occur when samples of the materials are in contact through a common water phase. The process appears to be slow, especially as far as penetration into deeper layers (tenths of millimeters) is concerned. Even after 300 days the systems are still a long way from equilibrium.

3.2.5. Pore water equilibrium composition.

A simplified model of water chemistry in contact with concrete was developed at Risø in connection with a previous contract /21/. Later a set of experiments where hardened granulated cement paste was equilibrated with increasing amounts of water was performed. The analytical results were in reasonable agreement with the model as shown by Fig. 32. where the punctated curves are calculated values and the points connected with unbroken lines represents analyses. Work of this type is persued in a more systematic way in studies made in connection with other EC contracts /23/ and has therefore not been continued at Risø.

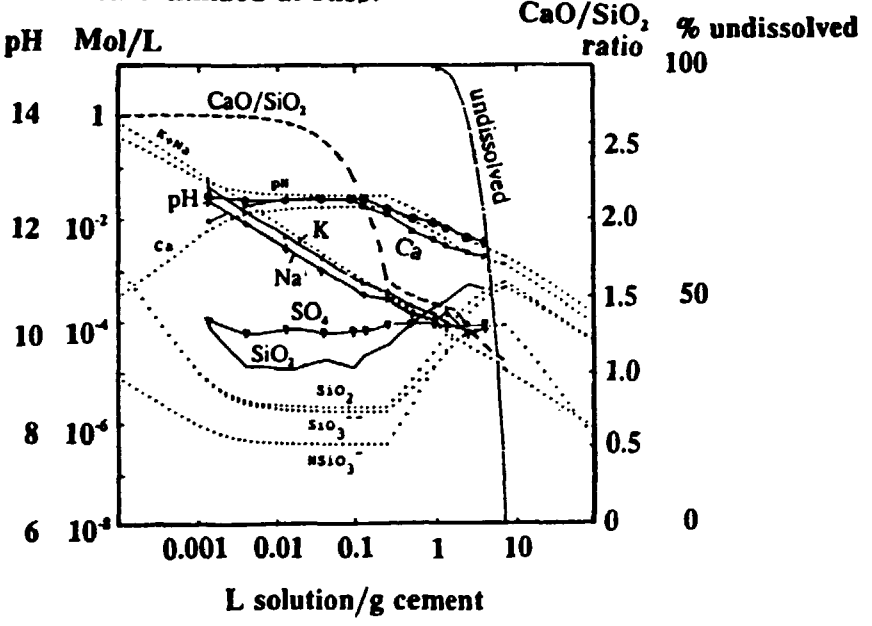

Fig. 32. Na, K, Ca, $SiO_{2(total)}$, pH and SO_4 analyses of solutions equilibrated with decreasing amounts of granulated, hardened SRPC paste. The analytically determined concentrations are compared with model calculations. However, the calculation of the CaO/SiO_2 ratio is too simplistic in this model.

3.3. SANS measurements on cement and bentonite.

Experiments have been carried out with the purpose of studying the microstructure of composite materials using the technique of Small Angle Neutron Scattering (SANS), which is a non-destructive method for studying structural features in the nanometer(nm)-size range.

Cements and clays are materials, which may be studied using this experimental technique. When pulverized cement clinkers are mixed with water the resulting hydrated cement contains a rigid calcium silicate (C-S-H) gel-structure with numerous, sometimes liquid-filled pores. The size of pulverized cement particles varies typically between 1000-2000 nm, but upon hydration C-S-H gel-particles are formed and these have diameters averaging around 10 nm, while inhomogeneities in the form of interstitial pores can be in the 1-100 nm range. During the hydration process calcium hydroxide is produced, and if silica fume (SF) - a material consisting of nearly spherical SiO_2-particles with a diameter around 100-200 nm - has been added to the mixture, then silica fume and calcium hydroxide may react undergoing the so-called pozzolanic reaction forming additional calcium-silicate-hydrate gel, C-S-H.

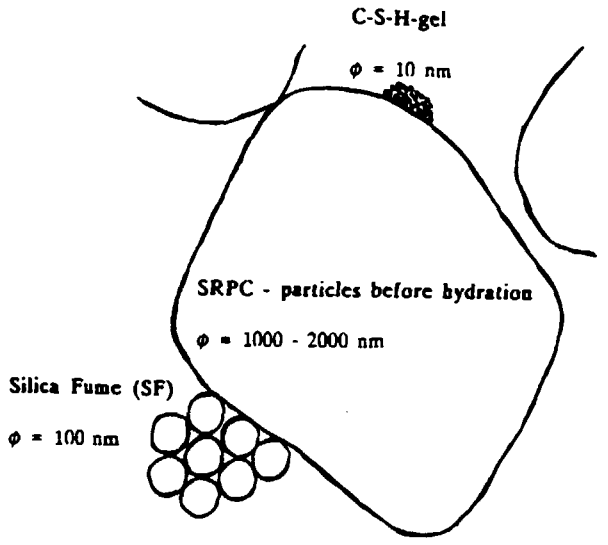

Fig. 33. Diagram of particle sizes in hydrating cement.

The hydrated hardened cement is quite susceptible in time to chemical and physical changes. Among these are general ageing (i.e. conversion towards more thermodynamically stable components or fractions), reaction with materials from the environment, and corrosion or leaching of components from the cement, all of which would be expected to affect the microstructure of the cement. This is important for the long-term development of the material, and therefore for the safety aspects of cementious materials used for waste conditioning and as barrier material.
SANS is well suited for the study of microporosity in cement paste since it measures the difference in scattering power between the general background and small particulate regions. Matrix inhomogeneities ranging in size from 2 nm to more than 100 nm can be detected.

3.3.1. The SANS equipment.

A study of the microstructure of cement and bentonite using the technique of SANS was initiated under this contract in 1986, but the study was interrupted in 1987, when the SANS instrument at the Risø DR3-reactor was demounted for renovation. In its place a new, more versatile facility has been built, and this facility was ready again for experimental use in september 1989.
The new SANS instrument, which is of flexible length, consists of four units: a mechanical velocity selector, A, a collimation section, B, a sample chamber, C and a tank, D with the neutron detector, E.
Neutrons with wavelengths between 0.3 and 2.5 nm are supplied from the cold source at the DR3 reactor through a 22 m long guide tube and enters the instrument at A. The mechanical velocity filter consists of a rotating drum with tilted slits, and it selects a neutron wavelength band from the continuous cold-source neutron spectrum. By varying

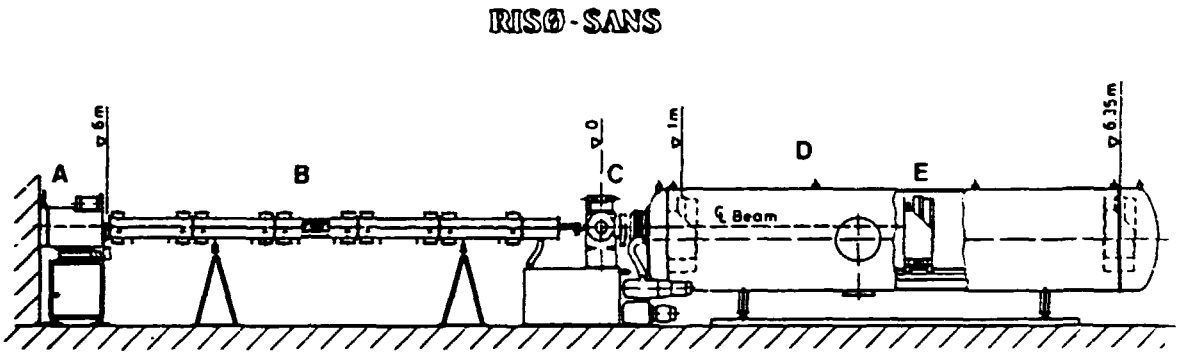

Fig. 34. Diagram of the SANS-instrument at the Risø DR3-reactor.

the speed of revolution and the tilt, both the wavelength and the resolution can be controlled. Usually the system is operated with a resolution of 0.18 FWHM.
The collimator section consists of six 1 meter units. In five of these it is possible to replace collimation apertures with Ni-coated neutron guides, moving in effect the source closer to the sample.
The neutron detector is a ^{3}He multiwire detector, 60 cm in diameter. Cd-beam-stops either 40 mm or 60 mm in diameter absorb the direct neutron beam during measurements. The neutron detector is mounted on a slide, so the sample to detector distance can be varied between 1 and 6 meters.
The sample chamber can be fitted with windows to allow for measurements at normal pressure, and it is built to contain various kind of sample environments such as a thermostated sample changer, which provides an option for mounting up to 7 different samples in the neutron beam.
A MicroVax computer controls the experimental variables and collects data on the parameters mentioned below. Further data treatment is carried out on a Vax-8700 computer.
The momentum transfer normally called the Q-vector measures the scattering, and its size is dependent on the incident neutron wavelength - between 3 and 20 A (Angstrom) at the Risø SANS equipment - and on the scattering angle, which in SANS is less than five degrees. The range of momentum transfer has been increased significantly in the renovated Risø SANS instrument, and the size range of scattering features, which can be studied, has thus been extended considerably.
The property measured as a function of Q in a SANS experiment is called either the differential scattering cross section, or the intensity per unit solid angle. The width, intensity and profile of the small angle scattering intensity as a function of the Q-vector contains the information desired, and can be interpreted either by assuming the presence of pores/particles or by adopting the fractal interpretation of the data.

3.3.2. Experimental.

3.3.2.1. Materials, sample cuvettes and sample preparation.

The following materials were used to prepare samples for SANS measurements:

1) Low alkali Sulphate Resistant Portland Cement (SRPC). A detailed description of this material is given in a previous report /1/. Typical particle size: more than 1000 nm, and a content of CaO of 64.8%.
   Complete hydration of the minerals in 1 gram of SRPC-paste require about 220 mg of water and results in the formation of 387 mg of hydrated calcium silicate gel = C-S-H and of 214 mg of calcium hydroxide = $Ca(OH)_2$.
2) Silica fume (SF) consists of nearly spherical particles with a diameter between 100 and 200 nm. Chemically, it is pure silicium dioxide with a few % of carbon black.
   Silica fume and calcium hydroxide can undergo the so-called pozzolanic reaction forming C-S-H-gel, approximately according to,

$$3\ Ca(OH)_2 + 3\ H_2O + 2\ SiO_2 \rightarrow 3CaO_2.2SiO_2.6H_2O$$

   The Ca/Si ratio in C-S-H-gel may vary continuously from 0.9 to 1.8, see /22/. When SF is added to SRPC + water, the 214 mg of calcium hydroxide formed during hydration of 1 g of cement clinker minerals, may react quantitatively with 200 mg of silica fume according to the pozzolanic reaction. The use of SF results in a more dense type of cement paste. Details about this product can be found in an earlier report /20/.
3) A superplasticizer (SP) with the commercial name of 'Mighty' must be added during preparation of the cement paste, when the w/c ratio is small. Chemically the superplasticizer is the sodium salt of a naphtalene-sulphonic-acid formaldehyde condensate.
4) Bentonite, a commercial clay on Na^+-form.

Microscopy slide glass, which does not contain neutron-absorbing boron, cut into 17 mm * 45 mm pieces has been used for cuvettes. The desired thickness of the cuvette is obtained by gluing stainless steel wire of the appropriate diameter along the edges. The samples are placed in-between the pieces of glass, and the sides are closed and glued together with epoxy resin.
The transmission of neutrons through the empty cuvettes as measured against vacuum has been found to be 98.0% ± 3.7% (average of 5) at 5 A and 94.0% ± 5.0% (average of 4) at 20 A.

The samples for the SANS measurements must have the dimension of about 15 mm * 30 mm and a thickness of preferably 0.3 mm and not higher then 0.5 mm. The latter in order to minimize the possibility of multiple scattering.
The samples were prepared as follows.

1) To demonstrate the pozzolanic reaction: Stoichiometric amounts of 1 g silica fume (16.7 mmole) + 1.4 g CaO (25 mmole) were mixed with 1.5 g of water. The paste was placed in the sample cuvette, which was then closed. In one series the amounts of added CaO were 0.7 g, 1.4 g and 2.1 g.

2) Cements: The cement samples were cast between two sheets of polyethylene by way of the Risø thin-plate technique /21/, and hardened for 3-4 weeks at 100% humidity in a CO_2-free atmosphere.
The following samples were cast and hardened.

SRPC,	w/c = 0.4
SRPC + 0.2*SF,	w/c = 0.4
SRPC + 0.2*SF + 0.004*SP,	w/c = 0.25

The weight of the hardened cement plates was 0.22 g ± 0.02 g for plates with the size of 10 mm * 20 mm * 0.35 mm.
Freshly prepared samples of cement paste in water, were made by placing the moist mixture in the sample cuvettes, which were then closed.

3) Bentonite: 1 g of bentonite + 1.4 g CaO (25 mmole) were mixed with 1.5 g of water. The paste was placed in the sample cuvette, which was then closed.

3.3.2.2. Leaching of the cement samples.

Special precautions has to be taken after leaching of the thin plates, since the samples are very frail, and only with great difficulty can be transferred to the measuring cuvette. As a consequence the following procedure was adopted: The cast and hardened samples were placed between two glass plates glued to a frame of spacing-wire long enough to provide a handle. The cuvettes were open in both ends and the plates were somewhat thinner than the distance between the glasses. Passage of leachant was therefore possible.

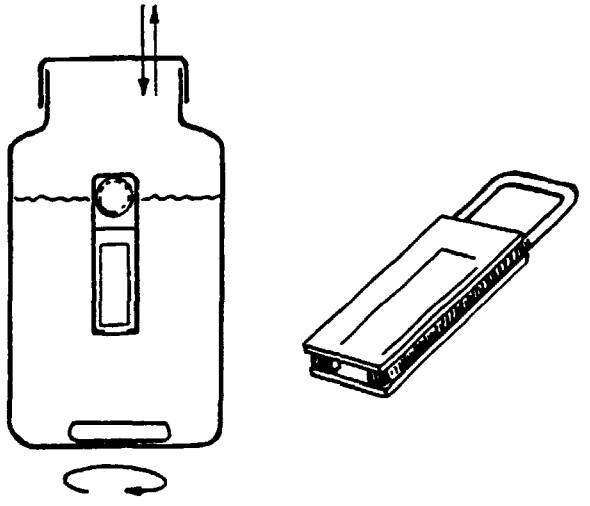

Fig. 35. Setup for leacing of 'thin-plates' of cement paste

Details are shown in Fig. 35. which also show the set-up for the leaching experiment itself. The sample was suspended in 500 ml of the leachant by an air-filled plastic cylinder tied to the handle. Magnetic stirring helped to ensure continuous leaching. The leachants were analyzed for calcium by atomic absorbtion and/or by titration with a Ca-electrode, and pH was also measured.

Leaching of thin cement plates in water with weekly complete changes of the 500 ml liquid showed after a five week period that 89% of the calcium had been leached from SRPC with w/c=0.4; 75% from SRPC + SF with w/c=0.4; and 71% of the calcium from SRPC + SF with w/c=0.25. When cement plates were leached in 500 ml of 0.1 N HCl, the removal of calcium was 100% within a 24 hour period for all the three types of cement.

The cement plates were subjected to other regimes of leaching, normally in closed systems with no access to CO_2 from the air. Some results are given as function of time in Fig. 36a,b. The complete change of liquid each time sampling takes place leads in all cases to a rapid extraction of calcium from the thin plates, whereas extraction of calcium rapidly levels off when the sample is kept in the same liquid used for the whole leaching period. Fig. 36c,d. show that pH declined slowly when water alone was the leachant in the closed systems. With 3% aq. NaCl, the decrease in pH is more rapid. In open systems with access to CO_2 from the atmosphere the leached calcium can precipitate as $CaCO_3$ and the amount of calcium in solution is determined by the solubility product of $CaCO_3$. Considerable pH decreases were observed. The leaching data have been summarized in Table 9.

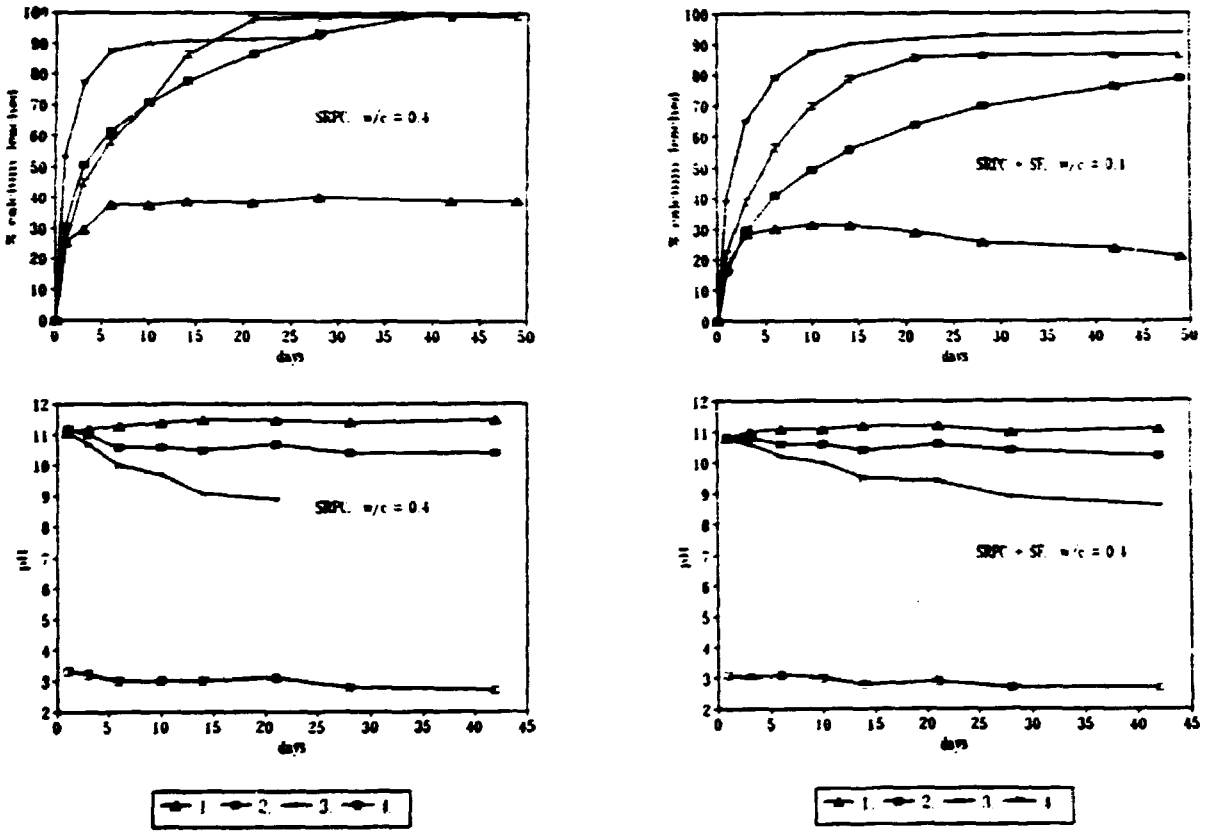

Fig. 36a,b,c,d. Calcium removed from cement plates and pH in the leachates during different regimes of leaching.

1. CO_2-free water, 20 ml out of 500 ml at sampling, no replenishment
2. CO_2-free water, complete (= 500 ml) change of liquid at sampling
3. 3% aqueous NaCl, complete (= 500 ml) change of liquid at sampling
4. 0.002 N HCl, complete (= 500 ml)change of liquid at sampling

Table 9. Summary of the leaching experiment.

leachant			SRPC, w/c=0.4			SRPC+SF, w/c =0.4		
soln	$\pm CO_2$	ml aliq.	plate cont. mg	leach-ed mg	left in plate mg	plate cont. mg	leach-ed mg	left in plate mg
H_2O	-	9* 20	76.2	20.9	44.5	69.7	21.6	47.0
H_2O	+	9* 20	76.9	38.4	35.0	77.2	30.0	58.0
H_2O	-	9*500	69.3	70.3	9.0	68.2	52.7	15.0
H_2O	+	9*500	66.7	54.2	20.0	78.6	41.1	14.0
3% NaCl	-	9*500	63.4	57.6	-	54.0	50.0	2.5
$2*10^{-3}$ N HCl	-	9*500	75.2	73.5	0.3	65.0	55.4	0.3

small errors during analysis and/or small amounts of precipitated $CaCO_3$ may be the reason for discrepancies in the amount of Ca accounted for.

3.3.2.3. SANS Measurements.

Measurements were carried out at ambient temperature using the previously mentioned SANS equipment at the Risø DR3-reactor. The scattered neutrons were recorded by the area-sensitive detector, and the resulting 2-dimentional spectrum transferred to a multichannel analyzer, and on to the MicroVax computer. The attenuation of the neutron beam due to absorption and scattering was recorded by measuring the transmission of the sample.

In the preliminary study neutron wavelengths were chosen, which correspond to Q-vector values of 0.005 - 0.08 A^{-1}, but in the recently resumed investigation neutron wavelengths as well as sample-detector distances can be varied. By doing this, it is possible by performing five consecutive measurements on the same sample to cover the Q-range of 0.003 A^{-1} to 0.35 A^{-1} with a 33% overlap in each of the Q-ranges studied.

During the initial period of measurement in 1986/87 knowledge was gained about various aspects of the SANS technique. SANS measurements at Risø are normally carried out in vacuum (10^{-6} mbar) in order to obtain maximum information from weak scatterers, but it proved extremely difficult to prepare vacuum-tight samples of in particular leached cement pastes. As luck would have it, cement samples are such strong scatterers, that vacuum can be omitted, and the SANS measurements are now carried out at ambient pressure (~ 760 mm Hg).

The samples measured are all isotropic, and therefore the spectra consist of circularly distributed intensity values. The spectra are normalized with the 'flat' spectrum of water, and then radially averaged. The spectra covering several ranges of Q-values are combined to one spectrum covering the entire Q-range. The data are then ready for further data handling.

3.3.2.4. Data Evaluation.

The normalized data can be evaluated according to the theory that the scattering is due to the existance of pores/particles /24/. Provided $Q * R_g \leq 1$, the Guinier single-particle approximation of the scattering law may be applied. The Guinier approximation assumes that all pores/particles are randomly oriented and of the same size, in which case, $I(Q) \propto \exp(-Q^2R_g^2/3)$ or $\log I(Q) \propto Q^2$. R_g is called the radius of gyration, and is a measure of the size of the pores/particles. If $Q * R_g >> 1$, then the Porod single-particle approximation of the scattering law can be applied. The Porod approximation can be used to obtain an estimate of a surface to volume ratio.
The data may also be evaluated on the assumption that the small angle neutron scattering is caused by a self-similar fractal system formed by e.g. aggregation. A fundamental parameter in the description of a self-similar (or scale-invariant) cluster (or aggregate) is called the fractal dimension, which describes how the mass of the cluster increases with its linear dimension, $M(r) \propto r^{D_f}$. M(r) is the mass of the aggregate of the linear dimension, r and D_f is the fractal dimension which can take on non-integer values. Theoretical considerations have shown that the intensity, I(Q) of small angle scattering from such a system scales as Q^{-D_f} and thus would be expected to follow a power law in Q over a Q-range corresponding to the fractal i.e. the scale-invariant size range. Experimentally it has been found that the small angle neutron scattering from heterogeneous disordered system appears to include power laws in the scattering vector Q.
For volume fractals the relationship is the following, $I(Q) \propto Q^{-D_f}$ with the volume-fractal dimension, D_f having a value between 2 and the Euclidian dimension of 3.
For surface fractals in a three-dimensional system it is the surface roughness, which is fractal, and the surface fractal dimension, D_s varies between 3 and a value of 2 in the case of a smooth surface. The relationship for surface fractals is, $I(Q) \propto Q^{(D_s-6)}$, and it follows that small angle neutron scattering solely from a smooth surface should give the relationship, $I(Q) \propto Q^{-4}$, often called the Porod approximation mentioned above.

3.3.3 Results.

3.3.3.1. The pozzolanic Reaction.

Freshly prepared aqueous samples of silica fume mixed with varying amounts of CaO were measured with 14 hours interval over a 5 day period, and then again 30 days later. The integrated SANS-intensities were found to vary with time reflecting on-going changes in the sample, but differently in the three overlapping Q-ranges as shown in Fig. 37. The scattering from the coarse and medium structures are decreasing in intensities while the intensities for the fine structure is increasing.
Each point of the curves in Fig. 37. represents an individual spectrum and each of these have been subjected to analysis by applying the Guinier assumption and by looking for a log I / log Q linear relationship. It was not possible clearly to identify a Guinier relationship in any of the spectra, whereas within certain Q-ranges, a linear relationship between log I and log Q was evident.

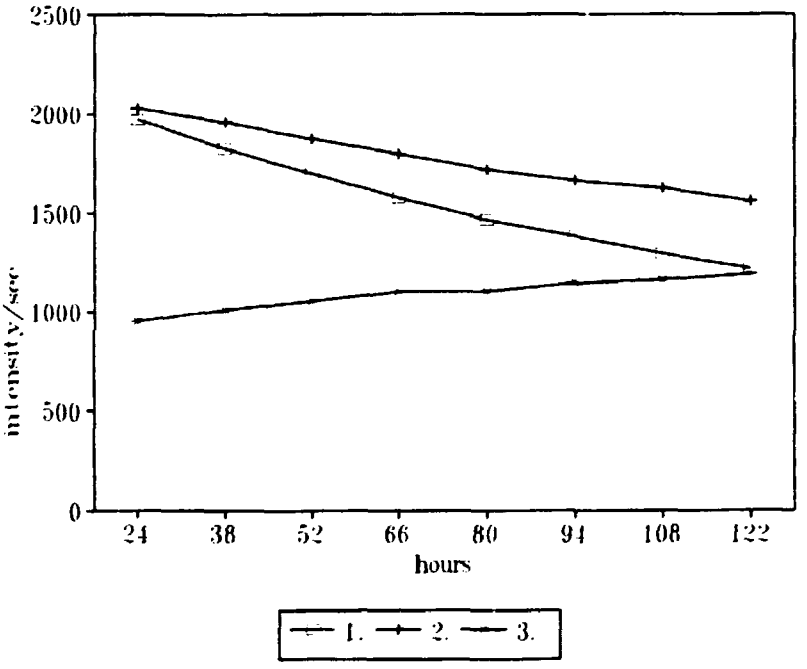

Fig. 37. The integrated SANS-intensity as a function of time measured in three overlapping Q-ranges in a sample containing stoichiometric amounts of silica fume and calcium oxide in water. The sample was freshly prepared at time = 0 hours.
1. Q: 0.007 - 0.04 A^{-1} ~scattering from coarse structure
2. Q: 0.010 - 0.08 A^{-1} ~scattering from medium structure
3. Q: 0.050 - 0.25 A^{-1} ~scattering from fine structure

The spectra recorded at the different times were combined to single spectra, and these combined spectra were fittet over the Q-range of 0.008 - 0.25 A^{-1} with the power-law relationship,

$$\text{differential scattering cross section} = I(Q) = \alpha * Q^{-x} + \beta$$

In Fig. 38. are shown the value of the exponent x representing the fractal dimension as a function of time, for 3 samples consisting of SiO_2, water and different amounts of CaO. The value of x decreases as a function of time probably reflecting the progressing formation of the C-S-H gel from silica fume and CaO. The rate of reaction appears to depend on the amount of CaO present.
SANS-measurements covering the wide Q-range of 0.008 to 0.45 A^{-1} were repeated on the three samples 30 days after preparation. The combined data could be fitted over the whole Q-range with the expression shown above, as seen in Fig.39. for the sample made from 1.0 g silica fume, 1.4 g CaO and ~ 3 g of water. The exponent x had the values of 2.29 ± 0.01, 2.28 ± 0.01 and 2.34 ± 0.01 for the samples containing respectively 0.7 g CaO, 1.4 g CaO and 2.1 g CaO.

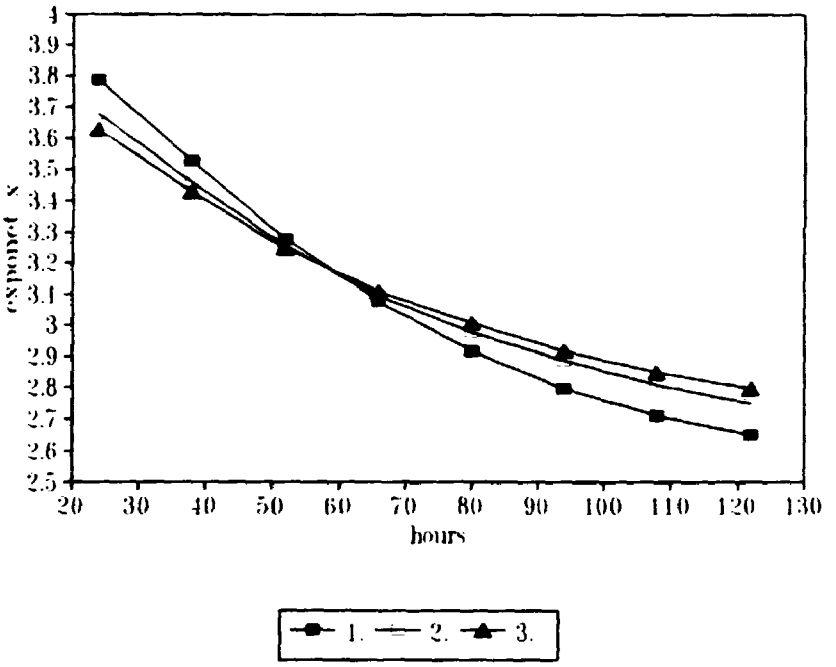

Fig. 38. The change in the exponent x, as a function of time during the formation of C-S-H-gel by the pozzolanic reaction
1: 0.7 g calcium oxide + 1.0 g silica fume + water
2: 1.4 g calcium oxide + 1.0 g silica fume + water
3: 2.1 g calcium oxide + 1.0 g silica fume + water

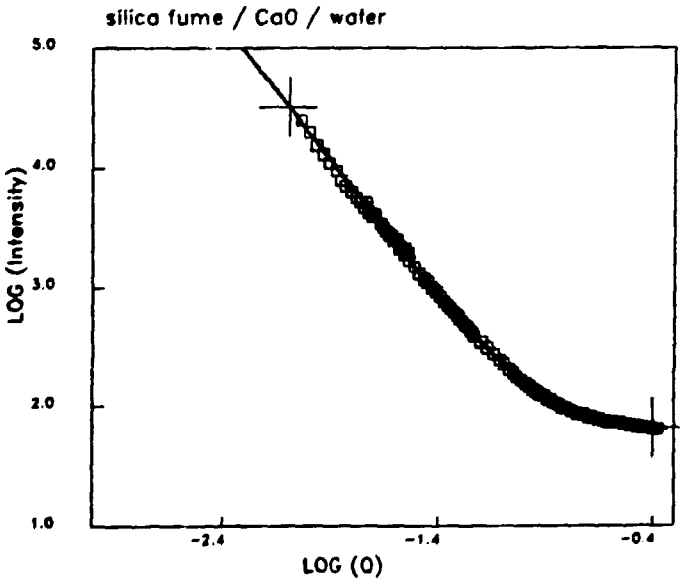

Fig. 39. Log Intensity (arbitrary units) versus log Q for the combined SANS-spectrum of a sample of C-S-H-gel formed from the pozzolanic reaction between 1.0 g silica fume and 1.4 g CaO measured 30 days after preparation.

An aged sample (> 6 months) of C-S-H-gel formed from the pozzolanic reaction in water between SiO_2 and CaO, was studied over the Q-range of 0.008 to 0.15 A^{-1}. It showed no Guinier relationship but a nearly linear log I - log Q relationship as seen in Fig. 40. The exponent x was found to be 2.27 ± 0.02.

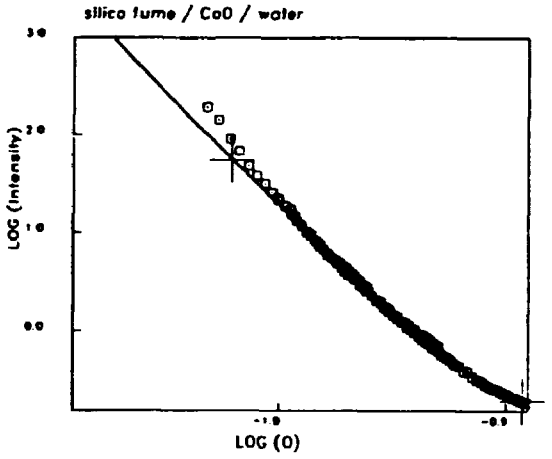

Fig. 40. Log Intensity (arbitrary units) versus log Q for the combined SANS-spectrum of an aged sample (>6 months) of C-S-H-gel formed from the pozzolanic reaction between silica fume and CaO.

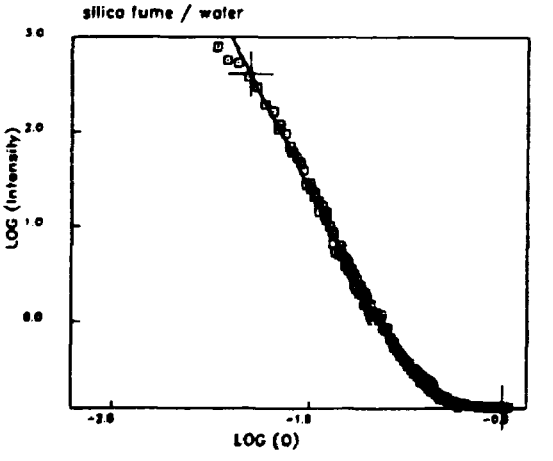

Fig. 41. Log Intensity (arbitrary units) versus log Q for the combined SANS-spectrum of an aged sample (>6 months) of silica fume in H_2O.

An aged sample (> 6 months) of pure silica fume in water was also studied over the same Q-range of 0.008 A^{-1} to 0.15 A^{-1}. Application of the Guinier assumption showed no linear relationship between log I versus Q^2. The data was then evaluated for a possible log I - log Q relationship, and it was found, that a linear relationship does exist as shown in Fig. 41. For such a sample containing only silica fume in water, a slope of 4.04 ± 0.03 was found, which is the value to expect according to the Porod approximation if scattering occurs solely from the surface of a relatively coarse material 'in casu' the silica fume globules with diameter ~100-200 nm..

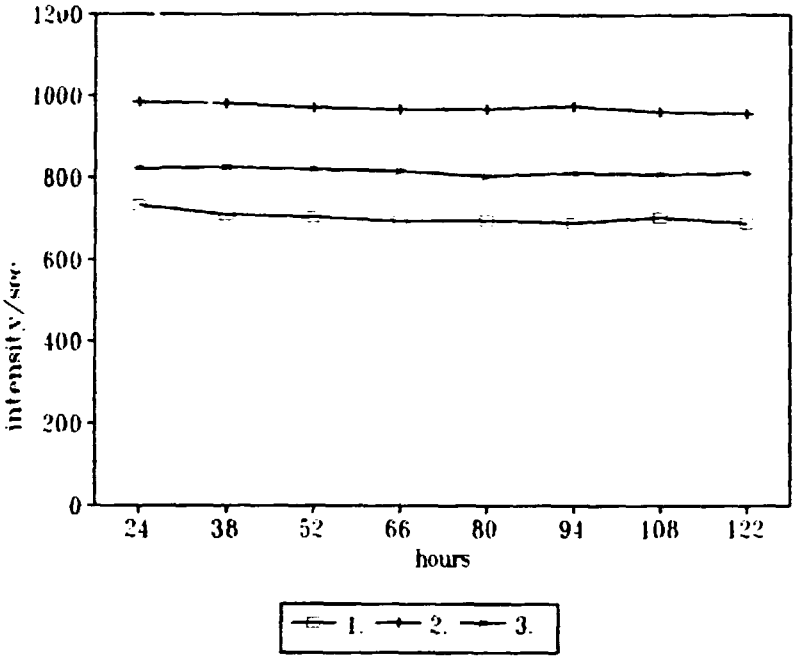

Fig. 42. The integrated SANS-intensity as a function of time measured in three overlapping Q-ranges. The sample of SRPC, w/c=0.4 was prepared at time = 0 hours.
1. Q: 0.007 - 0.04 A^{-1} ~scattering from coarse structure
2. Q: 0.010 - 0.08 A^{-1} ~scattering from medium structure
3. Q: 0.050 - 0.25 A^{-1} ~scattering from fine structure

3.3.3.2. Cements.

Freshly prepared samples of SRPC-paste, w/c=0.4 were measured by SANS, eight times with 14 hours intervals starting 24 hours after preparation.The intensities did not vary much within the time-range studied as shown in Fig. 42.

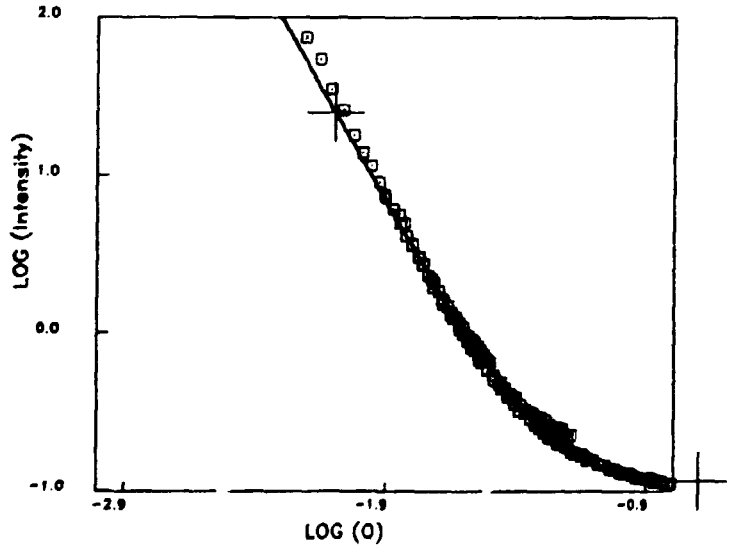

Fig. 43. Log Intensity versus log Q for the combined spectrum of a thin plate sample of SRPC-paste, w/c=0.4, 51 days old.

Analysis of the individual spectra applying the Guinier assumption did not reveal a linear relationship between log I and Q^2. The combined spectrum covering the Q-range, 0.008 - 0.20 A^{-1} was fitted with the previously mentioned power-relationship and a value for x of 2.88 ± 0.03 was found. Apparently the formation of the C-S-H-gel is already well under way before start of the measurements. The sample was measured again 30 days after preparation and this time a value for x of 2.86 ± 0.03 was found.
A pre-cast thin plate of SRPC, w/c=0.4, hardened for 35 days was placed in a cuvette in water for 16 days and then measured by SANS. Upon fitting between Q-values of 0.008 and 0.2 A^{-1}, a value for x of 2.85 ± 0.03 was found (see Fig. 43.).
Hardening of SRPC with silica fume additive results in a more dense type of cement supposedly with a smaller population of coarse pores. Samples of the (SRPC + SF)-cement with two different w/c-ratios, 0.4 and 0.25 have been used.
A sample of SRPC + SF, w/c=0.25 in water measured at 16 days after completed hardening gave x = 2.86 ± 0.03 for the Q-range 0.008 - 0.2 A^{-1}. Thus, no particular effect of the w/c ratio can be seen when pure SRPC, w/c=0.4 and the much more dense SRPC + SF are compared, althogh the pure SRPC, w/c=0.4 material should contain a higher fraction of coarse pores.
A sample of SRPC + SF, w/c=0.4 was measured several times following the initial hardening of 35 days In order to study the possible effect of ageing. Each time the spectra covering different Q-ranges were combined and then fitted between Q = 0.008 A^{-1} and Q = 0.2 A^{-1} using the previously mentioned power law relationship. For each measurement a values of x ~ 2.7 resulted, so no effect of ageing was in evidence. (see Table 10.

Tabel 10. Exponent x ~ the fractal dimension.

	SRPC + SF, w/c = 0.4		SRPC + SF, w/c = 0.25	
	water	Q-brine	water	Q-brine
16 days	2.68		2.86	
106 days	2.73	3.03		3.02
136 days	2.66			

Q-brine (sat. $MgCl_2$, NaCl solution) is known to corrode cement and precipitate $Mg(OH)_2$. A hardened sample of SRPC + SF, w/c=0.4 placed for 106 days in Q-brine gave x = 3.03 ± 0.05, and a sample of SRPC + SF, w/c=0.25 treated similarly gave x = 3.02 ± 0.03 both for the Q-range 0.008 - 0.2 A^{-1}. Apparently the precipitating material fills out the empty space in the cement aggregate moving the volume fractal dimension from ~2.8, to x ~3.0, the euclidian dimension.
Thin plates of SRPC and of SRPC + SF both with a w/c-ratio of 0.4 were subjected to leaching for 49 days (see section 3.3.2.2.) before the SANS-measurements were performed. Values for x obtained by fitting with the power law are given in Tabel 11. together with the pH end-values of the leachants and the residual Ca-content in the plates. The Ca/Si mol-ratios in the measured plates are also given.
Some of the plates were leached to an extreme degree leaving nearly pure silica gel. This results for the SRPC samples in rather low values for the exponent x. The leaching is less pronounced for the SRPC + SF plates and the x values appear rather erratic. Further measurements are clearly needed.

Table 11. The leaching procedure, end-values for pH in the leachates, Ca-content and Ca/Si mol-ratios in the remaining mixture together with the value for the exponent x obtained from the SANS measurements.

Leachant			SRPC, w/c=0.4				SRPC+SF, w/c =0.4			
soln	$\pm CO_2$	aliq.	pH	x	%Ca	Ca/Si	pH	x	%Ca	Ca/Si
H_2O	-	9* 20	11.2	2.75	58.4	1.59	10.8	2.50	73.7	1.03
H_2O	+	9* 20	8.1	2.42	45.5	1.24	8.1	2.43	75.1	1.15
H_2O	-	9*500	10.4	2.52	13.0	0.36	10.2	2.53	22.0	0.34
H_2O	+	9*500	8.2	2.27	30.0	0.82	8.3	2.69	17.8	0.27
3% NaCl	-	9*500	8.7	-	-	-	8.6	2.82	4.6	0.07
$2*10^{-3}$ N HCl	-	9*500	2.7	1.78	0.4	0.01	2.7	3.06	0.5	0.01

3.3.3.3. Bentonite.

A few samples of bentonite have been measured. Bentonite alone in water studied over a Q-range of 0.008 - 0.20 A^{-1} show Porot surface scattering with a slope of 4.11 ± 0.02 as seen in Fig. 44. Addition of CaO to the bentonite slurry gave as the result a slope of 3.79 ± 0.02 (see Fig.45.). This value may indicate some beginning roughening of the particle surfaces.

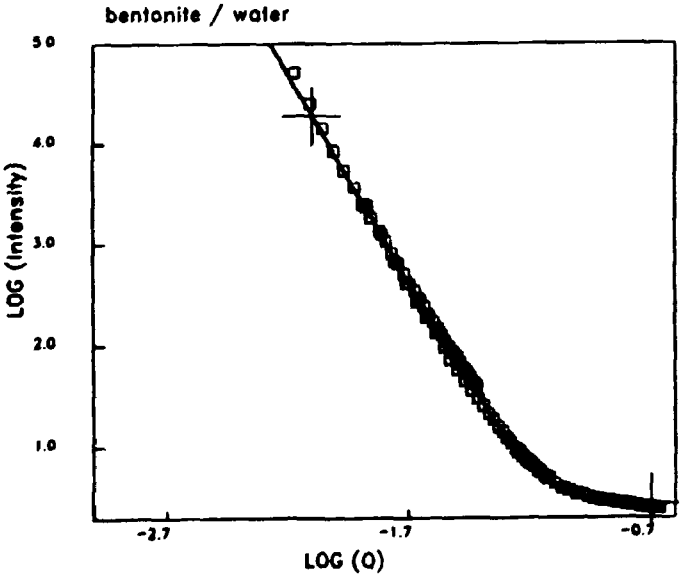

Fig. 44. Log Intensity versus log Q for the combined spectrum of bentonite in water.

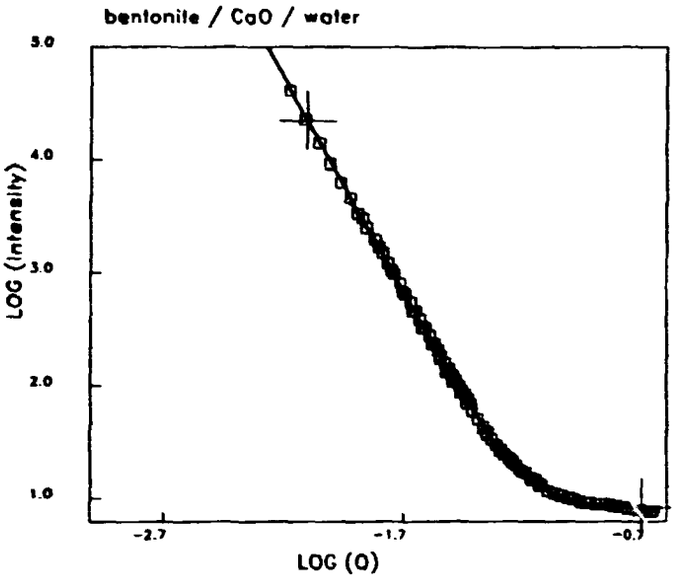

Fig. 45. Log Intensity versus log Q for the combined spectrum of bentonite and CaO in water.

3.3.4. Discussion

Small angle neutron scattering from hetorogeneous porous materials is as a rule complicated to analyze. The single-particle scattering approximations i.e. the Guinier- and Porod approximations are of use when a descrete size population of scattering features is present, and the Debye scattering law, which treats random systems can be used when the randomness is within single scale lengths. However, a heterogeneous disordered or porous structure generally has a wide range of scale lengths and most often gives rise to small angle scattering from a large non-characteristic size range of scattering features, which might be interpreted in terms of a power law in the porosity. On the other hand, a power-law relationship also arises from random aggregation processes, which tend to produce self-similar fractal systems according to, $M(r) \propto r^{-Df}$. Different types of aggregation processes lead to different values of the non-integer fractal dimension, but the scale invariance appear to be universal. Such structures also give rise to small angle scattering following a power law in Q over a Q-range corresponding to the scale-invariant size.

It has been suggested by Allen et al /24/, that the formation of the C-S-H-gel in cement is taking place by way of single particle diffusion-limited aggregation of calcium-silicate-gel globules, and that a self-similar structure with a fractal dimension of ~2.4 in the lower Q-range is the result. Our findings are in agreement with this suggestion.

The aim of the current investigation is to study the effect of degradation in the form of corrosion and leaching on the microstructure of cement. Some tentative results have been obtained and the experimental methods are now well established. It was found important that the measurements have to take place not in vacuo but at normal pressure.

It is the intention to look at the samples over the largest possible range of the Q-vector and to look for the coarsening effects of corrosion and leaching. A better quantitative interpretation is also on the agenda.E

4. INTERACTION BETWEEN BARRIERS AND WASTE.

4.1. Integral experiments.

Experimental studies of model systems simulating selected parts of repositories on a relatively small scale or in a simplified manner are valuable for the understanding of interaction phenomena which may be important for the over-all behaviour of the system. The results from such experiments may be used for model validation, and since the parameters probably are better controlled, also may be more suitable for the purpose than full-scale or in-situ experiments. Such a study involving cemented waste, iron (from drums) and various clay or concrete barrier materials is reported in the following.

4.1.1. Diffusive transport from cemented sodium nitrate (RMA8) through barriers of kaolin or concrete.

An integral experiment to determine the rate of release of ^{134}Cs and ^{85}Sr from cemented $NaNO_3$ (a simplified version of RMA8) through ~2 cm thick layers of kaolin or inactive concrete has been performed. Sixteen different systems were employed representing various combinations of the two barrier materials - in some cases with a layer of corroding iron at the interface between sample and barrier - with 4 different storage condtions, i.e. under oxidizing or reducing conditions, and with the presence or absence of HCO_3^- in the leach solution. Two of the samples were enriched in potassium content and one contained complexing agents as specified for RMA8. The systems are shown schematically in Fig. 46.

The materials were prepared from 2 L simulated waste containing 300 g $NaNO_3$ + 0.2 g KNO_3 per litre mixed with 4.44 kg SRPC. ^{134}Cs and ^{85}Sr together with Cs- and Sr-carriers were dissolved in the concentrate before mixing with the cement. Additional K^+ (samples X1 and X2) or oxalate + citrate + EDTA (sample X3) were added to portions of the mixture.

The samples were cast as ~4 cm thick layers filling the lower part of 500 ml polyethylene bottles. They were hardened for one month with closed caps.

After hardening, some of the samples were covered by a ~2 cm thick kaolin layer or with a ~2 cm thick layer of low quality concrete (100 SRPC+600 sand+130 water, corresponding to a water-filled porosity of about 28 %). Low quality barrier materials were employed to ensure break-through of activity within reasonable time. However, in the case of the kaolin this was accidentally carried too far (a material with 50 weight % water was employed instead of the intended 50 volume %) resulting in very short break-through times.

The systems intended for leaching under anaerobic conditions were prepared in a glove box with a N_2+5 % H_2 atmosphere. The leaching took place in 0.001 M NaCl or 0.001 M NaCl + 0.1 M $NaHCO_3$ solution under aerobic or anaerobic condtions. 100 ml out of 200 ml was replaced by fresh solution every fortnight. The systems were stored with closed caps at room temperature in the laboratory or in the above-mentioned glove box.

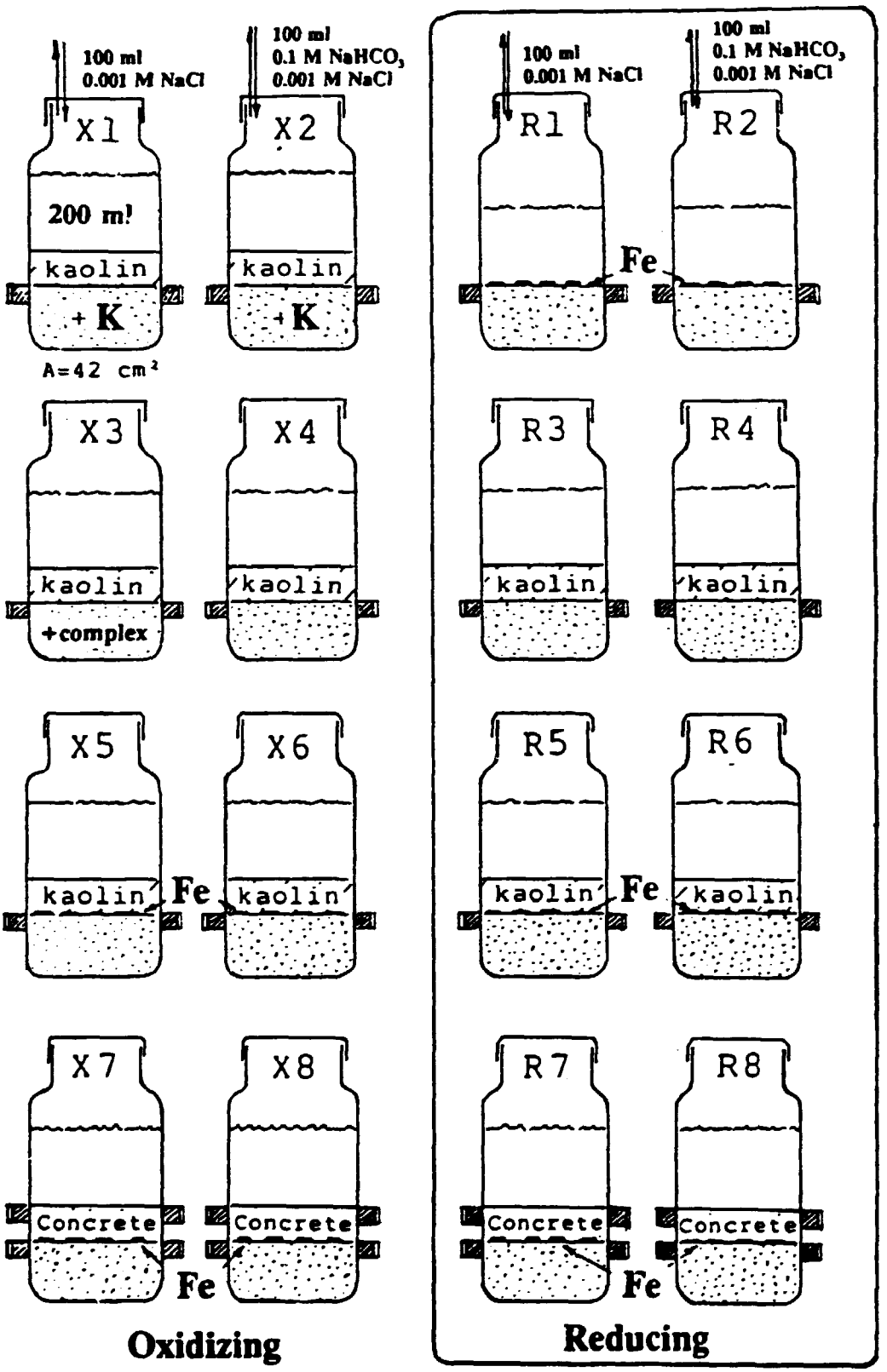

Fig. 46. Integral experiment combining leaching from cemented sodium nitrate, with effects of corroding steel and diffusion through kaolin or concrete barriers under oxidizing or reducing conditions and with and without HCO_3^- present.

In some experiments ~1 g activated iron in form of thin steel pins was placed evenly distributed on top of the concrete sample before covering by the barrier material. In no cases, not even when the steel pins lay freely exposed on top of the sample, have significant γ-countings for ^{59}Fe been attained for the leach-water samples. Measurements of the ^{59}Fe contents in the kaolin or adsorbed on the cemented waste product (extracted by HCl etching at the end of the experiment) indicated, however, that some corrosion takes place, and that the corrosion products are nearly completely fixed on the solid materials in the system. The Fe-precipitates do not seem to have any significant influence on the release rates for ^{134}Cs or ^{85}Sr.

After the last sampling the Cs- and Sr-activities in mixed samples of most of the kaolin layers were also determined.

Figs. 47abcd show the amounts of released ^{134}Cs and ^{85}Sr found in the water samples for the 4 systems with kaolin + iron and the 4 corresponding ones with concrete barriers. The results are given as the equivalent accumulative leached thicknesses plotted against the square root of time. The activities found in the kaolin layers at the end of the experiment are given as the equivalent ticknesses to the right in Figs. 47ab.

The leach curves show, as expected, a certain delay before the release of significant amounts of activity. Apparent effective diffusion coefficients and break-through times obtained from linear approximations to the last part of the curves are given in Table 12 for all 16 systems.

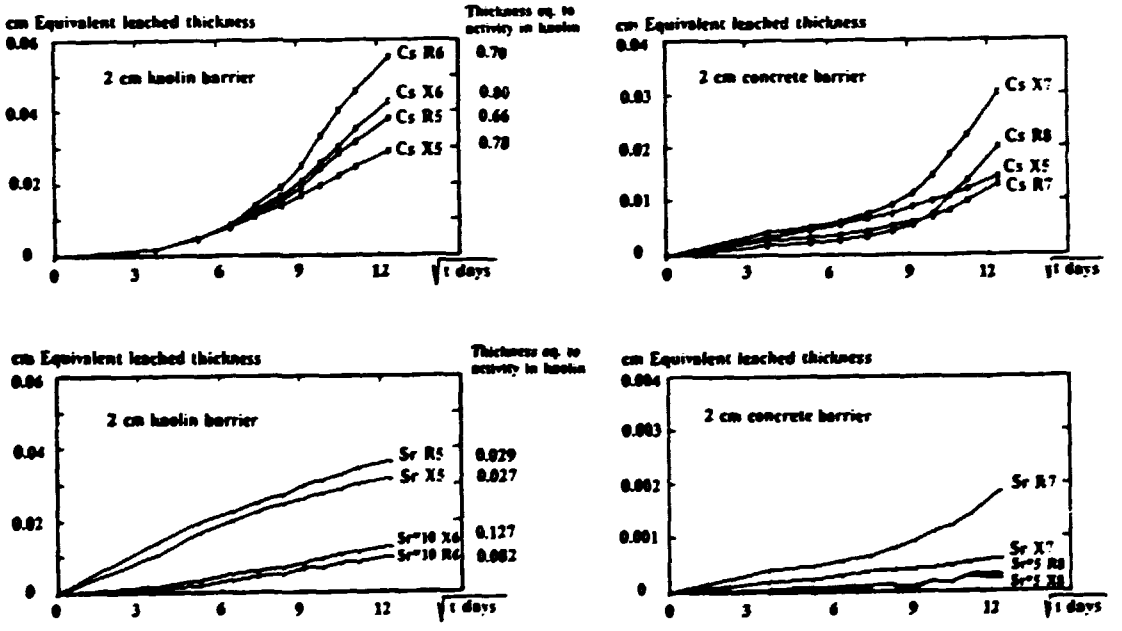

Fig. 47. Releases of ^{134}Cs and ^{85}Sr from cemented sodium nitrate through kaolin (with 50% water) or cement mortar (w/c = 1.4). Experiments under oxidizing conditions are marked (X) and reducing (R). Even numbers are with HCO_3^- present.

Table 12. Apparent effective diffusion coefficients and time-lags found in experiments with low-quality barrier layers of kaolin or concrete covering simulated RMA8.

D_e in 10^{-12} cm^2/sec (Time lag in days)

	Aerobe		Anaerobe	
	0.001 M NaCl	0.1 M $NaHCO_3$	0.001 M NaCl	0.1 M $NaCO_3$
^{134}Cs				
2 cm kaolin	X1 + extra K 750 (8)	X2 + extra K 1230 (26)	R1 no barrier 8500 -	R2 no barrier 10700 -
2 cm kaolin	X3 + complex 3800 -	X4 310 (33)	R3 360 (33)	R4 800 (37)
Fe+2 cm kaolin	X5 132 (22)	X6 400 (36)	R5 300 (33)	R6 690 (37)
Fe+2 cm concrete	X7 26 (15)	X8 57 (50)	R7 310 (53)	R8 225 (70)
^{85}Sr				
2 cm kaolin	X1 + extra K 51 -	X2 + extra K 0.13 -	R1 no barrier 87 -	R2 no barrier 0.075 -
2 cm kaolin	X3 + complex 89 -	X4 0.16 -	R3 57 -	R4 0.21 -
Fe+2 cm kaolin	X5 36 -	X6 0.19 -	R5 58 -	R6 0.11 -
Fe+2 cm concrete	X7 0.03 -	X8 0.0004 -	R7 0.9 (40)	R8 0.0022 (60)

The following general conclusions can be drawn from the figures, the values given in Table 12, and other information obtained in the experiment:

- Cs-release from systems with kaolin barriers is enhanced by increased Na^+ and especially K^+ concentrations, mainly as an effect of decreased retention in the barrier.
- The presence of complexing agents in the cemented waste increases the Cs-release as well as the leaching from the material itself.
- Cs-release is enhanced under reducing conditions. This is especially the case for the systems with concrete barriers.
- Cs concentration is increased slightly in the surface layer of a concrete sample when leaching takes place in a carbonate-containing solution (retention on $CaCO_3$?).
- Sr-release is considerably lower than Cs-release and is less influenced by the parameters mentioned above.
- Sr-release is strongly decreased in carbonate-containing water and Sr is enriched in the surface layer of the concrete sample or in the kaolin layer above (precipitation of $SrCO_3$?).

In addition, some experiments with 'equilibrium' extraction (no CO_2 present) of small broken pieces of the cemented waste product indicate that:

- Cs under such circumstances is leached rapidly and nearly completely. A small fraction is bound strongly or in a protected way.
- Sr is initially also leached rapidly, but only the first ~20 %. Leaching of the remaining ~80 % is slow, probably because of solubility limitations associated with the high content of Sr carrier naturally present in the cement (0.14 weight % in this SRPC). Comparison of chemical Sr analyses with Sr concentrations based on activity measurements indicates that all the strontium naturally present in the cement is able to act as carrier for the added ^{85}Sr.

4.1.2. Diffusive transport from cemented sodium nitrate (RMA8) through barriers of kaolin, chalk or concrete.

The main features of the experimental systems are similar to the ones described above. A simplified and slightly modified simulated RMA8 waste was prepared by hand-mixing of Danish SRPC with a sodium nitrate solution containing ^{134}Cs and ^{85}Sr + cesium and strontium carriers. A special version of the material with some of the $NaNO_3$ substituted by KNO_3 was also made. The composition of the products is given in Table 13 based on the analysis of SRPC given in /6/.

Table 13. Composition of simulated solidified sodium nitrate waste product (RMA8). Density: 2.07 g/cm³, w/c ratio: 0.37

	Water	Ca	Sr	Na	K	Cs	SO_4^-	NO_3^-	^{85}Sr	^{134}Cs
	g								MBq	
Contents in 1 L = 1.19 kg simulated concentrate	879	-	0.001	84.5 (66.7)	- (25.3)	0.0027	-	228 (220)	55	10
Contents in 2.38 kg SRPC	~10	1102	3.42	2.7	3.8	-	71.4	-	-	-
Total in 3.57 kg = 1.73 L	889	1102	3.42	87.1 (69.4)	3.8 (29.1)	0.0027	71.4	228 (220)	55	10
	mg/cm³								Bq/cm³	
Concentrations: simulated product	515	639	1.98	50.2 (40.2)	2.2 (16.9)	0.0016	41.4	132 (128)	31900	5800
% from the cement	~1	100	~100	3.0 (3.8)	100 (12.9)	0	100	0	-	-

The values in parantheses represents the material with some of the sodium nitrate substituted by potassium nitrate.

The products were again cast as ~4 cm thick layers in the bottom of soft LD-polyethylene bottles. The samples intended for leaching under reducing conditions were hardened in an anaerobic box with a N_2 + 5% H_2 atmosphere containing about 100 ppm O_2. In this case the lid of the bottels was opened occationally during the hardening period to remove oxygen, but otherwise the bottles were kept closed to prevent water loss or, for the samples under oxidizing conditions, contact with CO_2 from the air. After hardening the bottles were fitted with an external rubber ring and a steel ring squeezing the soft polyethylene wall of the bottles tightly against the sample. The systems are shown schematically in Fig. 48.

8 bottles with the ordinary product (even numbers) and 8 with increased potassium content (odd numbers) have been prepared.

Immediately before the leaching was initiated the samples in 8 bottels (Nos. 11-14 and R11-R14) were covered by a ~3 cm thick layer of kaolin containing 48 vol% water, i.e. a somewhat thicker layer with considerably less water than in the previous experiment.

In 4 bottles (Nos. 15,16,R15,R16) the samples were covered by a layer of chalk (precipitated, chemically pure $CaCO_3$) with 39 vol% water.

In the last 4 bottles (Nos. 17,18,R17,R18) a ~3 cm thick layer of inactive concrete (100 SRPC + 45.5 sand + 70 water) was cast on top of the samples and hardened 2 days before the leaching was initiated. This period is not included in the leach time although some diffusive transport will have occured. The concrete was of relatively low quality (i.e. high porosity, w/c=0.7), but considerably better than the product in section 4.1.1. (w/c=1.3).

For all the samples intended for leaching under reducing conditions (samples marked R) the dry barrier materials were mixed with de-aerated water in the anaerobic glove box. Reducing conditions should therefore be ensured in the barriers from the beginning of the experiment.

Before the barrier layers were placed in position, about 2/3 of the surface of the samples (except Nos. 11,12,R11,R12) was covered by bits of ordinary mild steel. The material was taken from the lid of a 200 l steel drum. It was cleaned and cut into pieces: ca. 5 • 5 • 1 mm, specific surface ~3.97 cm^2/g. Each bottle contained about 30 g. At the end of the experiment the weight losses were determined. In all cases the mean corrosion rate over the exposure period was found to be 0.5 - 0.1 μm/year or less, but the variability was large between systems which should have behaved rather similarly. No systematic difference between the corrosion rates under oxidizing and reducing conditions could be seen.

All the systems were leached in CO_2-free 0.001 M NaCl solution. In the case of the anaerobic systems, oxygen was removed by argon bubbling followed by storage in the anaerobic box. Each system contains 200 ml solution (+ water in the sample and barrier material). 100 ml was sampled after 7, 14, 28 and then every month, and replaced by fresh solution. The samples were analysed for pH, ^{134}Cs, ^{85}Sr, Na, K and Ca.

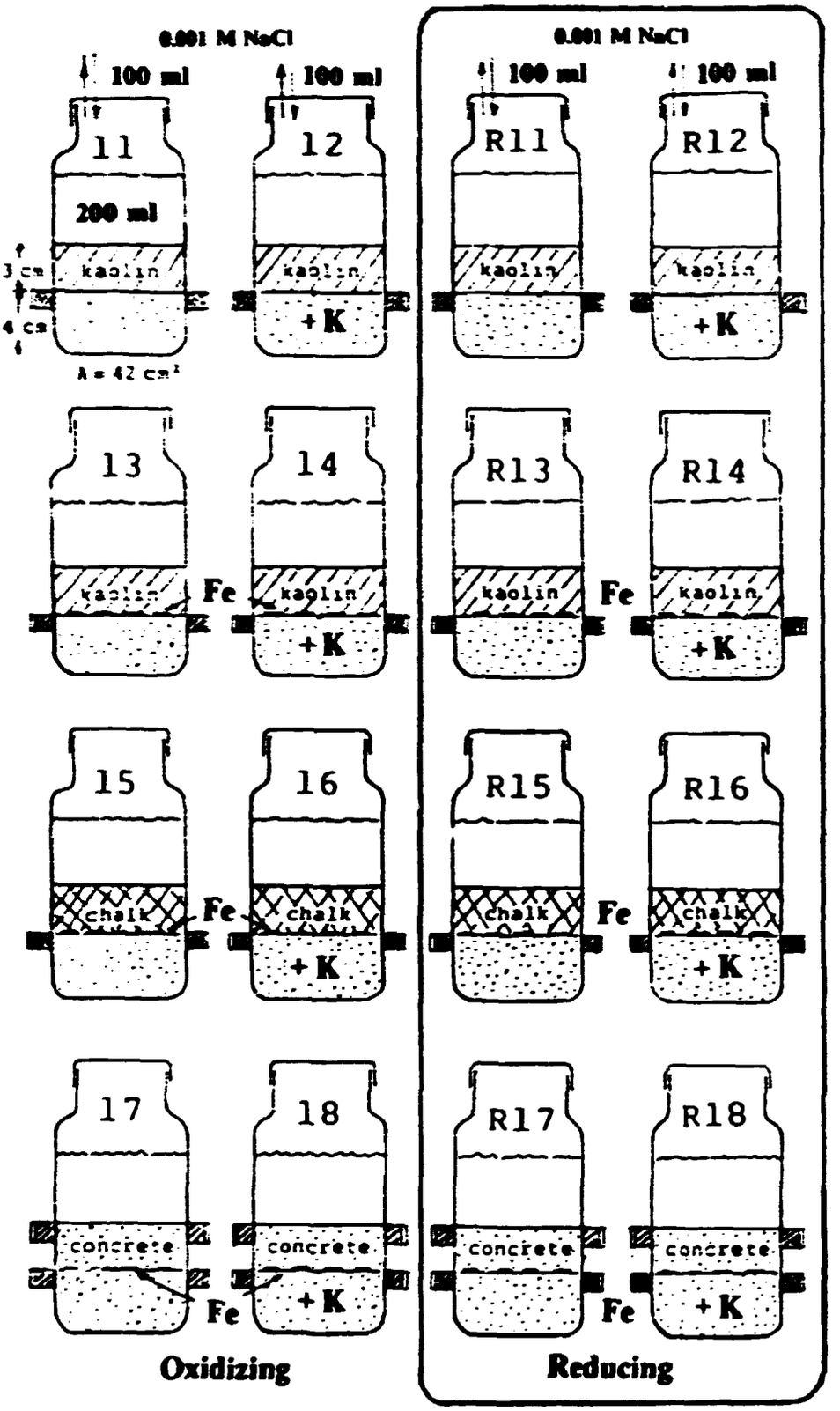

Fig. 48. Integral experiment combining leaching from cemented sodium nitrate, with effects of corroding steel and diffusion through kaolin ,chalk or concrete barriers under oxidizing or reducing conditions. The waste products in half of the systems were enriched in potassium.

For the systems with chalk or concrete barriers pH ~12.3 was reached nearly immediately. For the systems with kaolin the pH in the solution on top of the barrier also reached 12.0 to 12.2 but with a delay of one to two months. After 8-9 months and contact with 1.3 litres of water, pH began to decline slightly but remained above 12 for most systems.

Results concerning the Cs- and Sr-release are shown in Figs. 49a-h. As previously done and for convenience of presentation the results are shown as equivalent leached thickness plotted against the square root of time. Table 14 gives the apparent effective diffusion coefficients calculated from the slope of the curves, together with values for the time-lag.

For the systems with kaolin, the break-through for ^{85}Sr occurs after ~25 days and is nearly simultaneous with ^{134}Cs break-through in the systems with additional potassium. For the ordinary product the Cs break-through is delayed to about 140 days. There is not much difference between the systems with and without the presence of iron bits on the sample surface, but the previously noticed increase in the rate of Cs transport in reducing systems compared with similar oxidizing ones (Nos. 11 and 13 compared with R11 and R13) can again be seen. However, the effect is smaller than the influence of additional potassium and is not pronounced for the systems with extra K.

For the samples covered by $CaCO_3$, break-through of ^{134}Cs as well as ^{85}Sr occurs after only one to three days and the release proceeds at a considerable rate probably mainly determined by the leach rate from the waste product itself. There is not much difference between the four systems, although in this case increased potassium content appears to have a decreasing effect on both Cs and Sr releases.

For the samples covered by inactive concrete, Cs break-through occurs after about 100 days. The rate of release is increased greatly for the ordinary product under reducing conditions (compare Nos. 17 and R17), but the effect disappears also in this case for the systems with additional potasium (Nos. 18 and R18). The Sr releases are low and rather uncertain due to low countings. The inital relase for R18 could be due to contamination.

The releases of K, Na and Ca from the cemented product through the barriers are shown in Fig. 50a-f for the four systems with kaolin but without steel bits. Equivalent leached thicknesses as well as concentrations in the solution in contact with the barrier are given. It is seen that the potasium concentrations fall in two groups dependent on whether the sample contains additional K or not. The sodium concentrations are more uniform.

The Cs and Sr concentrations in the solutions as calculated from the measured ^{134}Cs and ^{85}Sr activities and the contents of carriers present in the waste materials are shown in Figs. 50g and h.

After the experiment the systems were taken apart. The kaolin and chalk barriers were sectioned into three layers and the activity profiles determined. In the systems with concrete barriers the layer was removed, dissolved in HCl and the total activity contents determined. The amounts found in the layers together with the accumulative amounts removed with the leach water during the experiment are reported in Table 15. The concentrations of Cs and Sr in the various layers relative to the initial concentration in the simulated waste material are also given.

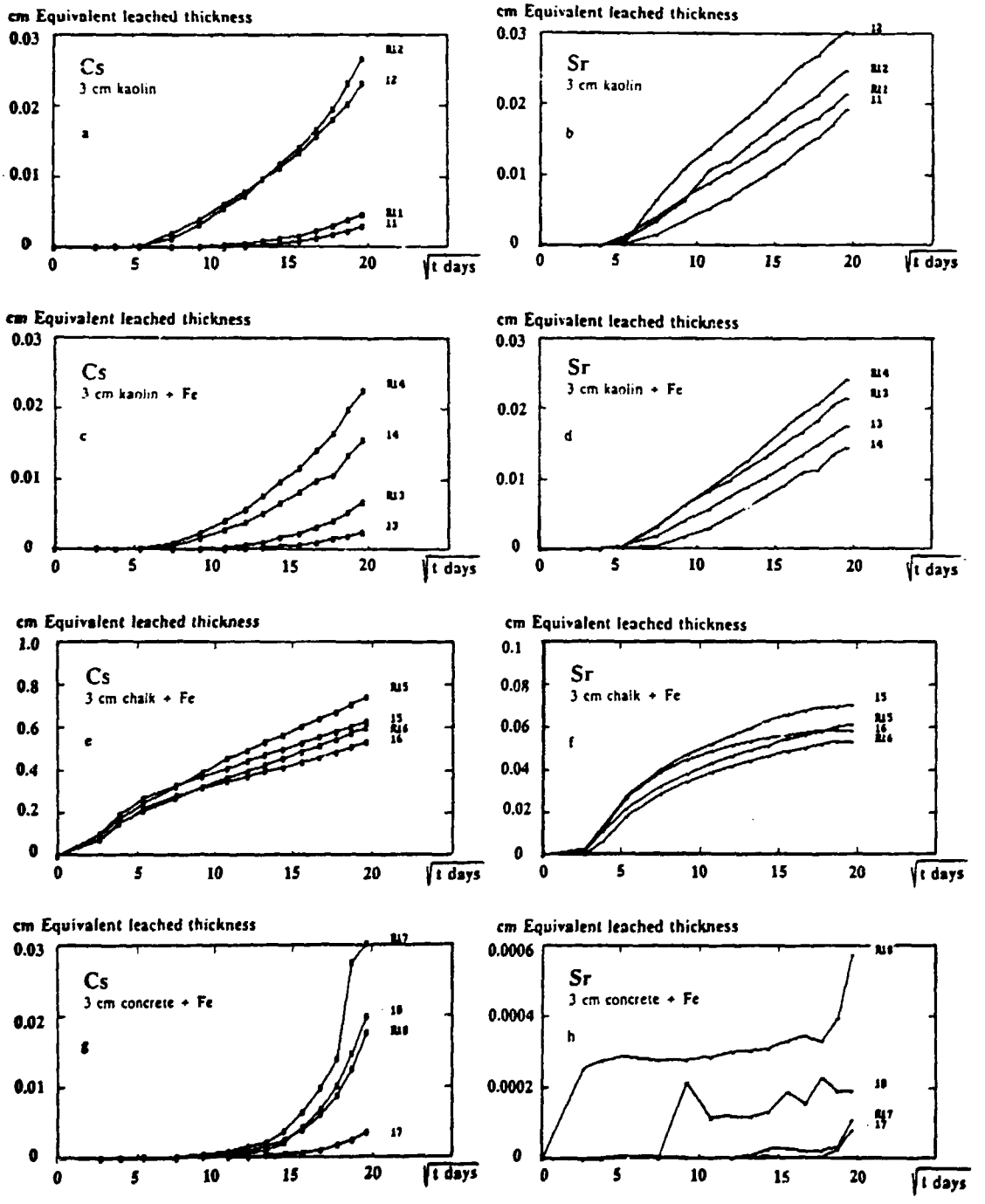

Fig. 49a-h. Break-through curves for ^{134}Cs and ^{85}Sr for the 16 systems shown in Fig. 48. For convenience the results are given as equivalent leached thickness of the original waste product plotted against the square root of time.

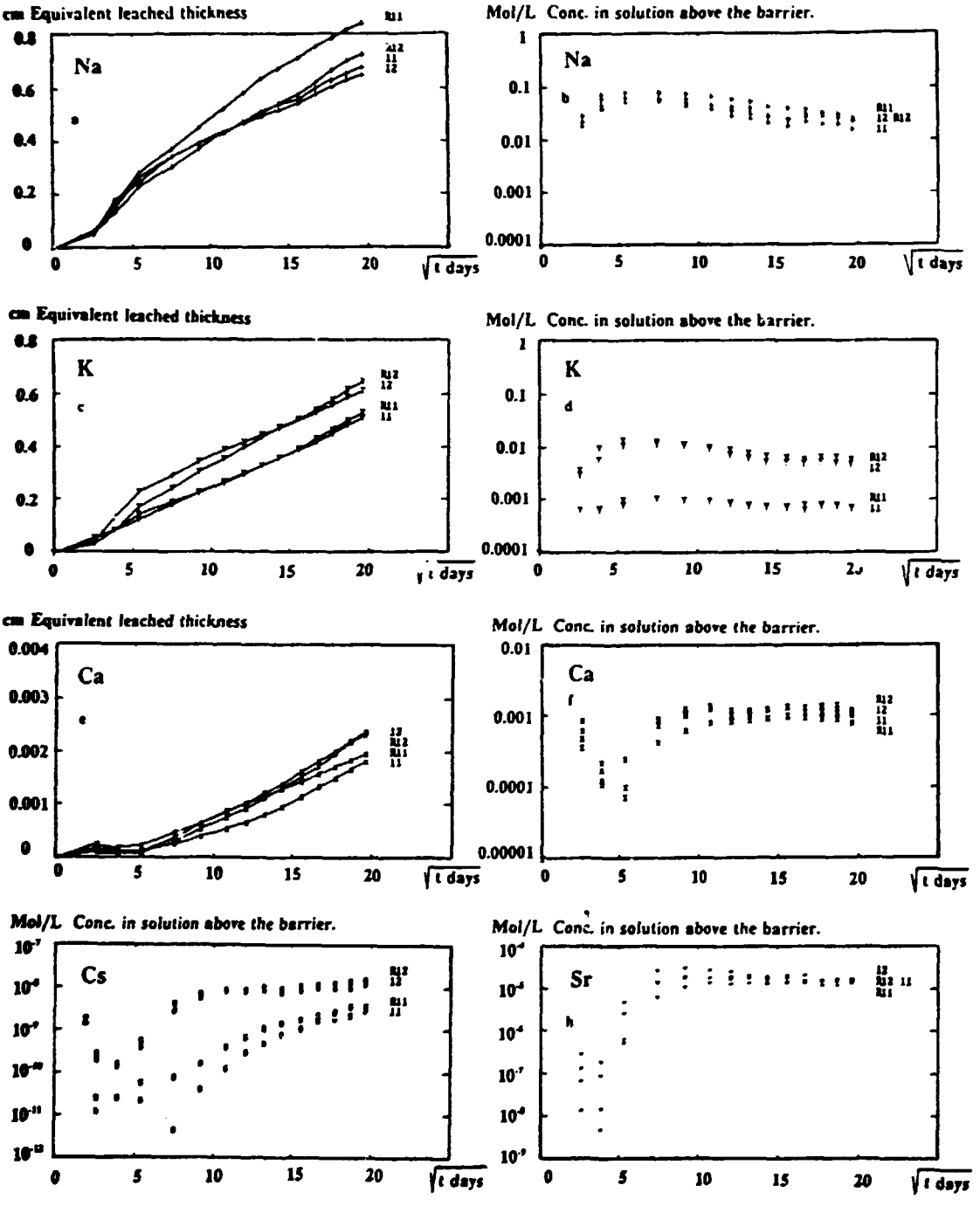

Fig. 50a-h. Break-through curves for Na, K and Ca together with the concentration development with time for the same 3 elements and Cs and Sr for the four systems with kaolin barriers but without corroding iron.

Table 14. Effective diffusion coefficients D_e and time-lags for the 16 experiments with diffusion from samples of cemented sodium nitrate through barriers of kaolin, chalk or concrete.

D_e in 10^{-12} cm^2/sec Time-lag in days

System	Aerobe				Anaerobe			
			With extra K				With extra K	
	D_e	time-lag	D_e	time-lag	D_e	time-lag	D_e	time-lag
3 cm kaolin	**11**		**12**		**R11**		**R12**	
Cs	0.97	142	27.1	51	2.7	141	38.2	63
Sr	22.7	60	34.4	14	17.9	20	27.2	26
K	6070	-	6140	-	7070	1	9760	-
Na	7670	-	7400	-	14300	-	10900	-
Ca	0.16	41	0.23	30	0.14	14	0.23	32
Fe + 3 cm kaolin	**13**		**14**		**R13**		**R14**	
Cs	1.16	173	18.2	88	6.9	156	29.2	68
Sr	15.3	38	15.4	72	20.0	27	27.5	33
K	5730	1	5980	-	9930	2	9740	-
Na	7530	-	5660	-	16500	-	10500	-
Ca	0.14	12	0.09	43	0.12	18	0.22	20
Fe + 3 cm chalk	**15**		**16**		**R15**		**R16**	
Cs	6320	-	3960	-	11300	-	69100	-
Sr	57.2	-	37.2	-	63.6	-	48.2	-
K	4750	-	6000	-	11200	-	10700	-
Na	7750	-	6080	-	12800	-	9540	-
Ca	(0.8)	-	(1.8)	-	(3.4)	(2)	(2.5)	(7)
Fe + 3 cm concrete	**17**		**18**		**R17**		**R18**	
Cs	3.06	203	101	202	264	204	39.3	163
Sr	0.001	227	0.001	-	0.001	178	0.001	-
K	(7230)	-	1250	(15)	(11800)	-	1680	(10)
Na	628	27	990	(56)	2210	(29)	1540	(24)
Ca	(0.8)	-	(0.5)	-	(1.2)	-	(1.2)	-

(Values in parantheses are much influenced by leaching from the barrier material itself.)

Tabel 15. Total activity removed in solution and activity contents in the barriers at the end of the experiment. The kaolin and chalk barriers were sectioned into three layers (Upper: 43 weight %, middle: 35 % and bottom: 22 % ± 4 %). The activities are given as equivalent thickness of the original waste material and as relative concentrations: c/c_o where c is the concentration in the layer (Bq/cm^3 corrected for decay) and c_o the original concentration in the waste product.

	mm	c/c_o %	mm	c/c_o %	mm	c/c_o %	mm	c/c_o %
3 cm kaolin		**11**		**12**		**R11**		**R12**
Cs in solution	0.030		0.234		0.047		0.267	
Upper layer	1.25	11	1.51	14	1.38	13	1.69	14
Middle -	2.69	27	2.18	20	2.83	25	3.19	31
Bottom -	2.67	51	2.34	40	3.14	49	2.66	57
Σ Cs loss	6.64		6.26		7.40		7.81	
Sr in solution	0.195		0.31		0.218		0.249	
Upper layer	0.212	1.8	0.168	1.4	0.166	1.5	0.157	1.3
Middle -	0.160	1.6	0.123	1.2	0.105	0.9	0.101	1.0
Bottom -	0.289	5.4	0.243	5.6	0.375	5.9	0.191	3.5
Σ Sr loss	0.86		0.84		0.86		0.70	
Fe + 3 cm kaolin		**13**		**14**		**R13**		**R14**
Cs in solution	0.026		0.157		0.068		0.227	
Upper layer	1.18	10	1.48	12	1.58	13	1.42	12
Middle -	2.79	26	2.00	21	2.26	23	2.01	21
Bottom -	2.09	48	1.55	32	2.15	40	2.34	36
Σ Cs loss	6.08		5.18		6.06		5.99	
Sr in solution	0.178		0.147		0.217		0.245	
Upper layer	0.141	1.3	0.164	1.3	0.243	2.0	0.113	1.0
Middle -	0.152	1.4	0.046	0.5	0.148	1.4	0.139	1.4
Bottom -	0.055	0.9	0.142	2.9	0.171	3.6	0.234	3.6
Σ Sr loss	0.53		0.50		0.78		0.73	
Fe + 3 cm chalk		**15**		**16**		**R15**		**R16**
Cs in solution	6.34		5.35		7.45		6.01	
Upper layer	0.084	0.8	0.080	0.8	0.076	0.7	0.065	0.6
Middle -	0.061	0.7	0.054	0.7	0.063	0.7	0.034	0.3
Bottom -	0.036	0.8	0.047	0.7	0.038	0.6	0.035	0.5
Σ Cs loss	6.52		5.54		7.63		6.15	
Sr in solution	0.710		0.591		0.623		0.537	
Upper layer	0.072	0.7	0.031	0.3	0.025	0.2	0.023	0.2
Middle -	0.036	0.4	0.022	0.3	0.021	0.2	0.019	0.3
Bottom -	0.057	1.2	0.071	1.1	0.040	0.6	0.108	1.5
Σ Sr loss	0.87		0.72		0.71		0.68	
Fe + 3 cm concrete		***17***		***18***		**R17**		**R18**
Cs in solution	0.036		0.200		0.303		0.177	
In barrier	2.88	9	2.10	7	3.52	12	2.58	9
Σ Cs loss	2.92		2.30		3.82		2.76	
Sr in solution	0.0008		0.0020		0.0011		0.0058	
In barrier	0.114	0.3	0.137	0.3	0.227	0.6	0.145	0.4
Σ Sr loss	0.115		0.138		0.228		0.151	

The results can be summarized as follows:

For the samples covered by kaolin the break-through of Cs occurs practically simultaneously with the break-through of Sr for the waste material containing additional potassium. For the normal product the break-through of Cs is considerably delayed. However, when comparing the concentration profiles and the total amounts of Cs released from the waste material itself, as given in Table 15 for samples 11 and 12 or R11 and R12, it is seen that there is not much difference and that especially the total loss of Cs from the waste samples are nearly the same. The effect of the additional potassium on the Cs release to the water must therefore mainly be due to competition about the available ion-exchange sites on the kaolin, while there is nearly no effect on the behaviour inside the waste sample itself.

The break-through curves for K and Na (Figs. 50a and c) show much greater releases to the water than the curves for Cs for the same four kaolin covered samples (Fig 49a). However, the loss from the waste samples are more or less the same when calculated as equivalent leached thicknesses at the end of the experiment: 0.65 to 0.85 cm for Na, 0.52 to 0.65 cm for K (excluding what may be bound on the kaolin thereby explaining the difference between systems 11,R11 and 12,R12 in Fig. 50a) and 0.63 to 0.78 cm for Cs (including what is bound on the barrier, see Table 15). All three alkali-metal ions are therefore behaving rather similarily inside the cemented waste.

The concentration curves in Figs. 50b,d and g show - after a short initial period - a steady decrease for K and Na in the water while the Cs concentration is nearly constant (for the systems with waste with additional potassium) or is still increasing. This is also an effect of the competing ion-exchange reactions. When the potassium concentration is decreasing some increase in Cs retention should be expected, but the effect is apparently not so large that it results in decreasing Cs concentrations towards the end of the experiment.

A slightly faster release of Cs to the water occurs in the reducing systems compared with the corresponding oxidizing systems (compare R12 and 12, R11 and 11, R14 and 14, R13 and 13). The fact that also the total amounts of Cs found in the kaolin layer at the end of the experiment are somewhat higher in the reducing than in the oxidizing systems support that increased releases of Cs from cemented materials under reducing conditions is a real phenomenon. However, the explanation could also be quite trivial, e.g. less compaction of the kaolin layers in the reducing systems, or temperature differences since the oxidizing systems were kept thermostated at 20°C while this was not possible for the systems stored in the anaerobic box where the temperture was about 23 ± 2°C.

Since the diffusion coefficients are temperature dependent in more or less the same way this should have resulted in a general increase of the same relative size for the releases of all species from the R-systems. Such a tendency can be seen, but not in a consistent way.

An example is the Sr releases which are not influenced in a systematic way by the redox conditions (or temperature difference) and also much less than Cs by the additional potassium. The Sr-releases to water is higher or similar to the values for Cs and the retention on the kaolin is considerably less, reflected e.g. in the much lower c/c_o values and in the total Sr losses given in Table 15.

Ca break-through occurs somewhat slower than for K and Na, but simultaneous with Sr break-through (compare Figs. 50e and 49b). The concentration development for Ca and Sr in the water phase is also similar resulting in nearly constant concentrations in the later period. The ratio between the Ca and the Sr concentration in the water is about 100 while the ratio in the waste product is 320. The reason could be that only part of the Ca in the cemented waste is available for easy leaching.

The presence of the corroding iron bits between the waste sample and the kaolin barrier results in slightly decreased total Cs loss and in a somewhat more pronounced decrease in the total Sr loss from the waste samples, but in this case only under oxidizing conditions. (Compare 13 and 14 with 11 and 12 in Table 15).

For the samples covered by chalk Cs appears to be leached more or less as from an uncovered sample. (The D_e values for R15 may be compared with the corresponding values found for the uncovered sample R1, see Table 12). For Sr, however, the shape of the curves in Fig. 48f show that the release rates diminish more rapidly than corresponding to a $\sqrt{t}$ law. The retention of especially Cs but also Sr in the chalk layers is much lower than for the kaolin barriers. No explanation of the abnormal shape of the Sr break-through curves is obvious from the Sr profile in the chalk barrier. Maybe carbonate from the chalk is influencing the Sr behaviour inside the concreted waste.

For the samples covered by inactive concrete (w/c=0.7) break-through of Cs occurs between 100 and 200 days. There is in this case so much difference between the release rates to water for the reducing and the oxidizing systems (R17 and 17) that this hardly can be due to differences caused by temperture differences or by unintended variations in the casting of the barrier. A similar clear tendency was also observed in the previous experiment of this type where a concrete barrier with w/c=1.3 was employed.

Sr break-through appears to take place at about 400 days, but the results are rather uncertain since the countings are low due to the high degree of retention and to decay of the ^{85}Sr.

It is obvious from the values given in Tables 14 and 15 that concrete - even of a relatively low quality as employed here - is a more efficient barrier material than the kaolin and chalk.

4.1.3. Modelling.

It is obviously of interest to use the measurements on these integral experiments for comparison with modelling results. This has been attempted for systems No. 11 and 12 with kaolin barriers where a suitable set of distribution coefficients are available /19/. A one-dimensional model DIFMIG /25/ was found to be suitable for the purpose.

DIFMIG, originally written in FortranIV is now called DIFMIG2 after being revised and rewritten in the C-language. DIFMIG2 calculates one-dimensionally the diffusive migration of single substances through multi-barrier systems according to the equation,

$$\delta C/\delta t = D'(t) \cdot \delta^2 C/\delta x^2 + F'(C,t)$$

where D'(t) is the effective diffusion coefficient, which is a product of the (possibly time-dependent) retention factor R_f and the diffusion coefficient, D in the liquid phase. F'(C,t) is a function responsible for the time-dependent changes in concentration other than dispersion/diffusion, e.g. radioactive decay. The diffusion equation is solved by a finite difference implicit method with the resulting trigonal matrix equation being solved by standard methods.

Within the cemented waste product the retention factor will mainly be determined by the pore structure although some chemical retardation or solubility related phenomena may also be involved, especially in case of strontium. In the calculations R_f's = 0.005, 0.001 and 0.00001 are assumed for K, Cs and Sr in the waste product.

In the kaolin R_f may be calculated from the formula:

$$R_f = \frac{\epsilon}{\epsilon + (1-\epsilon) \cdot \rho \cdot K_D} = \frac{1}{1+2.81 \cdot K_D}$$

for kaolin (ρ=2.6 g/cm^3) with 48 vol% water, since pore structure related retardation will be slight in this uncompacted and relatively coarse material.

The distribution coefficient K_D for Cs and Sr on kaolin in high pH solutions containing various concentrations of Na^+ and K^+ has been determined previously /19/ Some results are cited in Table 16 together with the R_f values calculated from the formula above. K_D and R_f are seen to be strongly dependent on the concentration of the major ions, especially the competition between potassium and cesium is pronounced. The divalent Sr-ions are less influenced except at very high concentration of alkali metals in agreement with usual ion-exhange theory.

Table 16 Distribution coefficents K_D ml/g for Cs^+ and Sr^{2+} on kaolin at different Na^+, K^+ and Ca^{2+} concentrations. The OH^- concentration was ~0.01 M giving somewhat increased K_D for Sr, but not for Cs compared with determination in neutral solutions. Cs and Sr-carrier concentrations: 10^{-6} eq/L.

Main ions			Cs		Sr	
Na	K	Ca	K_D	R_f	K_D	R_f
mMol/L			ml/g		ml/g	
8	-	0.8	230	0.0015	49	0.007
-	8	0.8	30	0.012	34	0.010
8	8	0.8	27	0.013	20	0.018
80	-	0.8	91	0.0039	18	0.019
-	80	0.8	7.4	0.046	11	0.031
80	80	0.8	5.3	0.063	7.5	0.045
400	-	8	33	0.011	1.7	0.17
400	8	8	11.5	0.030	2	0.15
320	80	8	5*	0.07	0.1*	0.8
-	400	8	2*	0.15	0.05*	0.9

* Estimate from measurements in neutral solution.

Typical values for the concentrations measured in water sampled from the integral experiments are 0.8 mM Ca, 50-20 mM Na for all the systems and ~8 respectively ~1 mM K depending on whether the waste was enriched in potassium or not. R_a values around 0.06 and 0.02 for Cs and 0.06 and 0.01 for Sr in the two types of experiments (systems no 12 and 11) could therefore be selected for example calculations. However, solutions saturated by $NaNO_3$ and 0.17 respectively 1.3 M in KNO_3 will initially be present in the pore water in the cemented waste and transient, but also quite high concentrations of major ions can be expected in the pore water in the kaolin. This will result in much reduced retention of Sr and also Cs when the potassium concentration is high. This is in agreement with the experimental observations. However, calculation examples with the model are not given here since some further refinements are needed.

4.2. Diffusive transport of tritiated water through bentonite as influenced by contact with concrete.

A preliminary experiment using three diffusion cells to see whether contact with concrete is influencing the diffusion of tritiated water through bentonite. The cells have been employed previously, se Section 3.1.1. to study diffusion of tritiated water through slabs of the five types of concrete specified in Table 6.

The experimental set-up is shown in Fig. 51. About 1 cm thick layers of bentonite containing ~24.5 % water were placed between two ~one cm thick slabs of concrete (type a from the study mentioned above) or similar slabs of very porous ceramics.

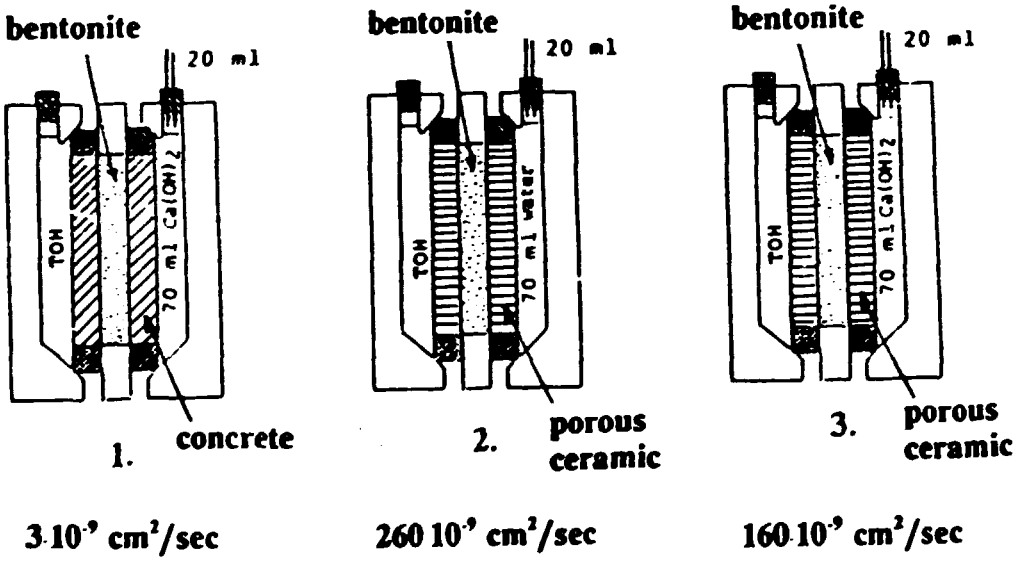

Fig. 51. The three diffusion cells employed in a preliminary experiment with diffusion of tritiated water through bentonite as influenced by concrete and nummerical values for the diffusive permeabilities for TOH migration assuming the main resistance is in the clay layer.

Three systems were employed:

- No. 1 with concrete slabs around the bentonite using $Ca(OH)_2$-saturated water in the two cell chambers. The left chamber contains in addition 0.3 MBq TOH/ml. Samples are removed regularily from the right chamber and analysed for tritium. The samples are replaced by fresh calcium hydroxide solution.
- No. 2 have slabs made from ceramics and pure water (with TOH as above) is used in the chambers and as replacement after sampling.
- No. 3 is similar to No. 2 except that $Ca(OH)_2$-saturated water is used instead of pure water.

The systems were followed with tritium analyse for about 3 months, and the diffusive permeabilities given in the figure were calculated from the slope of the linear part of the break through curves. Since the permeability of the type a concrete in previous experiments was found to be a factor ~10 lower ($18 - 26 \cdot 10^{-9}$ cm^2/sec, see Table 6) the contribution from the two concrete slabs to the overall permeability value is supposed to be slight and the resistance to water migration mainly due to the clay layer. The same is expected to be the case for the two clay layers contained between slabs of very porous ceramics.

The reason for the low permeability of the clay between the concrete slabs compared with the other two systems is not obvious. The properties of the clay may have changed due to contact with the concrete, but it could also be that the concrete slabs have been partly clogged by the clay or silica from the clay. However, trivial experimental errors in mounting the clay in the diffusion cells is also a possibility, and these three experiment are far too few for any conclusions to be drawn.

The interaction between bentonite or other clay materials used as backfill and concrete in waste or barriers or migration of water and ions in the materials is, however, an important issue in safety analysis and should be studied further using this or other methods.

4 REFERENCES

1 Brodersen, K., Nilsson K.
Mechanisms and interaction phenomena influencing release in low- and medium level waste disposal systems.
Progress report January-June 1987 for CEC contract FI 1W-0089-DK (B) Risø 1987,
(available on request).

2 Same, Annual report 1987.

3 Same, Progress report January-June 1988.

4 Same, Annual Report 1988.

5 Same, Progress Report 1/1-30/6 1989.

6 Same, Annual Report 1989.

7 Characterization of Radioactive Waste Forms.
Progress report for 1986, Volume 1.
Ed. F.P. Glasser and C. McCulloch. EUR 11354 EN/1, CEC 1988.

8 Characterization of Radioactive Waste Forms.
CEC Progress report 1987, Volume 1.
Ed. Brodersen,K. Nilsson,K. EUR 12077 EN/1

9 Handbook of Reference Medium Active Waste (RMA). 1st Edition 1989.
CEC R&D Programme on Management and Disposal of Radioactive Waste.
EUR 12482 EN

10 Characterization of low and medium-level radioactive waste forms.
Final report - 2nd Programme 1980-84
Ed: P.E. Pottier, F.P. Glasser. EUR 10579 EN, CEC 1986.

11 Ibid, Revision 1. Revised reference waste forms compositions.

12 Brodersen. K. "The influence of water uptake on the long-term stability of conditioned waste", pp 147-162 in:
Testing, Evaluation and Shallow Land Burial of Low and Medium Radioactive Waste Forms. Vol. 13 of CEC monographs on Radioactiv waste management.
Ed. Krischer, W. and Simon, R. EUR 8979 Harwood Acad Publ. 1984.

13 Beijer, O.
Casting granular ion-exchange resins as medium active waste in cement.
Report Prav 1.36, Stockholm 1980. (English summary of work reported in Swedish.)

14 Nordic studies on radwaste.
Technical part III, Product characteristics
NKA/AO (81)5 1981.

15 Crank, J.
The mathematics of diffusion.
Clarendon Press. Oxford 1975.

16 Van Iseghem, P., Berghman, W., Timmermans, W.
Physico-chemical characterization of bituminized Eurochemic medium-level waste.
Final report for CEC contract FI1W/0094, SCK/CEN Mol 1990

17 Brodersen, K.
"Hygroscopic Water Uptake and Dry/Wet Cycling Compared With Normal Water Exposure of Cemented Waste Forms."
12th Int.Symp. on the Scientific Basis for Nuclear Waste Management
MRS, in Berlin Oct. 1988. Paper A/22.

18 Brodersen,K., Petersen,B.M., Vinther,A.
Comparative study of test methods for conditioned low- and medium level radioactive waste.
Annual report 1983 for CEC contract WAS-303-83-13-DK(G)

19 Same, Annual report 1984.

20 Brodersen, K., Vinther, A.
Contraction, density- and viscosity changes of bitumen and bituminized waste products during dry storage.
NKA: Safety research in energy production, Nordic Projects. AVF(84)238, 1985.

21 Brodersen, K.
Development of a waste unit for use in shallow land burial.
Final Report. EUR 10821 EN, 1986.

22 Guppy, R.
Autogeneous healing of cracks in concrete and its relevance to radwaste repositories.
Nirex safety studies, NSS/R105 Harwell 1988.

23 Glasser, F.P. Lachowski, E.E., Macphee, D.E.
"Compositional model for calcium silcate hydrate (C-S-H) gels. Their solubilities and free energies of formation." J.Am.Ceram.Soc. 70, pp 481-485, 1987.

24 Allen, A.J., Oberthur, R.C., Pearson, D., Sholfield, P. and Wilding, C.R.
The development of the fine porosity and the gel structure of hydrating cement systems.
AERE R 12187, Harwell 1986.

25 Bo, P. Carlsen,L.
DIFMIG - A computer program for calculation of diffusive migration through multi-barrier systems.
Risø-M-2262, Nov. 1981.

Risø National Laboratory

Risø - M - 2908

MECHANISMS AND INTERACTION PHENOMENA INFLUENCING RELEASES IN LOW- AND MEDIUM-LEVEL WASTE DISPOSAL SYSTEMS

Final Report 1986-1990

Knud Brodersen
Karen Nilsson

Date November 1990

Department or group
NUK (BEH)

Groups own registration number(s)

Project/contract no.
EC contract
FI 1W-0089-DK

Pages 94 Tables 16 Illustrations 51 References 25

ISBN 87-550-1694-4

Abstract (Max. 2000 char.)

Abstract. The report covers work done 1986-1990 at Risø National Laboratory as part of the third EC Research Programme on Radioactive Waste Management.

Waste product characterization:

- Leaching and volume stability of cemented ion-exchange resins. Wet/dry cycling was found to be an important degradation mechanism.
- Hygroscopic properties of cemented and bituminized radioactive waste. Water uptake from the air can be an important release mechanism when waste containing soluble salts are disposed of by shallow land burial.
- Water uptake and swelling of bituminized waste including studies on water migration in bitumen membranes and measurements of swelling pressures.
- Ageing of bituminized products was demonstrated to result in increasing stiffness of the materials.
- Nickel ferrocyanide in precipitation sludge was found to be unstable in contact with concrete.

Barrier material properties:

- The influence of the pore structure in concrete on the hydraulic or diffusive transport of water and ions through concrete barriers was investigated. The main parameter is the water/cement ratio. A theoretical interpretation is given.
- Healing of cracks in concrete barriers by precipitation of calcium carbonate was demonstrated experimentally and described by a simplified model.
- Transport of components between two thin plates of cement paste with different composition stored together in water was found to take place at a low rate.
- The structure of degraded cement paste was studied using SANS (small angle neutron scattering).

Interaction phenomena:

- Integral experiments with migration of radioisotopes from cemented waste through barriers made from kaolin, chalk or concrete were made under different external conditions. The results can be used for model validation and some preliminary work was done.

Descriptors - INIS

BITUMENS; CALCIUM CARBONATES; CEMENTS; CESIUM ISOTOPES; CONCRETES; CRACKS; DECOMPOSITION; DIFFUSION; FERROCYANIDES; HYGROSCOPICITY; INTERMEDIATE-LEVEL RADIOACTIVE; ION EXCHANGE; KAOLIN; LEACHING; LOW-LEVEL RADIOACTIVE WASTES; PERMEABILITY; POROSITY; PRECIPITATION; RADIOACTIVE WASTE DISPOSAL; RADIONUCLIDE MIGRATION; SMALL ANGLE SCATTERING; STRONTIUM ISOTOPES; SWELLING; WATER

Available on request from Risø Library, Risø National Laboratory, (Risø Bibliotek, Forskningscenter Risø), P.O. Box 49, DK-4000 Roskilde, Denmark.
Telephone +45 42 37 12 12, ext. 2268/2269. Telex: 43116, Telefax: +45 46 75 56 27

Available on exchange from:
Risø Library,
Risø National Laboratory,
P.O. Box 49, DK-4000 Roskilde, Denmark
Phone +45 42 37 12 12, ext. 2268 2269
Telex 43116, Telefax +45 46 75 56 27

ISBN 87-550-1691-4
ISSN 0418-6435